



**UCGE Reports  
Number 20169**

Department of Geomatics Engineering

**Urban Snow Hydrology and Modelling**  
(URL: <http://www.geomatics.ucalgary.ca/links/GradTheses.html>)

by

**Carrie Lee Ing Ho**

**December 2002**



**THE UNIVERSITY OF CALGARY**

**Urban Snow Hydrology and Modelling**

**by**

**Carrie Lee Ing Ho**

**A THESIS**

**SUBMITTED TO THE FACULTY OF GRADUATE STUDIES  
IN PARTIAL FULFILLMENT OF THE REQUIREMENTS FOR THE  
DEGREE OF MASTER OF SCIENCE**

**DEPARTMENT OF GEOMATICS ENGINEERING**

**CALGARY, ALBERTA**

**DECEMBER, 2002**

**© Carrie Lee Ing Ho 2002**

## **Abstract**

Urban winter hydrology has garnered very little attention due to the general notion that high intensity rainfalls are the major flood-generating events in urban areas. As a result, few efforts have been made to research urban snow and its melt characteristics. This study investigated the characteristics of urban snow that differentiates it from rural snow, and the impact of incorporating these characteristics in an urban snowmelt model. A field study was conducted from fall of 2001 to spring of 2002 at the University of Calgary campus. Data collected includes snow depth and density, soil moisture, soil temperature, snow albedo, net radiation, snow evaporation, and surface temperature. Snow cover was classified into several types; snow piles, snow on road shoulders, snow on sidewalk edges, and snow in open areas. This resulted in the development of four separate functions for the changing snow albedo values. Shortwave radiation was found to be the main source of energy for urban snow, and as a consequence, the albedo of urban snow is a very important factor in urban snowmelt modelling. In addition, urban elements such as vehicle traffic and buildings can influence the energy balance of the snowpack. A study of the frozen ground conditions reveals that antecedent soil moisture conditions had very little impact on frozen ground, and thus frozen ground acts as a near impervious area. In the modelling component of this study, urban snowmelt was modeled using the energy balance method with hourly time steps and the incorporation of snow redistribution, and hence the simulation of snow piles. Three simulated tests of varying conditions revealed that peak volume, time to peak and runoff period differs for areas with snow piles versus a uniform urban snow cover. Simulation of rain-on-snow events revealed a sharp increase in runoff peak volume. Hence, under the adverse condition of intense snowmelt, frozen ground, and rainfall, flooding in urban areas can easily occur. Improved flood forecasting for urban catchments in cold regions can only be achieved with accurate modelling of urban winter runoff that involves the energy balance method, incorporating snow redistribution and urban snow cover characteristics, and using small time steps.

## **Acknowledgements**

I would like to thank Dr. Caterina Valeo for the wonderful opportunity to study and work under her supervision. A mentor as well as a friend, I owe much of this very rewarding experience to her.

I would also like to thank the University of Calgary for funding my research and the Engineering for the Environment Program for additional funding.

My gratitude also goes out to Rick Smith and the Department of Geography for the use of the University Weather Station data.

For Dr. John Yackel, and Dr. Ivan Muzik, my sincere thanks for the helpful comments and suggestions to improve my thesis.

For C.T. Ling, thankyou for the laughter and the unwavering support, for putting up with my many bizarre moods.

For my parents, you have made this possible in many ways. My profound gratitude for all the sacrifices you have made, and for always believing in me. Whatever the future holds, know that you have shaped me, and given me the best possible start.

## Table of Contents

<b>Approval Page</b>	ii
<b>Abstract</b>	iii
<b>Acknowledgements</b>	iv
<b>Table of Contents</b>	v
<b>List of Tables</b>	ix
<b>List of Figures</b>	x
<b>Notation</b>	xii
<b>CHAPTER ONE</b>	<b>1</b>
INTRODUCTION .....	1
1.1 Introduction and Research Background.....	1
1.2 Thesis Objectives .....	2
1.3 Thesis Layout.....	3
<b>CHAPTER TWO</b>	<b>4</b>
LITERATURE REVIEW .....	4
2.1 Processes Governing Urban Snow .....	4
2.1.1 Snowmelt Processes .....	4
2.1.2 Snow Metamorphosis .....	10
2.1.3 Component of Energy Exchange Dominating Melt .....	10
2.1.4 Factors Influencing Melt in Urban Areas.....	11
2.1.5 Infiltration Capacity of Frozen Soil.....	13
2.1.6 Surfaces Contributing to Overland Flow During Snowmelt.....	14
2.1.7 Redistribution of Snow in Urban Areas .....	15
2.2 Snowmelt Models .....	15

2.2.1	Mathematical Method.....	15
2.2.2	Computer Models.....	16
2.2.2.1	NWSRFS SNOW-17.....	17
2.2.2.2	EPA SWMM.....	20
2.2.2.3	MOUSE RDII.....	21
2.2.2.4	HSPF.....	22
2.2.2.5	SSARR.....	27
2.2.3	Discussion on the Snowmelt Algorithms.....	30
<b>CHAPTER THREE</b>		<b>32</b>
	THESIS OBJECTIVES.....	32
3.1	Gaps in Knowledge.....	32
3.2	Detailed Thesis Objectives.....	34
3.3	Research Outline.....	36
<b>CHAPTER FOUR</b>		<b>37</b>
	METHODOLOGY.....	37
4.1	Field Location.....	37
4.2	Common Data Gathering Methods (From Literature).....	37
4.2.1	Snowfall Data.....	38
4.2.2	Snow Surveys Measurements.....	38
4.3	Temporal, Spatial Data Collected.....	40
4.3.1	Soil Moisture.....	44
4.3.2	Soil Temperature.....	46
4.3.3	Snow Albedo.....	48
4.3.4	Net Longwave Radiation.....	48
4.3.5	Snow Depth and Density.....	49
4.3.6	Evaporation of Snowpack.....	50
4.3.7	Surface Temperatures.....	51

4.3.8	Precipitation Events (to be noted) .....	51
4.3.9	University Weather Station .....	51
<b>CHAPTER FIVE</b>		<b>52</b>
	<b>FIELD STUDY RESULTS AND ANALYSIS .....</b>	<b>52</b>
5.1	Qualitative Analysis.....	52
5.1.1	Visual Survey of Northwest Calgary.....	52
5.1.2	Classification of Urban Snow Cover.....	53
5.1.3	Snow Plowing Practices .....	54
5.1.4	Precipitation Events.....	55
5.2	Quantitative Analysis.....	55
5.2.1	Snow Water Equivalent.....	55
5.2.2	Soil Moisture .....	60
5.2.3	Soil Temperature .....	62
5.2.4	Infiltration into Frozen Ground .....	69
5.2.5	Albedo of Snow.....	70
5.2.6	Net Longwave Radiation.....	76
5.2.7	Net Radiation Fluxes .....	77
5.2.8	Evaporation from the Snowpack .....	82
5.2.9	Net Energy Flux .....	85
5.2.10	Surface Temperature .....	86
<b>CHAPTER SIX</b>		<b>90</b>
	<b>URBAN SNOW MODELLING .....</b>	<b>90</b>
6.1	Introduction.....	90
6.2	USM Time Steps.....	91
6.3	Subcatchment Schematization .....	91
6.4	Calculating Snow Melt Using the Energy Balance Method .....	93
6.5	Areal Depletion Curve .....	101

6.6	Liquid Water Routing in Snowpack .....	102
6.7	Infiltration into Frozen Ground.....	103
6.8	Net Runoff .....	103
6.9	Input Variables.....	104
6.10	Output Files.....	106
6.11	Simulations of Urban Snowmelt.....	108
6.12	Results and Analysis of Simulations .....	109
6.12.1	Results and Analysis of Simulation A.....	110
6.12.2	Results and Analysis of Simulation B.....	125
6.12.3	Results and Analysis of Simulation C.....	132
<b>CHAPTER SEVEN</b>		<b>137</b>
CONCLUSION AND RECOMMENDATIONS .....		137
7.1	Major Results of Field Study .....	137
7.2	Major Results of Modelling.....	138
7.3	Recommendation for Future Field Study.....	139
<b>REFERENCES</b>		<b>140</b>

## List of Tables

Table 4.1: Measurement sites description.....	41
Table 5.1: Instantaneous snow measurements.....	56
Table 5.2: Summary of campus snow survey.....	59
Table 5.3: Summary of snow density values.....	60
Table 5.4: Snow albedo summary.....	75
Table 5.5: Albedo values for snow cover at sites A, C, and D.....	76
Table 5.6: Net longwave radiation measurements at sites E, P, and Q on cloudless days.....	77
Table 5.7: Evaporation loss measurements for dry, fine-grained snow.....	83
Table 5.8: Evaporation loss measurements for crusty, larger-grained snow.....	83
Table 5.9: Evaporation loss measurements for disturbed, piled snow.....	84
Table 5.10: Average surface temperature measurements.....	88
Table 5.11 Specific heat values.....	89
Table 6.1: Subcatchment surface classification.....	92
Table 6.2: User-defined input variables used to simulate catchment schematization.....	104
Table 6.3: User-defined input variables used to simulate snow redistribution.....	105
Table 6.4: Input variables needed to calculate snow melt rate.....	106
Table 6.5: Resultant graphs from simulation.....	107
Table 6.6: Simulation scenarios description.....	108
Table 6.7: Values for the user-defined input variables for simulation A.....	110
Table 6.8: Snow depth available for melt for each subcatchment type.....	112

## List of Figures

Figure 2.1: Components of the energy budget for a snowpack .....	5
Figure 2.2: Seasonal variation of the melt factor (modified from Anderson, 1996) .....	20
Figure 2.3: Example of snow cover depletion curve (taken from USACE, 1991) .....	29
Figure 4.1: Map showing the study area and measurement sites.....	40
Figure 4.2: Profile of the soil moisture Profile Probe in the ground.....	45
Figure 4.3: Profile of the temperature sensors in the ground.....	47
Figure 5.1: Snow cover types classified .....	54
Figure 5.2: Locations of snow pile measurement sites on the University of Calgary .....	58
Figure 5.3: Averaged soil moisture level in the 0-30 cm depth for the different measurement sites .....	61
Figure 5.4: Soil moisture variation with depth at Site C.....	62
Figure 5.5: 24-hr temperature averages from October 1, 2001 to April 30, 2002 .....	65
Figure 5.6: Hourly temperature fluxes from January 14, 2002 to March 4, 2002 .....	66
Figure 5.7: Hourly temperature fluxes for April, 2002 (Dashed line indicates date when complete ablation of snow cover is observed).....	67
Figure 5.8: Soil temperature variation with depth .....	68
Figure 5.9: Infiltration amount vs. SWE.....	69
Figure 5.10: Snow albedo measurements at four open area sites .....	71
Figure 5.11: Snow albedo measurements for four sites with snow piles.....	72
Figure 5.12: Albedo measurements for snow on road shoulders.....	73
Figure 5.13: Albedo of snow on sidewalk edges .....	74
Figure 5.14: Net radiation fluxes measured for snow piles .....	78
Figure 5.15: Net radiation fluxes measured for snow in open areas.....	79
Figure 5.16: Net radiation fluxes measured for snow on road shoulders .....	81
Figure 5.17: Net radiation fluxes measured for snow near building walls .....	82
Figure 6.1: Snow albedo values for large snow piles .....	95

Figure 6.2: Snow albedo values for small snow piles.....	96
Figure 6.3: Snow albedo values for natural snow cover.....	97
Figure 6.4: Areal Depletion Curve.....	102
Figure 6.5: Energy flux for large snow piles .....	113
Figure 6.6: (a) Melt rate for large snow piles; (b) Melt rate for small snow piles; and (c) Melt rate for uniform snow cover .....	117
Figure 6.7: Runoff rates for subcatchment type 5 (large snow piles).....	118
Figure 6.8: Runoff rates for subcatchment type 6 (small snow piles) .....	119
Figure 6.9: Runoff rates for subcatchment type 7 (uniform snow cover).....	120
Figure 6.10: Runoff volume for subcatchment type 5 (large snow piles) .....	121
Figure 6.11: Runoff volume for subcatchment type 6 (small snow piles).....	122
Figure 6.12: Runoff volume for subcatchment type 7 (uniform snow cover) .....	123
Figure 6.13: Total runoff volume for the whole catchment.....	124
Figure 6.14: Advected heat rain from rain into the snowpack.....	125
Figure 6.15: Runoff rates for impervious subcatchment type 1 (parking lots).....	126
Figure 6.16: Runoff volume for subcatchment type 1 (parking lots) .....	128
Figure 6.17: Runoff volume for subcatchment type 5 (large snow piles) .....	129
Figure 6.18: Runoff volume for subcatchment type 7 (uniform snow cover) .....	130
Figure 6.19: Total runoff volume for the whole catchment.....	131
Figure 6.20: Runoff rates for impervious subcatchment type 1 (parking lots).....	134
Figure 6.21: Runoff volume for subcatchment type 1 (parking lots) .....	135
Figure 6.22: Total runoff volume for the whole catchment.....	136

## Notation

### Symbols

#### English Alphabet

A	snow albedo
$C_m$	factor to correct melt values to field conditions
D	index to the dullness of snowpack
$E_\ell$	elevation (hundreds of meters)
$E_t$	total emitted longwave radiation energy ( $\text{mm}_e \text{sec}^{-1}$ )
$E_x$	mean elevation of land segment above sea level (ft)
F	average forest canopy cover
$F_m$	melt factor ( $\text{mm } ^\circ\text{C}^{-1}$ )
$F_r$	fraction of snow depth
$F_{cs}$	fraction of clear sky
$F_{ls}$	fraction of shaded land segment
$F_{max}$	maximum melt factor ( $\text{mm } ^\circ\text{C}^{-1}$ )
$F_{min}$	minimum melt factor ( $\text{mm } ^\circ\text{C}^{-1}$ )
$F_{t1a}$	fraction of excess Swe in type 1 subcatchment redistributed by plowing into big snow piles onto adjacent pervious area
$F_{t1b}$	fraction of excess Swe in type 1 subcatchment redistributed by plowing into small snow piles onto adjacent pervious area
$F_{t1c}$	fraction of excess Swe in type 1 subcatchment redistributed by trucking onto pervious area of another catchment
$F_{t2a}$	fraction of excess Swe in type 2 subcatchment redistributed by plowing into big snow piles onto adjacent pervious area
$F_{t2b}$	fraction of excess Swe in type 2 subcatchment redistributed by plowing into small snow piles onto adjacent pervious area

$F_{t2c}$	fraction of excess S <sub>we</sub> in type 2 subcatchment redistributed by trucking onto pervious area of another catchment
$F_{t3a}$	fraction of excess S <sub>we</sub> in type 3 subcatchment redistributed by plowing into big snow piles onto adjacent pervious area
$F_{t3b}$	fraction of excess S <sub>we</sub> in type 3 subcatchment redistributed by plowing into small snow piles onto adjacent pervious area
$F_{t3c}$	fraction of excess S <sub>we</sub> in type 3 subcatchment redistributed by trucking onto pervious area of another catchment
$H_e$	condensation heat flux to the snowpack (in. water equivalent/interval)
$H_p$	heat transfer from rain (in. water equivalent/interval)
$H_r$	net radiation heat flux to the snowpack (in. water equivalent/interval)
$H_s$	convective heat flux to the snowpack (in. water equivalent/interval)
$H_{lw}$	net longwave radiation (in. water equivalent)
$H_{sw}$	net shortwave radiation (in. water equivalent)
$I_i$	observed solar radiation on horizontal surface (langleys)
$I_{lw}$	incoming longwave radiation to the snowpack (langleys/interval)
$I_{sw}$	incoming shortwave radiation to the snowpack (langleys/interval)
$I_{swe}$	initial snow depth over the catchment (mm)
$L_s$	latent heat of vaporization (8.5 mm <sub>e</sub> mm <sup>-1</sup> )
$M$	amount of snowmelt (mm day <sup>-1</sup> )
$M_d$	amount of daily snowmelt (in. day <sup>-1</sup> )
$M_f$	melt factor (mm °C <sup>-1</sup> day <sup>-1</sup> )
$M_r$	melt rate (in. water per degree day)
$M_s$	amount of snowmelt (mm)
$M_{gm}$	maximum melt of rate caused by heat from the ground (in. water equivalent)
$M_{sr}$	melt rate (mm/hr)
$O_s$	liquid-water outflow from the bottom of the snow cover (mm)

$P_a$	atmospheric pressure (mb)
$P_r$	rainfall intensity (in/hr)
$P_x$	water equivalent of precipitation (mm)
$P_{xmm}$	rainfall intensity (mm/hr)
$Q_a$	incoming longwave radiation ( $mm_e$ )
$Q_e$	latent heat transfer ( $mm_e$ )
$Q_g$	heat transfer across the snow-soil interface ( $mm_e$ )
$Q_h$	sensible heat transfer ( $mm_e$ )
$Q_i$	incoming shortwave radiation ( $mm_e$ )
$Q_m$	heat transfer by mass changes ( $mm_e$ )
$Q_n$	net radiation transfer ( $mm_e$ )
$Q_{lw}$	net longwave radiation ( $W/m^2$ -hr)
$Q_{sw}$	net shortwave radiation ( $W/m^2$ -hr)
$T$	snow surface temperature ( $^{\circ}K$ )
$T_a$	the temperature of the air at $z_a$ ( $^{\circ}C$ )
$T_b$	base temperature ( $^{\circ}C$ )
$T_c$	total catchment area ( $m^2$ )
$T_i$	index air temperature ( $^{\circ}C$ )
$T_m$	mean air temperature ( $^{\circ}C$ )
$T_o$	snow surface temperature ( $^{\circ}C$ )
$T_p$	air temperature minus 32 ( $^{\circ}F$ )
$T_r$	air temperature ( $^{\circ}F$ )
$T_s$	snow surface temperature ( $^{\circ}F$ )
$T_w$	wet bulb temperature ( $^{\circ}C$ )
$T_{ba}$	base temperature ( $^{\circ}F$ )
$T_{mp}$	period temperature at median elevation of snowpack ( $^{\circ}F$ )
$T_{sp}$	snowpack temperature ( $^{\circ}F$ )
$T_{air}$	air temperature ( $^{\circ}F$ )

$T'_a$	difference between the air temperature measured at 10 feet and the snow surface temperature ( $^{\circ}\text{F}$ )
$T'_d$	difference between the dewpoint temperature measured at 10 feet and the snow surface temperature ( $^{\circ}\text{F}$ )
$U_b$	wind speed (mi/hr)
$V$	water vapor transfer (mm)
$V_g$	vapor transfer between snow and soil (mm)
$c$	specific heat ( $\text{cal gm}^{-1} \text{ }^{\circ}\text{C}^{-1}$ )
$d$	snow depth (m)
$e_a$	vapor pressure of the air at $z_a$ (mb)
$e_o$	vapor pressure at the snow surface (mb)
$e_s$	saturation vapor pressure at snow surface temperature
$e_{\text{sat}}$	saturation vapor pressure (mb)
$f(u_a)$	function of the wind speed, $u_a$ , at $z_a$ ( $\text{mm mb}^{-1}$ )
$k_e$	coefficient for calculation of latent heat transfer ( $\text{in/hr ft}^{1/3} \text{ mi/hr mb}^{-1}$ )
$k_r$	basin shortwave radiation melt factor
$k_w$	convection-condensation melt factor
$n$	day number beginning with March 21
$t$	time
$t_1$	total type 1 subcatchment area ( $\text{m}^2$ )
$t_2$	total type 2 subcatchment area ( $\text{m}^2$ )
$t_3$	total type 3 subcatchment area ( $\text{m}^2$ )
$t_5$	total type 5 subcatchment area ( $\text{m}^2$ )
$t_6$	total type 6 subcatchment area ( $\text{m}^2$ )
$t_8$	total area of pervious area of another catchment where redistributed snow is destined ( $\text{m}^2$ )
$u_a$	wind speed at $z_a$ ( $\text{km hr}^{-1}$ )
$v$	wind speed (miles/interval)

$v_{50}$	wind speed at 50 feet above the snow (miles/hr)
$w$	weight of snow core (kg)
$z_a$	height above the snow surface (m)
$z_b$	height above surface for wind speed measurements (ft)
$z_t$	height above surface for air temperature measurements (ft)
BaseDepth	depth of snow above which redistribution occurs (mm)
BaseDepth1	depth of snow above which redistribution occurs for type 1 subcatchment (mm)
BaseDepth2	depth of snow above which redistribution occurs for type 2 subcatchment (mm)
BaseDepth3	depth of snow above which redistribution occurs for type 3 subcatchment (mm)
Imperv	total impervious area ( $m^2$ )
Perv	total pervious area ( $m^2$ )
NRunoff	net runoff (mm/hr)
SnowD	depth of snow above which there is always 100% snow cover (mm)
Swe	depth of snow in water equivalent present in subcatchment any time (mm)

### **Greek Alphabet**

$\Delta t$	computational time interval (sec)
$\Delta P$	period length (hours)
$\Delta Q$	change in the heat storage of the snow cover ( $mm_e$ )
$\Delta T_{60}$	number of hours per interval
$\Delta WE_t$	change in total water equivalent of the snow cover (mm)
$\varepsilon$	emissivity in the longwave portion
$\sigma$	Stefan-Boltzman constant ( $1.7 \times 10^{-13} \text{ mm}_e \text{ } ^\circ\text{K}^{-4} \text{ sec}^{-1}$ )

$\gamma$	psychometric constant (mb °C <sup>-1</sup> )
$\rho$	snow density (kg m <sup>-3</sup> )
$\alpha$	cross sectional area of snow core (m <sup>2</sup> )
$\pi$	pi

### **Abbreviations**

ASC	fraction of snow covered area
DHI	Danish Hydraulic Institute
EPA	Environmental Protection Agency
FWC	free water holding capacity of snowpack (mm)
HSPF	Hydrologic Simulation Program – Fortran
NWSRFS	National Weather Service River Forecasting System
RDII	Rainfall Dependent Inflow and Infiltration
SSARR	Streamflow Synthesis and Reservoir Regulation Model
SWE	snow water equivalent (mm)
SWMM	Storm Water Management Model
USM	Urban Snow Model

## CHAPTER ONE

### INTRODUCTION

#### 1.1 Introduction and Research Background

Studies of urban hydrology have concentrated mainly on the response of urban catchments to rainfall events. Generally, high intensity rainfalls are assumed to be the major flood-generating events in urban areas (Buttle and Xu, 1988). However, in the northern hemisphere, flooding is observed every year during snowmelt in urban environments in Scandinavia, Canada and northern USA (Bengtsson & Westerström, 1992). Semádeni-Davies and Bengtsson (1998) reported that northern Sweden experiences its most severe urban flooding during spring melt. Similarly, Thorolfsson and Brandt (1996) reported that snowmelt and rain on saturated or frozen ground represents the most adverse runoff conditions in many urban areas in Norway.

Melt intensities of snow are much lower than rainfall intensities but it has been assumed that the processes and factors governing both urban and rural snow hydrology are the same. Thus, snow receives little interest in urban hydrological research. However, there are differences between the factors that control snowmelt and runoff generation in the two environments (Bengtsson & Westerström, 1992).

In urban flood analysis, the contribution of snowmelt and frozen ground to the generation of floods is not well understood. Frozen ground can lead to reduced soil infiltration and thus increases runoff contribution areas and extends concentration time. Floods can result from adverse combinations of precipitation and basin conditions such as antecedent

wetness, water stored in the snow cover, and frozen ground during the winter. In partially developed urban areas with a low degree of imperviousness, basin conditions are significant as the annual flood may result from a combined snowmelt-rainfall event or runoff from frozen ground, even though precipitation may not be particularly intense. A flooding situation can be further aggravated by high levels of receiving waters or reduced outfall drainage capacity. In these cases, it may be necessary to consider seasonal design events in the urban flood analysis.

In a case study of the Town of Milton in southern Ontario, it was found that the annual peak flow based on both existing land use and the simulated peak flow based on controlled future land use is typically the result of spring freshet (Farrell, et. al, 2001). This indicates that snow accumulation and melt is critical in the consideration of designing stormwater management systems or facilities.

In northern Scandinavia and other cold regions, waste and stormwater systems have been constructed according to standards set for rainfall dominated climates. This results in urban drainage systems that are often unable to cope with the high volumes of melt water, which can be sustained for several weeks (Matheussen and Thorolfsson, 1999; Semádeni-Davies, 2000). Thus, the study of snowmelt runoff in urban areas is essential for accurate modelling to design reliable drainage systems. It is also the first step in improving flood forecasting for urbanized catchments that experience significant snowmelt runoff. It may also assist efforts to study winter pollutant transport (Buttle and Xu, 1988).

## **1.2 Thesis Objectives**

The general objectives of this thesis are to:

- a) Conduct a comprehensive literature review in order to summarize and compare current models for urban snowmelt.
- b) Develop a field study to investigate urban snowmelt and accumulation.
- c) Develop a model for urban snowmelt

### **1.3 Thesis Layout**

This thesis consists of seven chapters, and the general contents of each chapter are outlined here. Chapter two will fulfill objective (a). It presents the processes governing urban snow hydrology, and details several snowmelt models currently in use. Chapter three will detail the thesis objectives, discusses any gaps in knowledge found through the literature review, and present the methodology of this study. Chapter four will fulfill objective (b), detailing the various data collection methods found in literature and the methods used in this study. Chapter five will present the results and analysis of the field study. Chapter six will fulfill objective (c), developing an urban snowmelt model. Chapter seven ends this thesis with conclusions and recommendations towards the improvement of the modelling of urban snow.

## CHAPTER TWO

### LITERATURE REVIEW

#### 2.1 Processes Governing Urban Snow

##### 2.1.1 Snowmelt Processes

Snowmelt rate is determined by the net energy flux to the snowpack. Under most conditions, and especially during melt periods, most of the energy exchange occurs at the snow surface (Anderson, 1973).

##### **Snow Cover Energy Balance Equation (Anderson, 1996):**

The components of the energy balance for a snowpack are illustrated in Figure 2.1. The energy balance equation is expressed as follows:

$$\Delta Q = Q_n + Q_e + Q_h + Q_g + Q_m \quad (1)$$

where  $\Delta Q$  is the change in the heat storage of the snow cover, which is comprised of the energy used to melt the ice portion of the snow cover, freeze liquid water in the snow, and change the temperature of the snow;  $Q_n$  is the net radiation transfer;  $Q_e$  is the latent heat transfer (related to water vapor);  $Q_h$  is the sensible heat transfer (related to heat content of air);  $Q_g$  is the heat transfer across the snow-soil interface; and  $Q_m$  is the heat

transfer by mass changes (advected heat). Note that the unit expressing energy transfer terms is  $\text{mm}_e$  (a mm of energy per unit area defined as the energy required to melt 1 mm of ice, at  $0^\circ\text{C}$ )

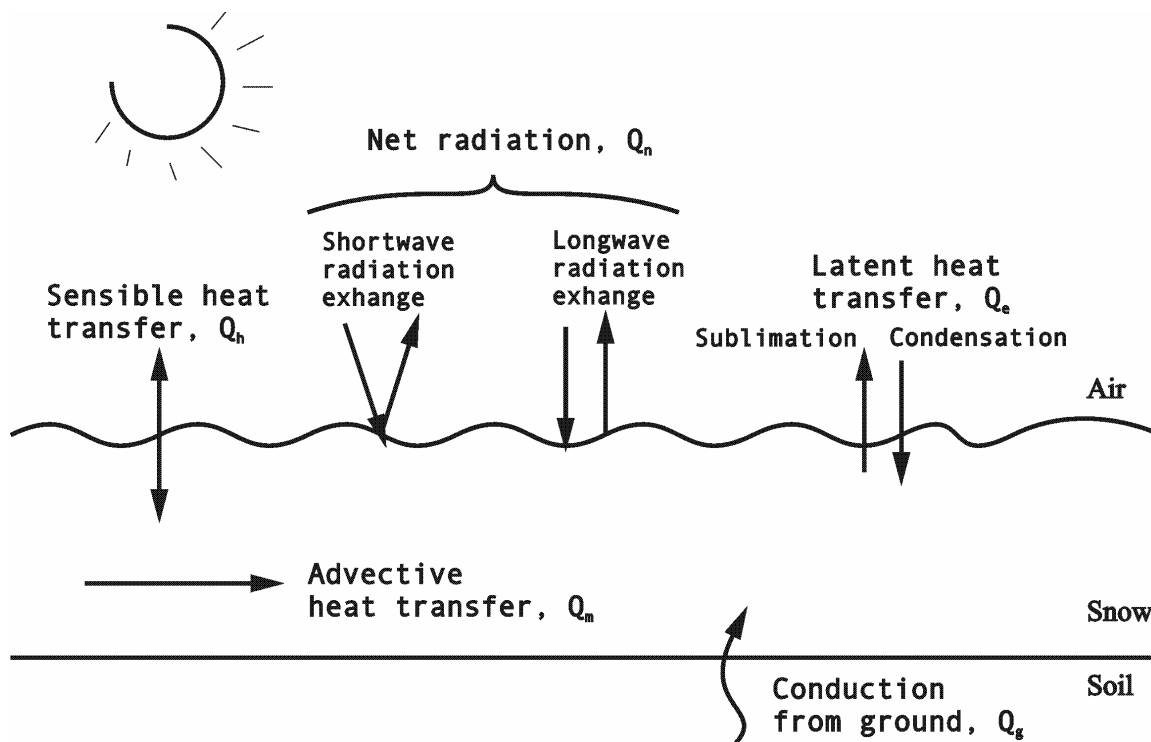


Figure 2.1: Components of the energy budget for a snowpack

**(a) Net Radiation Transfer**

The net radiation transfer can be expressed by the following:

$$Q_n = Q_i * (1 - A) + Q_a - \Delta t * (E_t) \quad (2)$$

where  $Q_n$  is the net radiation transfer for a snow cover;  $Q_i$  is the incoming shortwave radiation ( $\text{mm}_e$ );  $A$  is the snow albedo;  $Q_a$  is the incoming longwave radiation ( $\text{mm}_e$ );  $\Delta t$  is the computational time interval; and  $E_t$  is the total emitted longwave radiation energy given by Stefan's Law ( $\text{mm}_e \text{ sec}^{-1}$ ).

Stefan's Law:

$$E_t = \varepsilon * \sigma * T^4 \quad (3)$$

where  $E_t$  is the total energy emitted ( $\text{mm}_e \text{ sec}^{-1}$ );  $\varepsilon$  is the emissivity in the longwave portion of the energy spectrum;  $\sigma$  is the Stefan-Boltzman constant ( $1.7 \times 10^{-13} \text{ mm}_e \text{ }^\circ\text{K}^{-4} \text{ sec}^{-1}$ ); and  $T$  is the surface temperature ( $^\circ\text{K}$ ).

Snow has been found to be a nearly perfect blackbody with respect to the longwave radiation, thus emissivity,  $\varepsilon = 1.0$ . Substituting Equation 3 into Equation 2 gives the expression for net radiation transfer:

$$Q_n = Q_i * (1 - A) + Q_a - \Delta t * 1.0 * \sigma * (T_o + 273)^4 \quad (4)$$

where  $T_o$  is the snow surface temperature ( $^\circ\text{C}$ ).

### **(b) Latent and Sensible Heat Transfer**

Both latent and sensible heat transfer are turbulent transfer processes. Latent heat transfer involves the transfer of water vapor between the air and the snow surface. Latent heat is

either energy lost from the snowpack due to evaporation and sublimation or energy gained from condensation.

Latent heat transfer can be expressed as:

$$Q_e = L_s * V \quad (5)$$

where  $Q_e$  is the latent heat transfer;  $L_s$  is the latent heat of vaporization ( $L_s = 677 \text{ cal gm}^{-1}$  or  $8.5 \text{ mm}_e \text{ mm}^{-1}$ ); and  $V$  is the water vapor transfer (mm). For every unit of water vapor condensed, the release of the latent heat of vaporization ( $677 \text{ cal gm}^{-1}$ ) from the condensate will melt 7.5 times the amount of snow. Thus, to represent the condensate and its accompanying melt,  $L_s$  has the value of 8.5 that is,  $(1+7.5) \text{ mm}_e \text{ mm}^{-1}$ .

The rate at which water vapor is transferred depends on turbulence of air, which is related to windspeed. Thus, water vapor transfer can be expressed in an equation attributed to Dalton:

$$V = f(u_a) * (e_a - e_o) \quad (6)$$

where  $V$  is the water vapor transfer (mm);  $f(u_a)$  is the function of the wind speed,  $u_a$  ( $\text{km hr}^{-1}$ ), at a height,  $z_a$  (m), above the snow surface ( $\text{mm mb}^{-1}$ );  $e_a$  is the vapor pressure of the air at  $z_a$  (mb); and  $e_o$  is the vapor pressure at the snow surface (mb), assumed equal to the saturation vapor pressure at the snow surface temperature.

Substituting Equation 6 into Equation 5 gives the expression for latent heat transfer:

$$Q_e = 8.5 * f(u_a) * (e_a - e_o) \quad (7)$$

Sensible heat transfer is related to the heat content of the air. Similar to water vapor transfer, the rate of sensible heat transfer depends on the turbulence of the air. Since the mechanisms of transport are analogous, it is assumed that the turbulence transfer coefficients for heat and water vapor are equal. Thus, the sensible heat transfer is calculated using the Bowen's ratio, expressed as:

$$\frac{Q_h}{Q_e} = \gamma * \frac{T_a - T_o}{e_a - e_o} \quad (8)$$

where  $Q_h$  is the sensible heat transfer ( $\text{mm}_e$ );  $\gamma$  is the psychometric constant ( $\text{mb } ^\circ\text{C}^{-1}$ ) ( $\gamma = 0.00057 P_a$ , where  $P_a$  (mb) is the atmospheric pressure);  $T_o$  is the snow surface temperature ( $^\circ\text{C}$ ); and  $T_a$  is the temperature of the air  $z_a$  ( $^\circ\text{C}$ ).

Substituting Equation 7 into Equation 8, the resulting expression for sensible heat transfer is:

$$Q_h = 8.5 * \gamma * f(u_a) * (T_a - T_o) \quad (9)$$

### (c) Heat Transfer by Mass Changes

The mass balance of a snow cover can be expressed as:

$$\Delta WE_t = P_x - O_s + V - V_g \quad (10)$$

where  $\Delta WE_t$  is the change in total water equivalent of the snow cover (mm);  $P_x$  is the water equivalent of precipitation (mm);  $O_s$  is the liquid-water outflow from the bottom of

the snow cover (mm);  $V$  is the vapor transfer between snow and air; and  $V_g$  is the vapor transfer between snow and soil (mm).

If the temperature of the snow cover is assumed to be 0 °C, and the heat content of the transferred vapor is assumed to be negligible, then only the heat transferred by precipitation need to be considered. The wet-bulb temperature is a good approximation of temperature of precipitation because of the analogy between falling precipitation and a ventilated wet-bulb thermometer. Thus, the advected heat transfer due to mass changes is:

$$Q_m = \frac{c}{80} * P_x * T_w \quad (11)$$

where  $T_w$  is the wet bulb temperature (°C); and  $c$  is the specific heat (cal gm<sup>-1</sup> °C<sup>-1</sup>) (for snowfall,  $c$  equals the specific heat of ice, 0.5; for rainfall,  $c$  equals the specific heat of water, 1.0). Equation 11 is based on the relation between heat required to melt ice (80 calories per gram of ice) and the amount of heat given up by a gram of water when its temperature is decreased by one degree.

Substituting Equations 4, 7, 9, and 11 into Equation 1, the energy balance equation of a snow cover can be written as:

$$\begin{aligned} \Delta Q = & Q_i * (1 - A) + Q_a - \Delta t * 1.0 * \sigma * (T_o + 273)^4 + \\ & 8.5 * f(u_a) * [(e_a - e_o) + \gamma(T_a - T_o)] + \\ & \frac{c}{80} * P_x * T_w + Q_g \end{aligned} \quad (12)$$

In the case of a melting snowpack ( $T_o = 0$  °C), the heat transfer across the snow-soil interface,  $Q_g$  is negligible compared to energy exchange at the snow surface.

### **2.1.2 Snow Metamorphosis**

Freshly fallen snow exists in crystalline state, with relatively low density (snow specific gravity). As time passes, metamorphosis of the snow occurs, where individual snow crystals become bound together and into larger, coarser ice crystals, and density of the snow increases. This process is commonly known as “ripening” of the snowpack. In the early stages of the metamorphosis process, snow temperature may vary throughout the depth of the snowpack. However, as the snowpack ripens, a more isothermal pattern develops and when the snowpack is ripe, it is completely isothermal and near 0 °C. A snowpack ripe for melt also contains a small amount of free water. Thus, a snowpack is primed for runoff when it becomes isothermal at 0 °C and has reached its liquid water holding capacity (USACE, 1998).

Following several snowfall events, as each new layer of snow is deposited, the upper surface of the snowpack is weathered by radiation and wind. This causes the snowpack to become stratified, with distinct layers of ice layers or planes that separate individual snowfall deposits (USACE, 1998). Meltwater from snowpack mostly percolates vertically downward to the bottom of the pack.

### **2.1.3 Component of Energy Exchange Dominating Melt**

In urban areas, melt seems to be dominated by net radiation fluxes (Westerström, 1981 and Sundin et. al, 1999). Bengtsson and Westerström (1992) showed sensible heat flux to be minor when snowmelt took place and a higher daily melt in the city occurred compared to the rural environment, which was largely due to increased absorbed radiative energy in the snow. In a study plot in Lulea, Sweden, Semadeni-Davies and Bengtsson (1998) found that the contribution of turbulent exchange,  $Q_e$  and  $Q_h$  to the

total amount of energy available for melt was low in comparison to the net radiation. The temperature gradient at the snow-soil interface is usually small, so the heat exchange at the snow-soil interface,  $Q_g$  is negligible compared to the other terms (Marks and Dozier, 1992).

#### **2.1.4 Factors Influencing Melt in Urban Areas**

Snowpack energy fluxes are greatly influenced by the urban environment. Spatial variations in energy fluxes exist over the snowpack due to factors such as longwave radiation from buildings, full-sun/shadowed effect, and snow albedo variability (Bengtsson and Westerström, 1992; Semádeni-Davies, 1999).

##### **(a) Radiation Balance**

In urban areas, solar radiation may be reduced compared to the rural areas due to higher concentrations of water vapor, carbon dioxide and impurities (Thorolfsson and Sand, 1991).

In the absence of solar radiation, longwave exchanges dominate the radiation balance of snowpacks in open areas. For snow near buildings, the exchange is complicated by longwave radiation emitted from the building walls (Buttle and Xu, 1988). Factors such as cloud cover, snow albedo, wall temperature and wall to site distance influence the radiation balance of the snowpack (Semádeni-Davies and Bengtsson, 1998).

Bengtsson and Westerström (1992) found that two-storey houses influence the net longwave radiation of the snowpack up to 10 m from the buildings. Under clear sky

conditions, longwave radiation input to the snowpack 2 m from a building could increase by  $100 \text{ Wm}^{-2}$  (Bengtsson and Westerström, 1992). For snow surface near buildings, the influence of air temperature and atmospheric emissivity on the increased input of longwave radiation was minor (Bengtsson and Westerström, 1992).

## **(b) Albedo**

Albedo is the reflectivity of a body to shortwave radiation. Snow surface albedo depends on grain size, porosity, and impurities. Snow albedo is a very important factor in the snowmelt process. Snow albedo determines the amount of shortwave radiation adsorbed by the snowpack, which can lead to melting of the snowpack. Melting of the snowpack lowers the snow albedo, which in turn results in higher adsorption of shortwave radiation. This process is known as the snow albedo feedback mechanism. This mechanism can easily increase melt of a snowpack exponentially.

Snow albedo is lower in the city than in the rural areas due to pollution and the fact that much of the snow-covered areas are not left undisturbed. Thus, snow reflects less of the incoming shortwave radiation. The urban snow albedo ranges from values similar to undisturbed rural snow (0.8-0.4) to values less than 0.2 in the inner city (Bengtsson and Westerström, 1992). Snow plowed in piles near roads can be near black with albedo  $<0.3$  (Semádeni-Davies, 2000). Conway et. al (1996) found that a 30% decrease in albedo caused by soot particles resulted in a 50% increase in ablation from alpine snow cover, which carries significant implications for urban snowmelt processes.

Albedo of the urban environment as a whole is lower than the rural environment due to its canyon configurations, and thus causing increased solar energy absorption, air temperature, advection and longwave emittance by buildings (Semádeni-Davies, 2000).

### **2.1.5 Infiltration Capacity of Frozen Soil**

Infiltration into frozen soils at the beginning of the melt season is largely a function of the air-filled soil porosity and is inversely related to the ice-moisture content of the shallow 0-30 cm soil layer (Granger et. al, 1984). Granger et. al. (1984) also showed that the depth of infiltrating meltwater into uncracked soils averaged about 30 cm. The ice-moisture content depends on the moisture content of the soil at the beginning of winter soil freezing. For initial low soil moisture content, frozen soils retain a significant infiltration capacity. However, for high initial soil moisture content, frozen soils exhibit greatly reduced infiltration capacity (Granger et. al, 1984).

Several structurally and hydrologically different types of frost may form when the soil freezes. The type of frost that formed depends primarily on the moisture content of the soil at the onset of freezing. In literature, four types of frost have generally been recognised. They are “concrete frost,” essentially saturated ground that is completely frozen, “granular frost,” with small ice crystals intermixed with soil particles, “honeycomb frost,” which is similar to granular but with a higher degree of connectivity among the ice crystals and a lower porosity, and “stalactite frost” which describe small needle-like ice crystals aligned vertically and extending downward into the soil from a heaved surface (Dingman, 1975).

In his extensive review on frozen ground, Dingman (1975) found that American researchers generally observed that concrete frost is impermeable, while other types of frost, especially granular frost permits infiltration or had little effect on infiltration capacities.

At a study site in Ontario, Canada, Buttle (1989) found infiltration capacities were in excess of  $300 \text{ mmh}^{-1}$  even though ground surface at the study sites were frozen to a depth

of approximately 10 cm. He suggested the presence of honeycomb soil frost, which does not reduce infiltration capacity, unlike concrete frost.

Compared to rural areas, urban soils suffer heavy compaction due to activities such as construction, traffic and modification to the original soil stratification (Buttle and Xu, 1988). The overall effect is a reduction in the soil's infiltration capacity. Bengtsson and Westerström (1992) noted that no surface runoff occurred from a grassed surface plot during early melt, but in the late phase of the melt period, the runoff from the grassed plot almost equalled that from the asphalted plot. Westerström (1990) studied two snowmelt periods in Porsöberget residential area, Sweden and found that infiltration at the beginning of the melt period is great, but decreased substantially towards the end of the melt period. This suggests that infiltration capacity can be greatly reduced over an extended melt period, and that surface which contributes to runoff increases towards the end of the melt period.

#### **2.1.6 Surfaces Contributing to Overland Flow During Snowmelt**

Urban areas consist of both permeable and impermeable surfaces. During spring thaw, impermeable surfaces that contribute to quick overland flow during rainfall events are largely snow-free. Snow from streets, parking lots and pathways are usually plowed and piled along the edges of these areas or are removed to a dumpsite. Thus, roads, driveways, walkways and roofs are incorporated into the runoff contributing area only during rain-on-snow events (Buttle and Xu, 1988). This means that for snowmelt, it is the permeable areas that largely contribute to runoff. In addition, concrete ground frost can develop in permeable urban surfaces, which occurs when wet compacted soils undergo rapid freezing, hence, the soil can be rendered impervious (Semádeni-Davies, 2000). For

rain-on-snow events, this means that the area contributing to runoff increases considerably, and can be greater than for summer storms.

### **2.1.7 Redistribution of Snow in Urban Areas**

A major difference between snow in urban and rural areas is the snow removal practices in urban areas. Snow in urban areas is usually removed from impervious surfaces such as parking lots, roads, and driveways. Most of the snow is piled onto adjacent grassed banks. In highly impervious urban areas, the snow can be trucked to a dumpsite. Undisturbed, fairly uniform snow cover similar to rural snow can usually be found only in city parks and open grassed areas.

## **2.2 Snowmelt Models**

### **2.2.1 Mathematical Method**

The only way to correctly compute the amount of snowmelt is through an energy budget (Anderson, 1968). However, the energy balance equation for computing snowmelt requires good measurements of incoming solar radiation, albedo, incoming longwave radiation, wind speed, vapor pressure of the air, air temperature as well as precipitation. In most watersheds, these data are simply not available. Thus, practical operational procedures for snowmelt predictions generally rely on air temperature as the index of the energy available for melt (Gray and Male, 1981; Watt et. al., 1989; Westerström, 1990). It is a conceptual model whereby the *temperature index* or *degree-day method* replaces the full energy balance. It is physically sound in the absence of shortwave radiation when

much of the energy supplied to the snowpack is atmospheric longwave radiation, such as for heavily forested areas (Semádeni-Davies, 2000).

In its simplest form, the relationship between snowmelt and air temperature can be expressed by:

$$M = M_f(T_i - T_b) \quad (13)$$

where  $M$  is the snowmelt generated ( $\text{mm day}^{-1}$ );  $M_f$  is the melt factor ( $\text{mm } ^\circ\text{C}^{-1} \text{ day}^{-1}$ );  $T_i$  is the index air temperature, commonly maximum or mean temperature ( $^\circ\text{C}$ ); and  $T_b$  is the base temperature, commonly  $0^\circ\text{C}$ .

Snowmelt runoff simulated with the degree-day method assumes both a homogeneous snowpack and a heterogeneous snow coverage. Bengtsson (1984) showed that snowmelt from the heterogeneous urban environment cannot be adequately determined from temperature indices. Urban snow tends to be plowed into piles having a wide range of characteristics depending on location and landuse. Thus, the presence of snow piles can both reduce the maximum volume of melt and extend the melt period if determined using the degree-day method (Semádeni-Davies, 2000). Without modifications, this method is not theoretically suitable for urban snow runoff simulations (Semádeni-Davies, 2000).

### **2.2.2 Computer Models**

Computer-based models for snow accumulation and melt range from simple temperature index models to complex models based on energy balances requiring extensive data. These models are generally presented as components of more comprehensive runoff models. All snowmelt routines have two basic components: (1) the method of snowmelt

generation and (2) the method of handling snow cover accumulation and depletion (Watt, et. al, 1989).

### 2.2.2.1 NWSRFS SNOW-17

The National Weather Service River Forecasting System, NWSRFS is a collection of models that can perform a wide variety of hydrologic and hydraulic functions (NWSHL, 1996). One of the operations available in the NWSRFS is SNOW-17, a snow accumulation and ablation model. It is a conceptual model representing the physical processes of snow accumulation and snowmelt (Anderson, 1996). Air temperature is used as an indicator of the energy exchanges governing the snow-air interface. The model differentiates snowmelt during rain-on-snow periods from melt during non-rain periods to account for differences in magnitudes of the energy exchanges and the seasonal variation in melt rates.

Melt during rain is computed from an energy balance equation that calculates the net radiative, latent, sensible and rainwater heat transfer to calculate the amount of melt. It is assumed that during rain-on-snow periods, melt occurs at the snow surface.  $Q_g$  is negligible compared to energy exchange at the snow surface. Thus, the dominant energy transfers are known if a few reasonable assumptions are made. The assumptions are:

- a. Incoming solar radiation (shortwave) is negligible due to overcast skies
- b. Incoming longwave radiation is equal to blackbody radiation at the ambient air temperature
- c. Relative humidity is very high (assumed 90%)
- d. Snow cover is isothermal and melting;  $T_o = 0^\circ\text{C}$

In this case, the wet-bulb temperature is essentially the same as the air temperature,  $T_w = T_a$ . The vapor pressure is then assumed to be 90% of the saturation vapor pressure at the air temperature,  $e_{sat}$ . The saturation vapor pressure can be estimated using the following expression:

$$e_{sat} = 2.749 * 10^8 * \exp\left(\frac{-4278.6}{T_a + 242.8}\right) \quad (14)$$

where  $e_{sat}$  is the saturation vapor pressure computed from air temperature (mb).

The atmospheric pressure,  $P_a$  is computed from the elevation data using the ‘standard-atmosphere’ altitude-pressure relationship, which can be approximated using the following expression:

$$P_a = 1012.4 - 11.34 * E_\ell + 0.00745 * E_\ell^{2.4} \quad (15)$$

where  $P_a$  is the atmospheric pressure (mb); and  $E_\ell$  is the elevation (hundreds of meters).

The energy balance equation is reformulated to result in a melt equation for rain-on-snow periods (Anderson, 1996). Equation 12 can be rewritten to express snowmelt during a 6-hr rain-on-snow period as:

$$\begin{aligned} M_s = & 3.67 * 10^{-9} * (T_a + 273)^4 - 20.4 + \\ & 8.5 * f(u_a) * [(0.9 * e_{sat} - 6.11) + 0.00057 * P_a * T_a] + \\ & 0.0125 * P_x * T_a \end{aligned} \quad (16)$$

where  $M_s$  is the amount of snowmelt (mm).

Equation 16 is used when the amount of rain exceeds 2.5mm during a 6-hr period.

During non-rain periods, the melt is estimated using a temperature index method:

$$M_s = F_m * (T_m - T_b) \quad (17)$$

where  $M_s$  is the amount of snowmelt (mm);  $F_m$  is the melt factor ( $\text{mm } ^\circ\text{C}^{-1}$ );  $T_m$  is the mean air temperature ( $^\circ\text{C}$ ); and  $T_b$  is the base temperature ( $^\circ\text{C}$ ).

As the snow season progresses, due to an increase in the amount of solar radiation absorbed per degree of the temperature difference,  $T_m - T_b$ , the melt factor results in a seasonal variation. The seasonal variation of the melt factor can be expressed as:

$$F_m = \frac{F_{\max} + F_{\min}}{2} + \sin\left(\frac{n * 2\pi}{366}\right) * \frac{F_{\max} - F_{\min}}{2} \quad (18)$$

where  $F_m$  is the melt factor ( $\text{mm } ^\circ\text{C}^{-1}$ );  $F_{\max}$  is the maximum melt factor, assumed to occur on June 21 ( $\text{mm } ^\circ\text{C}^{-1}$ );  $F_{\min}$  is the minimum melt factor assumed to occur on December 21 ( $\text{mm } ^\circ\text{C}^{-1}$ ); and  $n$  is the day number beginning with March 21. Figure 2.2 shows a plot of the seasonal variation of the melt factor from October to April.

The areal extent of the snow cover is determined by the areal depletion curve, which should be reasonably unique for different areas. The areal depletion curve used in the model is a plot of the areal extent of the snow cover versus a ratio indicating how much of the original snow cover remains. After a new snowfall, the area reverts to 100 percent cover until 25 percent of the new snow ablates. Then, the area returns to the point where it was before the snowfall by a straight line.

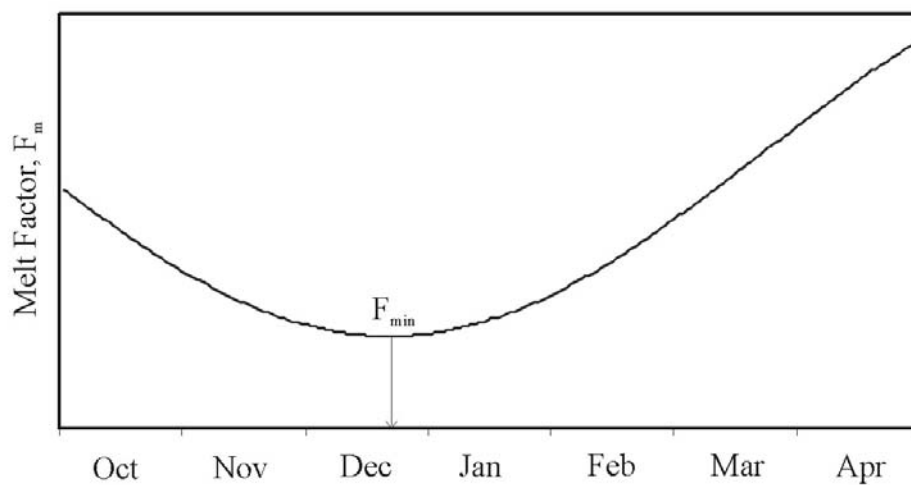


Figure 2.2: Seasonal variation of the melt factor (modified from Anderson, 1996)

In either rain-on-snow or non-rain periods, once the heat deficit of the snowpack has been satisfied, the available melt water is lagged and attenuated to simulate the transmission of water through snow.

#### 2.2.2.2 EPA SWMM

The U.S. Environmental Protection Agency (EPA) Storm Water Management Model, SWMM is a water quantity and quality simulation model developed primarily for urban areas. The model has the capability to be used for purposes that include routine drainage design, screening and planning for future drainage issues, water quality problems, complex hydraulic and flow routing issues, and many other engineering tasks. (Huber, 1995)

Snowmelt is optionally simulated using a degree-day type method during dry weather and energy balance method based on Anderson's U.S. National Weather Service procedures

(1973) during rainfall periods. Different degree-day melt factors can be used on different urban surfaces (pervious and impervious), and a sinusoidal maximum and minimum melt factors is fitted to simulate a seasonal day-to-day temporal variability.

SWMM simulates rain-induced melt based on the energy budget equation, assuming zero solar radiation, incoming longwave radiation equals blackbody radiation at the ambient air temperature, the snow surface temperature is 0 °C, and the dewpoint and rain water temperatures equal the ambient air temperature. Appropriate terms for each heat budget component are combined into one equation to produce the melt rate as detailed in Anderson (1973).

Urban snow removal and the linkage to quality of buildup to the presence of snow may also be simulated by subjecting snow cover to a user-defined areal depletion curve that simulates the diminishing snow covered area (Semádeni-Davies, 2000). However, snow piles are not simulated explicitly; instead, the fitted depletion curve is said to compensate for low melt rates.

### **2.2.2.3 MOUSE RDII**

MOUSE is a software tool developed by the Danish Hydraulic Institute (DHI), which simulate hydrology, hydraulics, water quality and sediment transport in urban drainage and sewer systems (DHI, 2000). One of the module available in MOUSE is the MOUSE Rainfall Dependent Inflow and Infiltration Module (RDII). MOUSE RDII is a hydrological model for continuous simulation of the land phase of the hydrologic cycle. It is a deterministic, conceptual, lumped drainage model, which calculates the precipitation dependent flow component.

MOUSE RDII consists of models to describe two types of components of flow hydrographs, the fast response component (FRC) and the slow response component (SRC). The FRC comprises of the rain induced inflow and fast infiltration, while the SRC comprises only the slow infiltration component. The FRC comes from impervious surfaces whereas the SRC originates from pervious areas and is highly dependent on antecedent conditions.

Snowmelt is applied in the surface runoff computations and is determined using the temperature index method. When temperature is above 0 °C, a degree-day coefficient is used to determine the velocity of emptying the contents in the snow storage to the surface storage. The coefficient can be estimated from analysis of the relation between temperature, water content in the snow storage and measured discharge.

The snowmelt routine was tested against drainage from a small (13ha) suburb in Lulea for three snowmelt seasons by Semádeni-Davies (2000). Many peaks were not captured, especially towards the end of the thaw period. Stormwater peaks were underestimated, and baseflow was overestimated (Semádeni-Davies, 2000).

#### **2.2.2.4 HSPF**

The Hydrologic Simulation Program – Fortran, HSPF is a mathematical model to simulate hydrologic and water quality processes in natural and man-made water systems. It has 3 application modules: PERLND, which simulates runoff and water quality constituents from pervious land areas in the watershed; IMPLND, which simulates impervious land area runoff and water quality; and RCHRES, which simulates movement of runoff water and its associated water quality constituents in stream channels and mixed reservoirs (Donigian et.al, 1995).

PERLND features a SNOW component to simulate snow accumulation and melt. Snowmelt is computed using a detailed energy budget method. Air temperature is used to determine whether precipitation is rain or snow. Energy exchanges that influence melt of a snowpack, net radiation transfer, convective heat transfer, latent heat of condensation, heat transfer from rain, and ground-induced melt are simulated. A combination of physical and empirical formulations are used to model processes such as fluxes and variables of snowfall accumulation, snowpack albedo, snowpack compaction, pack evaporation, atmospheric heat exchanges, snow, ice and water occurrence in the pack and melt from ground heat (Donigian et.al, 1995).

The equations used to simulate the energy exchanges that influence snowmelt are based on work by the U.S. Army Corps of Engineers (1956), Anderson and Crawford (1964) and Anderson (1968). The following details the expressions to compute heat transfer processes that influence snowmelt (Bicknell et. Al, 1997):

**(a) Net radiation heat**

Heat supplied by radiation is determined by:

$$H_r = \frac{(H_{sw} + H_{lw})}{203.2} \quad (19)$$

where  $H_r$  is the net radiation heat flux to the snowpack (inches of water equivalent/interval);  $H_{sw}$  is the net solar or shortwave radiation (langley/interval);  $H_{lw}$  is the net terrestrial or longwave radiation (langley/interval); and the constant 203.2 is the number of langley required to produce one inch of melt from snow at 32 °F.

Solar radiation is modified by the albedo and the effect of shading. The albedo or reflectivity of the snowpack is a function of the dullness of the snowpack and of the season. The equation for calculating albedo for the 6 summer months is:

$$A = 0.80 - 0.10 * (D / 24.0)^{0.5} \quad (20)$$

where A is the albedo; and D is the index to the dullness of the snowpack.

The corresponding equation for the winter months is:

$$A = 0.85 - 0.07 * (D / 24.0)^{0.5} \quad (21)$$

A is allowed a minimum value of 0.45 for summer and 0.60 for winter. Once the albedo of the pack is found then the net solar radiation ( $H_{sw}$ ) is modified according to the equation:

$$H_{sw} = I_{sw}(1 - A) * (1 - F_{ls}) \quad (22)$$

where  $I_{sw}$  is the incoming solar radiation (langleys/interval); and  $F_{ls}$  is the parameter indicating the fraction of the land segment which is shaded.

Unlike shortwave radiation, which is more commonly measured, incoming longwave radiation is estimated from theoretical consideration of the emitting properties of the snowpack and its environment. The following equations are based on Stefan's law of black body radiation. They vary only by the constants, which depend on air temperature. For air temperatures above freezing:

$$I_{lw} = F_{ls} * 0.26 * T_p + [(1 - F_{ls}) * (0.2 * T_p - 6.6)] \quad (23)$$

And for air temperatures at freezing and below:

$$I_{lw} = F_{ls} * 0.2 * T_p + [(1 - F_{ls}) * (0.17 * T_p - 6.6)] \quad (24)$$

where  $I_{lw}$  is the incoming longwave radiation (langleys/interval);  $T_p$  is the air temperature minus 32 ( $^{\circ}$ F); and 6.6 is the average back radiation lost from the snowpack in open areas (langleys/hr)

Since the constants in these equations were originally based on hourly time steps, both calculated values are multiplied by  $\Delta T_{60}$ , the number of hours per interval, so that they correspond to the simulation interval. In addition,  $I_{lw}$  is multiplied by the fraction of clear sky ( $F_{cs}$ ) when it is negative, to account for back radiation from clouds.

### **(b) Latent heat transfer by condensation**

The heat produced by condensation of moist air moving over the snowpack is calculated by an empirical relationship:

$$H_e = 8.59 * (e_a - 6.11) * C_m * 0.00026 * v \quad (25)$$

where  $H_e$  is the condensation heat flux to the snowpack (inches of water equivalent/interval);  $e_a$  is the vapor pressure of the air at the current air temperature (mb); 6.11 is the saturation vapor pressure at 32  $^{\circ}$ F, assumed to be the vapor pressure of the

snow surface;  $C_m$  is the parameter used to correct melt values to field conditions; and  $v$  is the wind speed (miles/interval). Latent heat from evaporation are considered less significant and thus, not simulated.

**(c) Sensible heat transfer**

Heat supplied by turbulent exchange with the atmosphere can occur only when air temperatures are greater than freezing. This convection of heat is calculated by the empirical expression:

$$H_s = (T_{\text{air}} - 32) * \left( 1.0 - 0.3 * \frac{E_x}{10000} \right) * C_m * 0.00026 * v \quad (26)$$

where  $H_s$  is the convective heat flux to the snowpack (inches of water equivalent/interval);  $T_{\text{air}}$  is the air temperature ( $^{\circ}\text{F}$ ); and  $E_x$  is the mean elevation of the land segment above sea level (ft).

In the simulation,  $H_s$  can only be positive or zero, that is, only incoming.

**(d) Heat from rain**

Heat transfer from rain water to the snowpack is calculated using a physically based equation:

$$H_p = \frac{P_r(T_{\text{air}} - 32)}{144} \quad (27)$$

where  $H_p$  is the heat transfer from rain (inches of water equivalent/interval);  $P_r$  is the rainfall (in.); 144 is the factor to convert to equivalent depth of melt; and 32 is the freezing point ( $^{\circ}\text{F}$ ).

**(e) Heat from the underlying ground**

The potential rate of ground melt is calculated hourly as a function of snowpack temperature ( $T_{sp}$ ) and a lumped parameter ( $M_{gm}$ ).  $M_{gm}$  is the maximum rate of melt in water equivalent caused by heat from the ground at a snowpack temperature of  $32^{\circ}\text{F}$ .  $M_{gm}$  would depend upon the thermal conductivity of the soil and the normal depth of soil freezing. The potential ground melt is reduced below  $M_{gm}$  by 3 percent for each degree that  $T_{sp}$  is below  $32^{\circ}\text{F}$  to a minimum of 19 percent of  $M_{gm}$  at  $5^{\circ}\text{F}$  or lower. As long as a snowpack is present, ground melt occurs at this potential rate.

The areal extent of the snow cover is determined by a snow cover depletion curve that relates snow covered fraction of the area to ratio of water equivalents.

**2.2.2.5 SSARR**

The Streamflow Synthesis and Reservoir Regulation Model (SSARR) was initially developed by the U.S. Corps of Engineers to enable simulation of a river system from rain/snowmelt runoff to regulation of runoff through a reservoir system (Speers, 1995). Modelling of the runoff process is constructed in the watershed module of the SSARR program. SSARR offers two basic methods of computing snowmelt, the temperature index method and the energy budget method.

The temperature index method relies upon a melt rate factor. The expression for calculating snowmelt runoff using the temperature index method is as follows:

$$M = (T_{mp} - T_{ba}) * M_r * \frac{\Delta P}{24} \quad (28)$$

where  $M$  is the snowmelt (mm);  $T_{mp}$  is the period temperature at the median elevation of the melting snowpack ( $^{\circ}\text{F}$ );  $T_{ba}$  is the base temperature ( $^{\circ}\text{F}$ );  $M_r$  is the melt rate, specified by the user or given as a function of accumulated runoff (in. of water per degree day); and  $\Delta P$  is the period length (hours).

The energy budget method uses a generalized equation for snowmelt applicable only for a partly forested area based on the Cooperative Snow Investigations research conducted by the Corps of Engineers.

$$M_d = k_r(1 - F)(0.004I_i)(1 - A) + k_w(0.0084v_{50})(0.22T'_a + 0.78T'_d) + F(0.029T'_a) \quad (29)$$

where  $M_d$  is the daily snowmelt (in/day);  $T'_a$  is the difference between the air temperature measured at 10 feet and the snow surface temperature ( $^{\circ}\text{F}$ );  $T'_d$  is the difference between the dewpoint temperature measured at 10 feet and the snow surface temperature ( $^{\circ}\text{F}$ );  $v_{50}$  is the wind velocity at 50 feet above the snow (miles/hr);  $I_i$  is the observed solar radiation on horizontal surface (langley);  $A$  is the average snow surface albedo;  $k_r$  is the basin shortwave radiation melt factor;  $k_w$  is the convection-condensation melt factor; and  $F$  is the average forest canopy cover.

Areal extent of the snow cover is computed by a standard snow cover depletion curve or by elevation bands. An example of the generalized depletion curve as used in the SSARR model is shown in Figure 2.3.

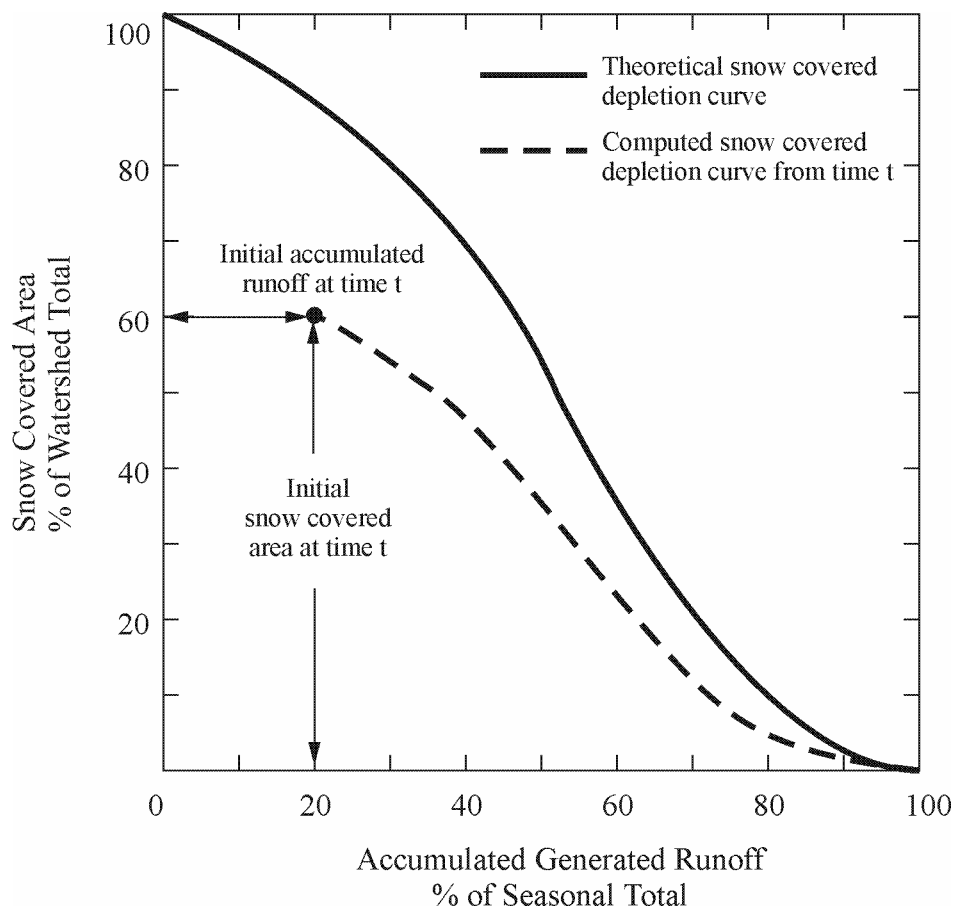


Figure 2.3: Example of snow cover depletion curve (taken from USACE, 1991)

The depletion curve simulates the catchments as an entity and depletes the snow-covered area as a function of seasonal accumulated runoff. A proportionally adjusted curve is used when the observed snow cover and runoff yields a point not on the theoretical curve, as shown in Figure 2.3. The elevation band option keeps an inventory of snow water

equivalent and soil moisture parameters on each elevation band (USACE, 1991). In the elevation bands option, each elevation band is treated as a separate watershed with its own characteristics and initial snow water equivalent. Each band must be either snow free or 100 percent snow covered.

### **2.2.3 Discussion on the Snowmelt Algorithms**

NWSRFS SNOW-17, SWMM, MOUSE RDII and SSARR have a temperature index to simulate melt. This method has been proven to be valuable in rural and alpine areas (WMO, 1986), but transferring the model to urban environment is questionable. The melt factor is fitted daily to observed air temperatures and reflects the average energy and snow conditions. Given the small catchment size and extreme spatial variability of snowpack location, albedo, depth, density, and energy availability, the representativity of the melt rate factor in urban areas is questionable (Semádeni-Davies, 2000).

Snow piles are a unique case in point, whose presence depends on the political and economic climate of the town. They are normally located near roads and pavements and are compacted and icy with low albedo. These factors will influence local melt conditions. Bengtsson (1984, 1986) noted that because degree-day melt routines make melt calculations only once daily, it masks the dynamics of runoff generation over impervious urban surfaces, thus it is unsuitable for urban areas.

Furthermore, the time scales of SWMM and MOUSE RDII have capabilities of minutes, thus daily time steps seem inadequate for snowmelt generation. In their investigation of simulation errors due to insufficient temporal resolution in urban snowmelt models, Matheussen and Thorolfsson (1999) determined that snowmelt induced runoff in urban areas should be measured and modeled with a one-hour time resolution or less.

Similarly, soil routines for continuous equations are not compatible with daily melt values. As overflow conditions in cold regions are associated with snowmelt (spring runoff), an improved temporal resolution could be warranted.

None of the models simulates ground frost. Thorolfsson and Brandt (1996), and Westerström (1984) showed that urban soils can become seasonally impervious, which suggests that a soil frost/thaw routine could be important.

## **CHAPTER THREE**

### **THESIS OBJECTIVES**

#### **3.1 Gaps in Knowledge**

One of the general objectives of this study was to conduct a comprehensive literature review to summarize and compare current urban snowmelt models. That literature review identified several gaps in knowledge and modelling of urban snowmelt. They are discussed below:

##### **(a) Contribution of frozen ground to urban snowmelt modelling**

The role of frozen ground in the generation of floods in urban areas has largely been ignored. In high-density urban areas due to the high degree of imperviousness, the generation of flood is generally controlled by the amount of the precipitation. High intensity precipitation typically occurs in the summer, so winter runoff and factors such as frozen ground have received minimal attention. However, in low-density urban areas, annual floods may result from runoff from frozen ground. The contributing areas to snowmelt runoff will increase substantially when considering frozen ground. In addition, snow from impervious areas is usually plowed and piled onto pervious areas. However, little guidance is available for considering the effects of frozen ground on snowmelt runoff computations in current urban runoff models.

**(b) Densities of urban snow**

In urban areas, snow removal practices alter the natural state of snow. Human activities, vehicle traffic, and snow plowing practices increase the amount of dirt and sand in snow. This results in an increase in the densities of snow in urban areas compared to snow in rural areas. However, few efforts have been made to investigate the densities of an urban snow cover. Gray and Male (1981) showed that initial density of a natural snow cover is usually 100 – 500 kg/m<sup>3</sup>. Sundin et. al. (1999) indicated that urban snow piles can have densities up to 700 kg/m<sup>3</sup>.

**(c) Rate of change of snow properties**

The rate of change of snow properties such as snow albedo and snow density over time is important for continuous modelling. However, a detailed study of the rate of change of snow properties in urban areas cannot be found in the literature.

**(d) Urban snowmelt models time-steps**

The optimum time resolution to use in an urban snowmelt runoff model is important for accurate modelling. However, the temporal scale appropriate for urban snowmelt models has not been discussed extensively in the literature. The study by Matheussen and Thorolfsson (1999) showed that the traditional temperature index model used in urban snowmelt models using daily time steps results in large errors. Their study indicated that urban runoff models applied to snowmelt situations should use a time step of 1-hour or less.

### **(e) Snow energy-balance models for different snow cover types**

Various types of snow cover can be found in urban areas. The most dominant types are snow piles and the natural snow cover on pervious areas. Others include snow on road shoulders, snow on rooftops, and snow near building walls. Energy balance models for each type of snow cover in the urban areas is different due to characteristics of the snow such as initial density values, the initial snow albedo values and the rate of change of the snow properties. In addition, urban elements such as buildings influence the radiation budget of the snowpack. There has been no attempt to apply separate energy models to the different snow cover types to achieve accurate modelling of snowmelt in urban areas.

## **3.2 Detailed Thesis Objectives**

### **(1) To investigate the spatial distribution of urban snow**

The spatial distribution of snow in the urban environment varies greatly compared to snow cover in rural area. Depending on the location of the snow cover, snow in urban areas is subjected to disturbances such as foot traffic, vehicle traffic, and redistribution (plowing). Snow is commonly plowed from streets, sidewalks and parking lots into windrows or piles. The snow is either left on road-shoulders, parking lot edges or removed to designated dumpsites. On the other hand, urban parks or playing fields may well have an undisturbed snow cover. The different snow cover types may have different SWE as well as different snow albedo values. In addition, snow cover near buildings is subject to different radiation intensity due to longwave radiation from building walls compared to undisturbed snow cover in an open area. As a result, melt characteristics of urban snow are markedly different from location to location due to the heterogeneity of

the snowpacks. Snow cover in urban areas cannot be assumed to be distributed evenly as is common in the rural areas. Hence, this thesis will investigate the spatial heterogeneity of urban snowpacks.

**(2) To investigate the temporal distribution of urban snow in terms of SWE, radiation balances, and snow albedo**

The properties of urban snow such as snow density and snow albedo change over time. As a consequence, the radiation balances for urban snow also changes with time. Documenting these changes is important in the modelling of urban snowmelt at a high temporal resolution.

**(3) To investigate frozen ground conditions and the significance of antecedent soil moisture levels**

Frozen ground is a common characteristic of an urban basin in a cold region. The effects of frozen ground on infiltration and hence, runoff is not well understood. Depending on meteorological factors, location, and soil moisture levels, impervious frozen ground may develop by the end of the winter period or the snow cover may act as an insulating layer preventing formation of frost. This is further complicated by the effects of Chinook winds due to the location of the study area. The Chinook is a warm, dry and gusty wind that comes from over the Rocky Mountains that is located to the west of the City of Calgary and can cause rapid temperature changes (Yackel, 1995). Winter Chinook winds are associated with rising temperatures that can reach above 0 °C. The study area is located in the City of Calgary, in southern Alberta and averages 45 winter Chinook days per year

(Yackel, 1995). Thus, mid-winter melt is quite frequent and can affect soil moisture levels and thaw frozen ground.

#### **(4) To develop an urban snow model**

Redistribution of snow cover in urban areas form a major difference between urban and rural snow hydrology. Redistribution of urban snow results in snow properties that are different than rural snow and as a result melt intensities for rural snow can be significantly different for urban snowpacks. Therefore, an urban snow model will be developed to generate runoff from snowmelt in an urban area using the energy balance method to compute snowmelt at an hourly time step. The aim of the model would be to demonstrate how different snow cover types that can be found in urban areas would result in different winter runoff patterns.

### **3.3 Research Outline**

To achieve the objectives beyond the literature review involves developing (a) a field study; (b) using information from the field study to gain insights into urban snow hydrology, and improve urban snowmelt models; and (c) developing and programming an urban snow model. The field study is conducted around the University of Calgary campus (which is representative of a low residential environment) in the period of October 2001 to April 2002 and involves the collection of a number of parameters to resolve issues mentioned above at a high spatial and temporal resolution.

## **CHAPTER FOUR**

### **METHODOLOGY**

#### **4.1 Field Location**

The study area is located at the campus of the University of Calgary, Alberta (51°04'N, 114°08'W). Surficial deposit over the area of the campus consists of lacustrine sediments, which are predominantly silts but also include clay and fine sand (Osborn and Rejewicz, 1998). From the surficial geology map of Calgary by Moran (1986, fig.5), sandy lacustrine sediments occur at the surface under the University of Calgary campus.

#### **4.2 Common Data Gathering Methods (From Literature)**

Field investigations of snow conditions remain an important task in collecting measurements of snow cover information. In a field study, snow surveys are conducted at regular intervals at designated stations throughout the winter to determine snow depth and vertically-integrated density so that the snow water equivalent (SWE) can be calculated for use in predicting spring runoff volumes. A snow course is a permanently marked traverse where snow surveys are conducted. Ground level observations offer the conventional and most direct measurement of snow conditions at single points within limited areas (Woo, 1997).

### **4.2.1 Snowfall Data**

Winter precipitation can be measured by several methods. The simplest method is by using snowboards to capture the amount of snow falling within a specified time period. The thickness of the snow on the board is measured by a graduated ruler. The board is reset on a new surface of the snow before the next snowfall. The depth of snow measured on the board is multiplied by an assumed density of  $100 \text{ kg/m}^3$  to obtain the SWE (Woo, 1997).

Other methods of measuring snow are by using precipitation gauges. Snow gauges measure SWE directly. In Canada, the MSC Nipher shielded snow gauge was designated as the official Canadian instrument for measuring SWE (Gray and Male, 1981). However, Woo (1997) identified several problems regarding snowfall measurements using snow gauges. This raises concerns regarding economic feasibility of setting up snow gauges in a small, easily accessible area compared to a large, remote location.

### **4.2.2 Snow Surveys Measurements**

#### **(1) Depth measurements**

For sampling shallow snow, a metal ruler is plunged vertically into the snow and the depth read directly on the ruler. For deep, hard packed snow, a snow rod can be used. It is recommended that the rod consist of a rounded, solid steel tip, attached to a hollow rod that is extensible. For very steep cornices, an alternative is to select a transect and survey the snow profile by levelling (Woo, 1997).

## (2) Density measurements

The standard method of determining snow density is by gravimetric measurement using a snow sampler to obtain a snow core. The snow sampler consists of a graduated tube with a cutter fixed to its lower end to permit easy penetration of the snow. Snow depth is read off from the sampler. The snow weight can be read directly from a special scale or the snow core can be retrieved to be weighed in the lab (Male and Gray, 1981).

$$\rho = \frac{w}{d\alpha} \quad (30)$$

where  $\rho$  is the snow density;  $w$  is the weight of snow core;  $d$  is the snow depth; and  $\alpha$  is the cross sectional area of the core.

Several types of snow samplers are used in Canada. These includes the Canadian MSC, the Standard Federal, and the Eastern Snow Conference or ESC-30. Generally, the larger the diameter of the cutter, the greater the snow core volume and hence, the more precise the density measurements (Woo, 1997).

## (3) Frequency of measurements

Separation of the sampling of depth and density can speed field surveys and still provide statistically varied areal water equivalents in shallow snowpack area, such as the Prairies, since there is less temporal and spatial sample variability in density than in depth (Male and Gray, 1981). However, this is not necessarily the case in towns (Semadeni-Davies, 1999). Dickinson and Whitley (1972) showed that the standard error of SWE was smallest when equal number of depth and density samples were taken. For a transect of

100 m length, there should be 20-40 depth measurements (Woo, 1997). Since snowpacks in urban areas are heterogeneous, it is recommended to take an equal number of density samples.

### 4.3 Temporal, Spatial Data Collected

In the field study carried out at the campus of the University of Calgary, various quantitative and qualitative data were collected. These include soil moisture, soil temperature, snow albedo, net all-wave and shortwave radiation of snowpacks, snowpacks depth and density, evaporation rate, and sky conditions. The locations of the sites where these measurements were taken are shown in Figure 4.1.

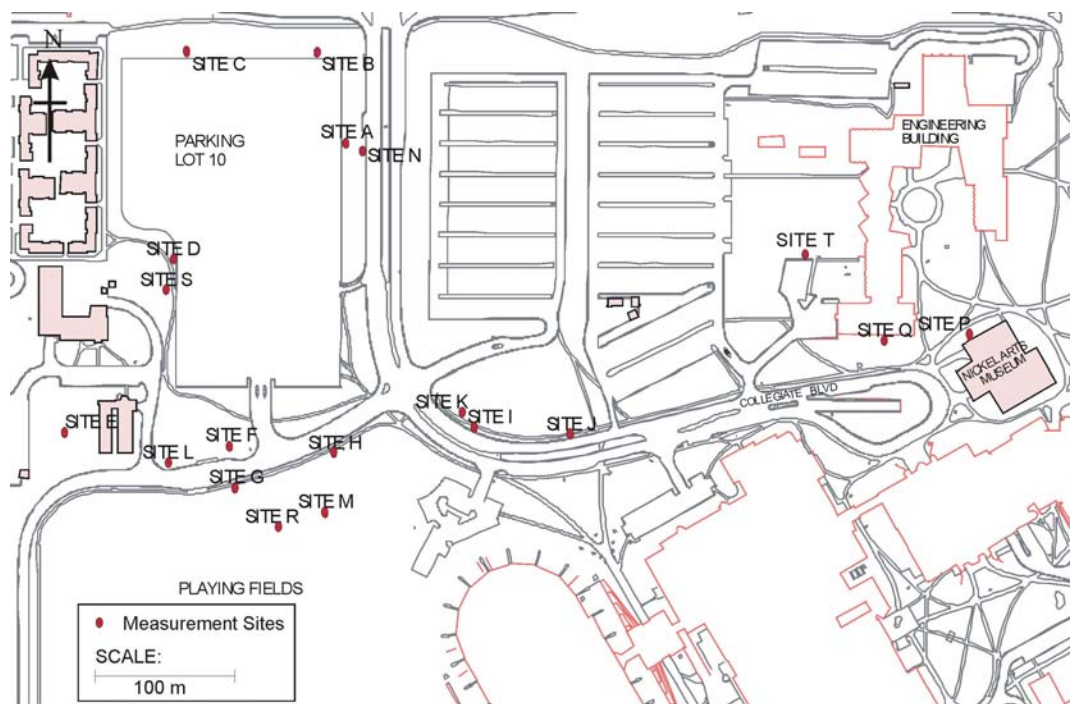


Figure 4.1: Map showing the study area and measurement sites

There are 19 measurement sites in total, and they are labeled alphabetically in Figure 4.1. Not all types of measurements are carried out at every site. The list of the measurement sites, a short description of each sites including its slope's aspect, and the type of measurements taken at each site are shown in Table 4.1.

Table 4.1: Measurement sites description

<b>Site Name</b>	<b>Site Description</b>	<b>Aspect</b>	<b>Types of Measurements</b>
A	Near edge of parking lot	West	<ul style="list-style-type: none"> <li>a. Soil Moisture</li> <li>b. Soil Temperature</li> <li>c. Snow Depth and Density</li> <li>d. Snow Albedo</li> <li>e. Radiation Flux</li> </ul>
B	Near edge of parking lot	South	<ul style="list-style-type: none"> <li>a. Soil Moisture</li> <li>b. Soil Temperature</li> <li>c. Snow Depth and Density</li> <li>d. Snow Albedo</li> <li>e. Radiation Flux</li> </ul>
C	Near edge of parking lot	South	<ul style="list-style-type: none"> <li>a. Soil Moisture</li> <li>b. Snow Depth and Density</li> <li>c. Snow Albedo</li> <li>d. Radiation Flux</li> </ul>
D	Near edge of parking lot	East	<ul style="list-style-type: none"> <li>a. Soil Moisture</li> <li>b. Soil Temperature</li> <li>c. Snow Depth and Density</li> <li>d. Snow Albedo</li> <li>e. Radiation Flux</li> </ul>

Table 4.1: Measurement sites description (continued)

<b>Site Name</b>	<b>Site Description</b>	<b>Aspect</b>	<b>Types of Measurements</b>
E	Open, undisturbed area	South East	<ul style="list-style-type: none"> <li>a. Soil Moisture</li> <li>b. Soil Temperature</li> <li>c. Snow Depth and Density</li> <li>d. Snow Albedo</li> <li>e. Radiation Flux</li> </ul>
F	Open area	South West	<ul style="list-style-type: none"> <li>a. Soil Moisture</li> <li>b. Snow Depth and Density</li> <li>c. Snow Albedo</li> <li>d. Radiation Flux</li> </ul>
G	Sidewalk edge	North	<ul style="list-style-type: none"> <li>a. Soil Moisture</li> <li>b. Soil Temperature</li> <li>c. Snow Depth and Density</li> <li>d. Snow Albedo</li> <li>e. Radiation Flux</li> </ul>
H	Sidewalk edge	North	<ul style="list-style-type: none"> <li>a. Soil Moisture</li> <li>b. Snow Depth and Density</li> <li>c. Snow Albedo</li> <li>d. Radiation Flux</li> </ul>
I	Road shoulder	South West	<ul style="list-style-type: none"> <li>a. Soil Moisture</li> <li>b. Snow Depth and Density</li> <li>c. Snow Albedo</li> <li>d. Radiation Flux</li> </ul>

Table 4.1: Measurement sites description (continued)

<b>Site Name</b>	<b>Site Description</b>	<b>Aspect</b>	<b>Types of Measurements</b>
J	Road shoulder	South East	a. Soil Moisture b. Snow Depth and Density c. Snow Albedo d. Radiation Flux
K	Sidewalk edge	South West	a. Snow Albedo b. Radiation Flux
L	Road shoulder	South West	a. Snow Albedo b. Radiation Flux
M	Playing field	North West	a. Snow Albedo b. Radiation Flux
N	Road shoulder	East	a. Snow Albedo b. Radiation Flux
P	Near North facing building wall	North	a. Snow Albedo b. Radiation Flux
Q	Near South facing building wall	South	a. Snow Albedo b. Radiation Flux
R	Playing field	North East	a. Snow Albedo b. Radiation Flux
S	Sidewalk edge	East	a. Snow Albedo b. Radiation Flux
T	Near edge of parking lot	South	a. Evaporation

### 4.3.1 Soil Moisture

Soil moisture data is collected during periods prior to the onset of winter as well as during the snowmelt season. The soil moisture data determines the antecedent wetness of the soil at the beginning of winter soil freezing, which helps determine the type of frost that might develop and indicates the infiltration capacity of the soil during the melt season. Since during the snowmelt season, it is the permeable areas in particular, that contribute to runoff, soil moisture and infiltration conditions determine the runoff to a large extent, as noted in section 2.1.4.

Soil moisture measurements are carried out using a Delta-T Profile Probe type PR1. It consists of a sealed composite rod, approximately 25 mm diameter, with electronic sensors in the form of pairs of stainless steel rings. The sensors are placed at fixed intervals along the length of the rod. The Profile Probe is used in a special access tube, also supplied by Delta-T. The soil moisture measurements, in % volume are recorded and stored using a Delta-T Moisture Meter type HH2, and later downloaded to a computer.

The access tubes are installed flushed to the soil surface at ten sites around the campus grounds. The Profile Probe measures soil moisture at 6 depths on each site; 10, 20, 30, 40, 60, and 100 cm. The Profile Probe is inserted through a spacer tube before inserting it into the access tube so that the sensors are placed at the correct depths. Refer to Figure 4.2.

Sampling at each site is carried out three times a day, around 9 a.m., 12 p.m., and 3 p.m.. To maximize the sampling at each location, three readings are taken, with the Profile Probe rotated through 120° each time, guided by three small screw heads on the cap of the Profile Probe. This procedure is necessary because there is a gap in the stainless steel rings, which means that the soil moisture detection is not the same all the way around the

probe. An average of the three readings is taken as the sampling value. When not all three of the readings taken at a particular depth registers on the moisture meter, then the sampling value is taken to be the average of two readings or is represented by a single reading alone. When all three readings do not register on the moisture meter, a sampling value of zero is assumed. When a precipitation event coincides with the approximated time of readings, then readings are delayed until the end of the rain or snow period.

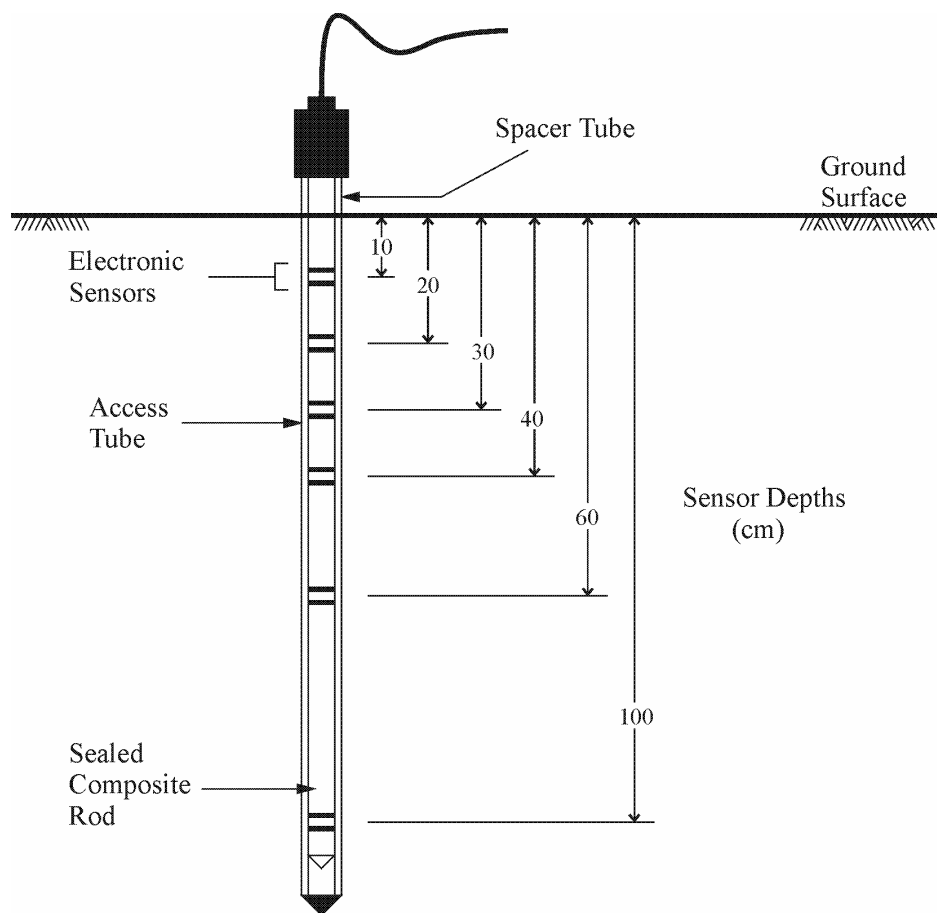


Figure 4.2: Profile of the soil moisture Profile Probe in the ground

During winter, the effects of Chinook winds may well melt snowpacks from previous snowfalls partially or completely. Thus, soil moisture measurements taken in the fall cannot always be accepted as a good indicator of soil moisture level at the time of active snowmelt. Exchanges of moisture at the soil and snow interface may result in moisture level changes in the soil. Therefore, at any time over the winter period, when soil temperature is above 0 °C, soil moisture measurements are also taken.

#### **4.3.2 Soil Temperature**

Soil temperature data is collected throughout the study period to aid investigation of the frozen ground condition as well as map ground temperature fluxes. The ground temperatures were measured using Onset TMCx-HA temperature sensors. The sensors have steel tips, which are 0.2" in diameter and have a measurement range between -40°C to +100°C. Readings from the temperature sensors are recorded continuously using a HOBO H8 Outdoor/Industrial Logger. The logger is housed in a custom-made steel housing case to protect the logger. The housing case is attached to a steel spike embedded into the ground to prevent acts of vandalism. Figure 4.3 shows how the temperature sensors are buried in the ground and also the steel housing for the data logger. A HOBO Shuttle is used to offload and transfer the recorded data to a computer.

Soil temperatures are measured at four depths; 0, 5, 10, and 50 cm in five different sites around the campus ground. They are sites A, B, D, E, and G, as shown in Figure 4.1. The depths into which the sensors are placed are based on depths recorded by the University of Calgary's weather station and by Environment Canada. The University of Calgary records soil temperature at depths of 0, 5, 10, 50, 100, and 300 cm while Environment Canada uses depths of 5, 10, 20, 50, 150, and 300 cm. The depths chosen in this study also considers the effects of Chinook winds. Frozen ground may thaw in mid winter,

especially closer to the surface of the ground. Therefore, three sensors are placed within the first 10 cm layer of soil.

The sites where soil temperature measurements are recorded coincide with the sites where soil moisture measurements are also taken. In all the sites, the location of the temperature sensors is within 1 m radius from the soil moisture access tube. A hand auger is used to drill a hole so that the temperature sensors can be buried at the four different depths.

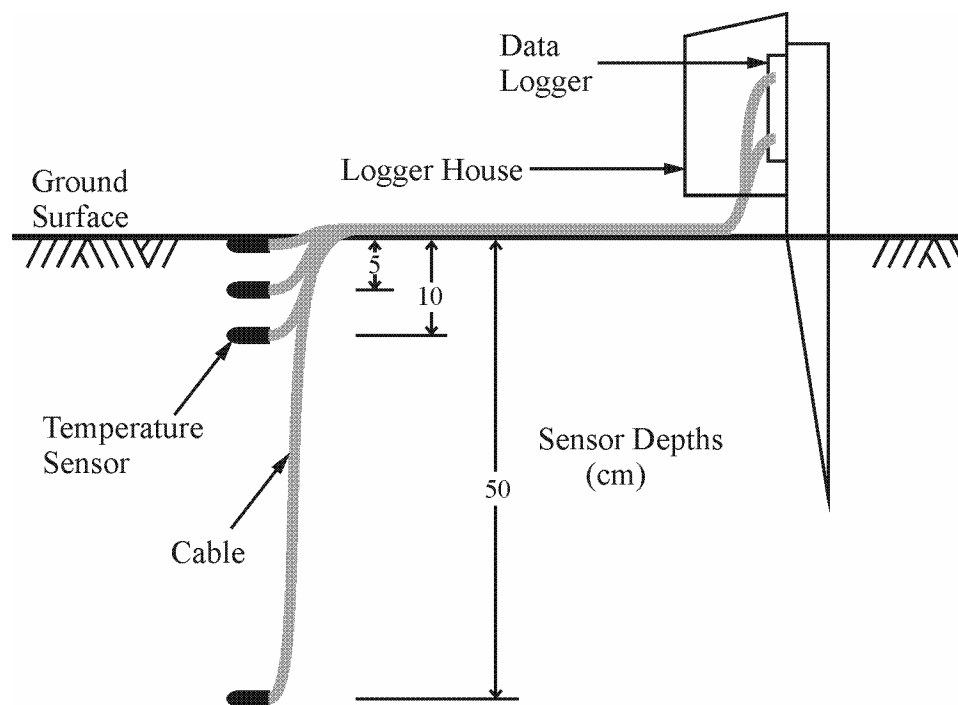


Figure 4.3: Profile of the temperature sensors in the ground

### 4.3.3 Snow Albedo

Snow albedo data is important in the investigation of urban snowpack heterogeneity. The albedo of snow is taken directly as the inverse ratio between observed incoming and outgoing solar radiation. An upward facing Kipp & Zonen pyranometer measures the incoming solar radiation into the snowpack and a downward facing pyranometer measures the outgoing solar radiation. The Kipp & Zonen pyranometer has a spectral range of 0.4 – 1.1  $\mu\text{m}$ . Therefore, the snow albedo measured in this study is based on measured shortwave radiation with wavelengths of 0.4 – 1.1  $\mu\text{m}$ .

The output of the Kipp & Zonen pyranometer, in Volts, is recorded by two digital multimeters, which have resolutions of 0.1 mV. The pyranometer has a sensitivity of 0.1 mV/Wm<sup>-2</sup>. Thus, the radiation intensity, in W/m<sup>2</sup> is calculated by dividing the output of the multimeter by the sensitivity of the pyranometer.

The snow albedo is measured at specific locations such as road shoulders, the sidewalk edges, in open areas, and of snow piles.

### 4.3.4 Net Longwave Radiation

The net longwave radiation of the snowpack is monitored to investigate the influence of factors such as building walls on the radiation balance of the snowpack. A Kipp & Zonen net radiometer measures the net all-wave radiation of the snowpack. The Kipp & Zonen net radiometer has a spectral range of 0.2 – 100  $\mu\text{m}$ . Two Kipp & Zonen pyranometer measure the net shortwave radiation of the snowpack. The net longwave radiation of the snowpack is then obtained by simply subtracting the net shortwave radiation from the net all-wave radiation measurements.

The output of the Kipp & Zonen net radiometer, in Volts, is recorded by a Wavetek<sup>®</sup> Meterman digital multimeter. The digital multimeter has a resolution of 0.01mV. The radiometer has a sensitivity of 0.01 mV/Wm<sup>-2</sup>. Thus, the radiation intensity, in W/m<sup>2</sup> is calculated by dividing the output by the sensitivity of the radiometer.

The radiation measurements are taken at locations such as near a North and a South facing building wall, in open areas, and of snow piles.

For this study area, longwave radiation into the snowpack can be complicated by Chinook events. Chinook conditions are usually accompanied by dense cloud cover, which can increase atmospheric reflectivity, and thus, influence the net longwave radiation into the snowpack.

#### **4.3.5 Snow Depth and Density**

Snow depth and density measurements are collected to calculate the SWE of the snowpacks throughout the study area. A SEAR 500 cm<sup>3</sup> Sampling Tube is used to collect snow samples and it's weighed using a 500 g Dial Spring Scale. The depths of the snowpacks are measured using a SEAR 2 m fiberglass folding ruler. Only the accumulated depth of the snow piles is measured. An equal number of depth and density samples are taken since different snow piles may have different depth and density values.

The snow depth and density measurements are also collected to demonstrate the spatial variability of point SWE in urban areas. For natural snow cover, the initial density of snow ranges from 100 to 500 kg/m<sup>3</sup> (Gray and Male, 1981). For urban snow cleared from

streets and piled up by an excavator, the initial density can reach up to  $700 \text{ kg/m}^3$  (Sundin et. al, 1999).

To study the heterogeneity of the SWE of the urban snow cover, the snow depth and density measurements are taken at every location where the soil moisture or the soil temperature measurements are taken.

#### **4.3.6 Evaporation of Snowpack**

Evaporation of the snow is measured to study latent heat loss from the snowpack. The study area is affected by Chinook conditions that bring warm, windy air during mid winter. Thus, ablation of the snow is accelerated by such conditions. The evaporation of the snowpack is measured using a weight system. Three light rectangular aluminium foil pans are used as evaporation pans. The pans have measurements of 20.3 cm x 12.7 cm x 2.5 cm. One of the pans is filled with icy, large-grained snow from snow piles and placed on top of a snow pile. The other two pans are filled with dry, small-grained, new snow and slightly larger-grained, older snow respectively and placed on ground level. A GBX-230 Gram Precision Balance from Osprey Scientific Inc. is used to measure the weight of the initial contents of the pans early in the morning and the final contents of the pans at the end of the day. The scale is sensitive to its surroundings and is affected by wind turbulence. As the weighing process takes place in the outdoors, the scale is placed in a card box and covered with another box that has a sealed plastic viewing window when the pans are being weighed.

#### **4.3.7 Surface Temperatures**

The surface temperatures of the road, parking lot, north and south facing building walls under different conditions are taken to monitor temperature changes that might contribute to snowmelt. Traffic vehicles supply heat energy to road surfaces, thus contributing to snowmelt on road surfaces (Ishikawa et. al, 1999). Parking lots might have a different surface temperature compared to roads, or sidewalks. The variability of the temperature of different surfaces is investigated using *quickTEMP*, a non-contact thermometer by Linear Laboratories. The thermometer uses infrared technology to obtain instantaneous reading of a surface temperature.

#### **4.3.8 Precipitation Events (to be noted)**

Precipitation events over the course of the study period are observed and recorded. The purpose of such observations is to note substantial snowfall events, so that snow measurements can be carried out. The notation also serves to record whether a rain on snow event occurred over the study period, as snowmelt under such conditions are calculated differently than non-rain periods.

#### **4.3.9 University Weather Station**

The Department of Geography at the University of Calgary maintains a weather station located at the Northwest corner of the university campus. Data collected from the University weather station will also be used in this study, to verify the field data collected as well as providing meteorological data for snowmelt computations.

## **CHAPTER FIVE**

### **FIELD STUDY RESULTS AND ANALYSIS**

#### **5.1 Qualitative Analysis**

Over the study period of October 2001 to April 2002, six significant snowfall events occurred in the study area. The dates for these events are: October 24<sup>th</sup>; October 29<sup>th</sup>; November 26<sup>th</sup>; December 10<sup>th</sup>; January 28<sup>th</sup>; February 25<sup>th</sup>; and April 6<sup>th</sup>. Most of the snowfall events were followed by Chinook conditions that resulted in snowmelt.

##### **5.1.1 Visual Survey of Northwest Calgary**

A drive around the Northwest communities in Calgary revealed that there is no marked difference in the spatial distribution of snow cover between a high-density residential area and a medium or low-density residential area. The visual survey was conducted on Feb 5<sup>th</sup>, 2002. In general, snow from the sidewalks and driveways are shoveled onto grassed medians and boulevards. This results in a snowpack with higher depth and density as compared to a natural snow cover. This is similar to snow on sidewalk edges around the campus after the snow on the concrete sidewalks has been brushed off. Snow from parking lots of commercial centers is plowed and piled onto grassed areas around the perimeter of the parking lots, which is typical and resembles the conditions of the parking lots around the campus grounds.

The snow piles consisted of a mixture of compacted snow, sand and gravel. Snow on road shoulders and road medians are dirty due to a high content of sand and gravel. The dirty snow extends to about half a meter away from the road edges. The visual survey of the snow cover around the Northwest area of the city showed that there are no significant differences between plowing practices around the city and the university campus. Therefore, the campus ground can be considered to be representative of a low-density urban area.

### **5.1.2 Classification of Urban Snow Cover**

The snow removal practices in the study area resulted in different snow covers that have distinct characteristics relative to each other. In this study, the common snow cover that can be found in urban areas is classified into four types; snow piles, snow on road shoulders, snow on sidewalk edges, and snow in open areas. Figure 5.1 shows the different snow cover types classified.

Snow piles are formed from removal of snow from large impervious areas such as parking lots and roads, and can usually be found along the pervious areas surrounding the parking lots. Snow piles are highly compacted and contain a high degree of dirt and gravel. Snow on road shoulders results from build-up of snow rolled to the sides by road-sanding machines. Snow on sidewalk edges accumulates from snow brushed from the sidewalk pavements. Snow in open areas such as recreational fields or parks are natural, and quite undisturbed except for the occasional foot traffic. The measurement sites selected covered all four types of the snow cover classified.



Figure 5.1: Snow cover types classified

### 5.1.3 Snow Plowing Practices

On the campus ground, for the first substantial snowfall, the snow is plowed onto medians along the road and onto islands in the parking lot. Snow from pedestrian sidewalks is brushed off the pavements. Snow from subsequent snowfalls is plowed into windrows along the parking lot edges and grassed clearings.

#### **5.1.4 Precipitation Events**

Observations and weather station data revealed that no rain on snow events occurred over the study period. This eliminates the necessity to consider rain induced melt in the computations of snowmelt.

### **5.2 Quantitative Analysis**

#### **5.2.1 Snow Water Equivalent**

Snow water equivalent (SWE) is the most important parameter in the study of snow hydrology. The SWE determines the amount of water stored in the snowpack, and hence the amount available for runoff in the winter. In urban areas, snow cover is often subject to redistribution due to the snow removal practices. This results in a heterogeneous spatial distribution of the SWE of the snow cover.

Table 5.1 shows the instantaneous snow depth and density values for the different snow cover types, measured after a snowfall on January 25<sup>th</sup>, 2002 and the corresponding snow water equivalent. The University weather station's Nipher gauge recorded this snowfall event as having a SWE of 1.6 cm. This is comparable to the SWE of 1.4 cm measured in the open area, and thus verifies the field measurements.

Table 5.1: Instantaneous snow measurements

Types of snow cover	Snow Depth (cm)	Snow Density (kg/m <sup>3</sup> )	SWE (cm)
Pile	130	380	49.4
Road Shoulder	20	190	3.8
Sidewalk Edge	22	160	3.5
Open Area	13	110	1.4

The snow depth and density measurements in Table 5.1 show that the SWE of the urban snow cover is spatially heterogeneous and is location dependent. Snow piles are usually compact, and have the highest depth and density values compared to the other snow cover types. Snow on road shoulders usually have a similar SWE as snow on sidewalk edges, and snow in open areas has the lowest SWE compared to the other types of snow cover.

An intense two-day snow depth and density survey was conducted on the 8<sup>th</sup> and 9<sup>th</sup> of January, 2002 to obtain snow water equivalent data of existing snow piles on the University of Calgary campus. A total of 90 samples were taken and varying depth and density values were obtained. Figure 5.2 shows the map of the University of Calgary campus and the locations where the snow sampling were carried out. It can be seen from the map that the snow sampling are concentrated along the perimeter of impervious areas such as parking lots and roadways. This shows that the snow on parking lots and roadways are plowed and deposited on the surrounding grassed banks. Natural snow cover on pervious areas had completely ablated at the time the snow survey was carried out.

Table 5.2 shows the summary of the results of the two day snow survey. The snow water equivalent of the samples vary between 14 – 92 cm, which is very high compared to the SWE of 2.4 cm measured at an open area after the snowfall event. Snow density of the piles ranges between 310 – 600 kg/m<sup>3</sup>. However, the snow piles surveyed contained a significant amount of gravel, which will overestimate the snow density values slightly. The snow density averages 470 kg/m<sup>3</sup> with a standard deviation of 50 kg/m<sup>3</sup>, which indicates that the average is a good representation of the density of snow piles. This shows that density values of snow piles are much higher than the snow densities of a natural snow cover.

The snow survey illustrates the common practice in urban areas to plow snow from large impervious areas and to pile them on surrounding grassed banks. This results in the redistribution of a uniform snow cover with low SWE into concentrated piles with high SWE. Table 5.2 shows that the snow piles are highly heterogeneous in terms of its depth and density, which results in a random distribution of the SWE. The snow survey also shows that snow piles, a dominant snow cover in urban areas have a longer melt period compared to other types of snow cover.

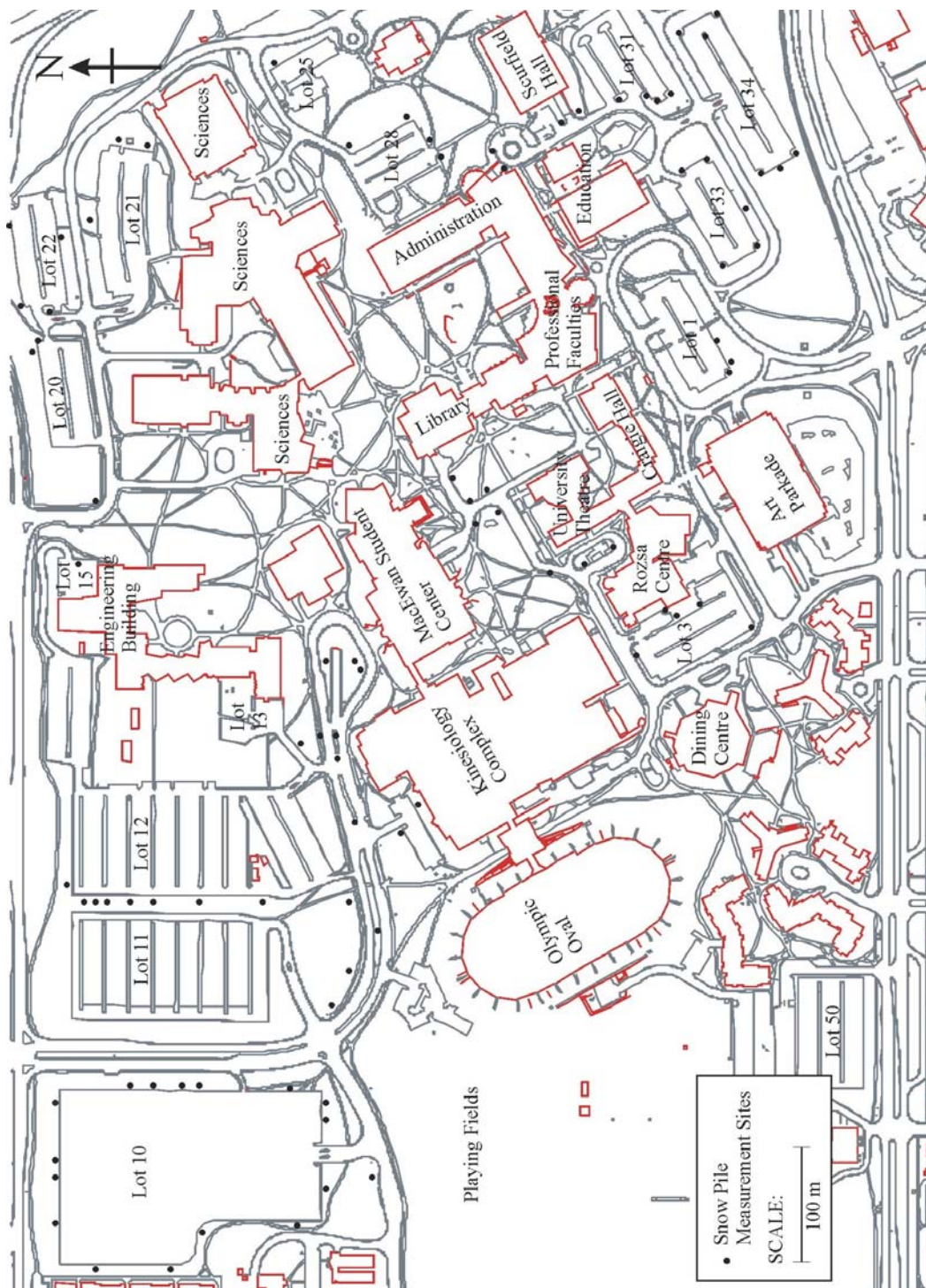


Figure 5.2: Locations of snow pile measurement sites on the University of Calgary

Table 5.2: Summary of campus snow survey

<b>Number of sample</b>	90
<b>Range of snow pile depth</b>	30 cm – 200 cm
<b>Range of snow pile density</b>	310 kg/m <sup>3</sup> – 600 kg/m <sup>3</sup>
<b>Range of snow water equivalent (SWE)</b>	14 cm – 92 cm
<b>Average snow density</b>	470 kg/m <sup>3</sup>
<b>Standard deviation of snow density</b>	50 kg/m <sup>3</sup>

Over the study period, snow depth and density of different snow cover types were measured after every significant snowfall event, and periodically between each snowfall. Table 5.3 shows the range of the snow density values measured for the different snow cover types, as well as the averaged snow densities and the averaged SWE. Average snow density for snow piles is about 500 kg/m<sup>3</sup>, whereas average snow density for snow in open areas is only about 200 kg/m<sup>3</sup>. Average snow densities for snow on road shoulders and snow on sidewalk edges are slightly higher than snow in open areas. Similarly, the average SWE for snow piles is much higher than snow in open areas, and average SWE for snow on road shoulders and snow on sidewalk edges is only slightly higher than snow in open areas. Snow samples measured over the study period show that although snow depth and density values varies for the different types of snow cover, average SWE for snow on road shoulders, on sidewalk edges, and in open areas are quite similar. Snow piles, on the other hand, have a distinctly higher SWE average. In addition, snow piles are a dominant snow cover in urban areas. Therefore, in modelling the spatial heterogeneity of SWE in urban areas, modelling snow piles is very important.

Table 5.3: Summary of snow density values

<b>Types of snow cover</b>	<b>Number of samples</b>	<b>Range of Snow Density (kg/m<sup>3</sup>)</b>	<b>Average Snow Density (kg/m<sup>3</sup>)</b>	<b>Average Snow Depth (cm)</b>	<b>Average SWE (cm)</b>
Piles	44	300 – 600	490	73	35.0
Road Shoulders	8	180 – 340	220	16	3.5
Sidewalk Edges	22	160 – 320	240	15	3.4
Open Areas	26	110 – 340	210	13	2.5

### 5.2.2 Soil Moisture

Soil moisture measurements were taken prior to ground freeze-up and during spring thaw. The measurements prior to ground freeze-up will give an indication of the moisture level at the start of infiltration in spring. Figure 5.3 shows the averaged soil moisture content in volumetric % for the 0-30 cm depth for different measurement sites. The measurements were taken on November 23<sup>rd</sup>, 2001, prior to the ground freeze-up. The averaged soil moisture content varies from one location to another, and ranges between 5-35 %. The measured soil moisture level is very low, reflective of the dry conditions experienced in the study area.

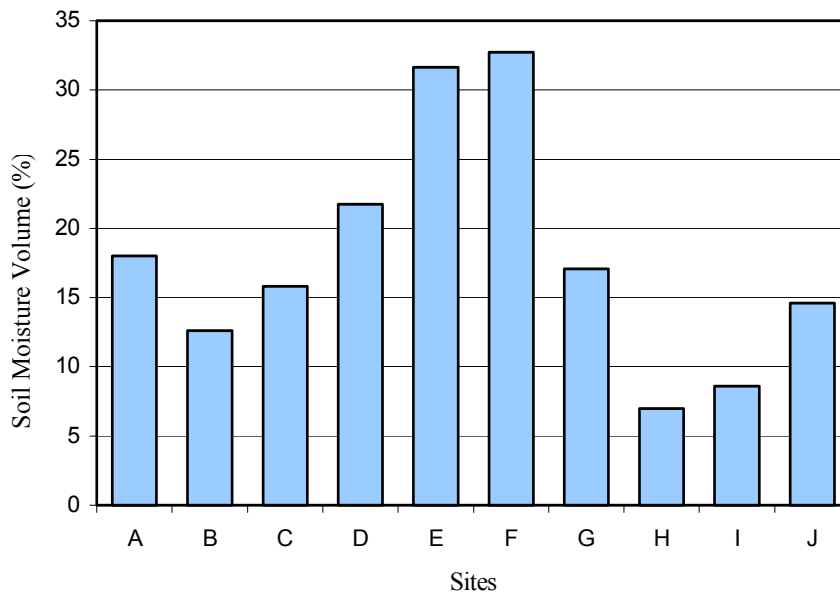


Figure 5.3: Averaged soil moisture level in the 0-30 cm depth for the different measurement sites

Figure 5.4 shows the vertical soil moisture profile for one of the measurement sites. The soil moisture content increases with depth for this site, but the patterns of the vertical soil moisture profile diverge substantially from one location to another. The soil moisture measurements reveal high spatial variability of the soil moisture content, which shows that the spatial scale of urban snow hydrology is very small (likely smaller than rural snow hydrology). Therefore, a very high density of point measurements is required for a good representation of the hydrological properties of the urban watershed.

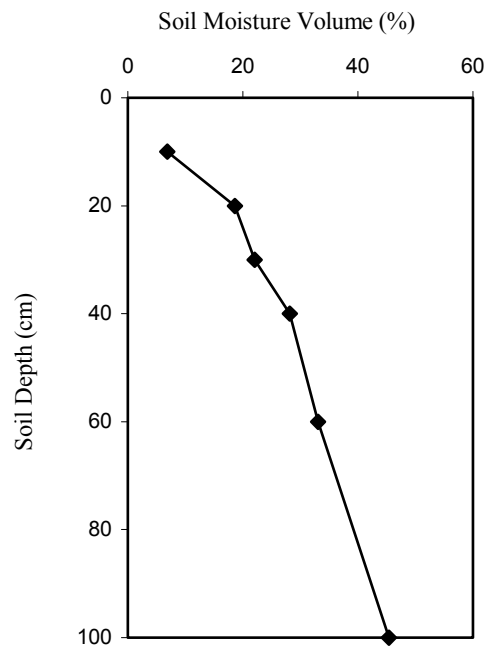


Figure 5.4: Soil moisture variation with depth at Site C

### 5.2.3 Soil Temperature

Hourly soil temperature measurements are used to aid the investigation of frozen ground as well as to map soil temperature fluxes. In this study, frozen ground is defined as when the soil temperature remained below 0 °C. Figure 5.5 shows 24-hour soil temperature averages for four depths at five measurement sites as well as for the air temperature, from October 1<sup>st</sup>, 2001 to April 30<sup>th</sup>, 2002. Air temperature reveals several periods of Chinook conditions that raised the air temperature above 0 °C during mid-winter. However, soil temperature data measured indicated that the ground remained frozen throughout the winter. Soil temperature data at all depths decreases to below 0 °C as the air temperature drops below freezing, and the soil temperature remained below 0 °C until the beginning of April.

The 24-hour temperature average plots show that soil temperature fluctuates with changes in the air temperature for all the measurement sites. Comparison of the soil temperature fluxes for the different sites reveals that with the exception of site E, all the other sites have similar soil temperature fluctuations prior to April. In addition, the magnitude of the temperature fluctuations for site E is not as high as for all the other sites. Site E is an open area with a natural snow cover throughout the winter, and sites A, B, D, and G usually have snow piles on the ground surface.

Figure 5.6 shows hourly temperature fluxes for measurement sites E, B, D, and G as well as the hourly air temperature. Figure 5.6 reveals how snow cover affects the soil temperature. Prior to January 25<sup>th</sup>, 2002, the snow cover for all measurement sites has started to deplete due to Chinook conditions. By January 21<sup>st</sup>, 2002, the snow cover had completely ablated. The temperature fluxes for all the measurement sites showed that the soil temperature at depths 0, 5, and 10 cm dropped sharply and showed a more pronounced fluctuation after January 21<sup>st</sup>. Heavy snowfall started on January 25<sup>th</sup>, 2002, and an accumulation of 15 cm was recorded by the University weather station. The effect of the thick layer of snow on the soil temperature can be seen by the significant change in the soil temperature fluctuations. Soil temperature fluctuations became less pronounced, and reacted less with the changes in the air temperature.

Figure 5.6 also shows that sites B, D, and G had a clear underlying trend of increase in temperature, similar to the air temperature. Soil temperatures at site E, however, remained at an average value. This could be the result of the type of snow cover overlying the ground surface at each measurement sites. As previously mentioned, site E is covered by a near-uniform natural snow cover, whereas sites B, D, and G are covered with snow piles. Factors such as ground slope and tree canopy at sites B, D, and G result in an uneven snow cover depth. Thus, even though a snow pile may cover the ground surface directly above the temperature sensors, thin snow cover at the surrounding area

can easily affect the soil temperatures. Site E, on the other hand, is well insulated due to the layer of snow covering a large area in the vicinity of the temperature sensors. This also explains the less pronounced temperature fluctuations exhibited at site E compared to all the other sites in Figure 5.5. Note that the ground is mostly snow covered between November 26<sup>th</sup>, 2001 and April 10<sup>th</sup>, 2002.

Figure 5.7 shows hourly temperature fluxes for five measurement sites and the air temperature for the month of April 2002. The dashed line in each soil temperature plot indicates the date when complete ablation of the snow cover at each measurement site is observed. Due to instrument malfunction, the start of ground thaw can only be reasonably assessed from sites E, B, and G. For these three sites, it can be clearly seen that the start of ground thaw coincides with the end of the snow cover depletion. Soil temperature increases to above 0 °C only after complete ablation of the overlying snow cover. Figure 5.7 also shows that the soil temperature measurements at the ground surface for all the measurements sites were higher than the air temperature on numerous days after the complete ablation of the snow cover. This is due to the fact that the temperature sensor at the ground surface is exposed to solar radiation, thus heating up to a temperature greater than the air.

The soil temperature plots showed that the snow cover acts as an insulating layer to a certain degree with the result of dampening the fluctuations in the soil temperature in reaction to the changes in air temperature. However, this effect is more pronounced when the snow cover is uniformly covering a larger extent of area. Other investigators have also shown similar result for near surface soil temperatures, which reaches an equilibrium temperature near 0 °C once a snowcover is established (Marks, et. al, 2000). The temperature plots also revealed the lack of spatial heterogeneity for the soil temperature fluxes from one measurement site to another measurement site.

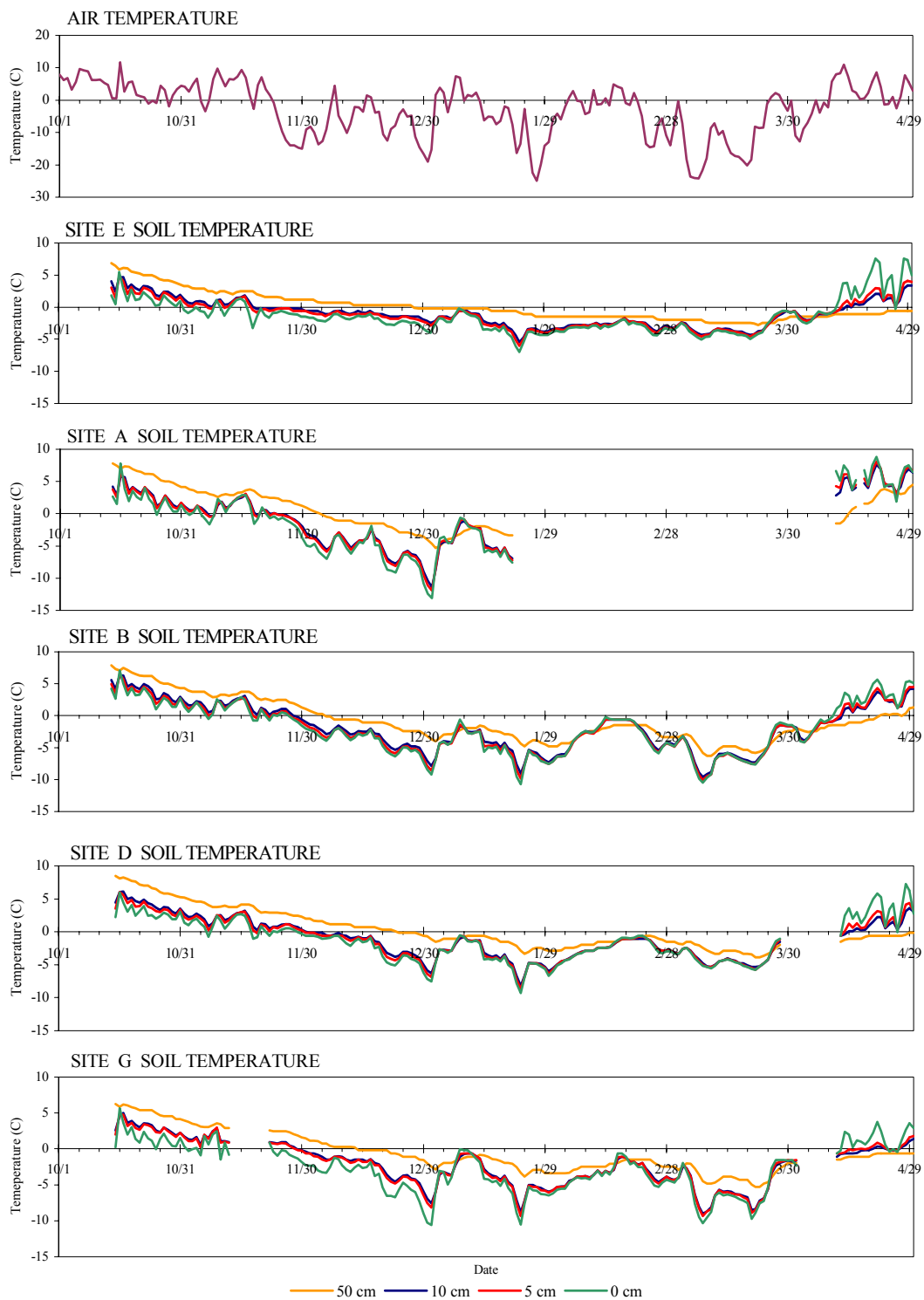


Figure 5.5: 24-hr temperature averages from October 1, 2001 to April 30, 2002

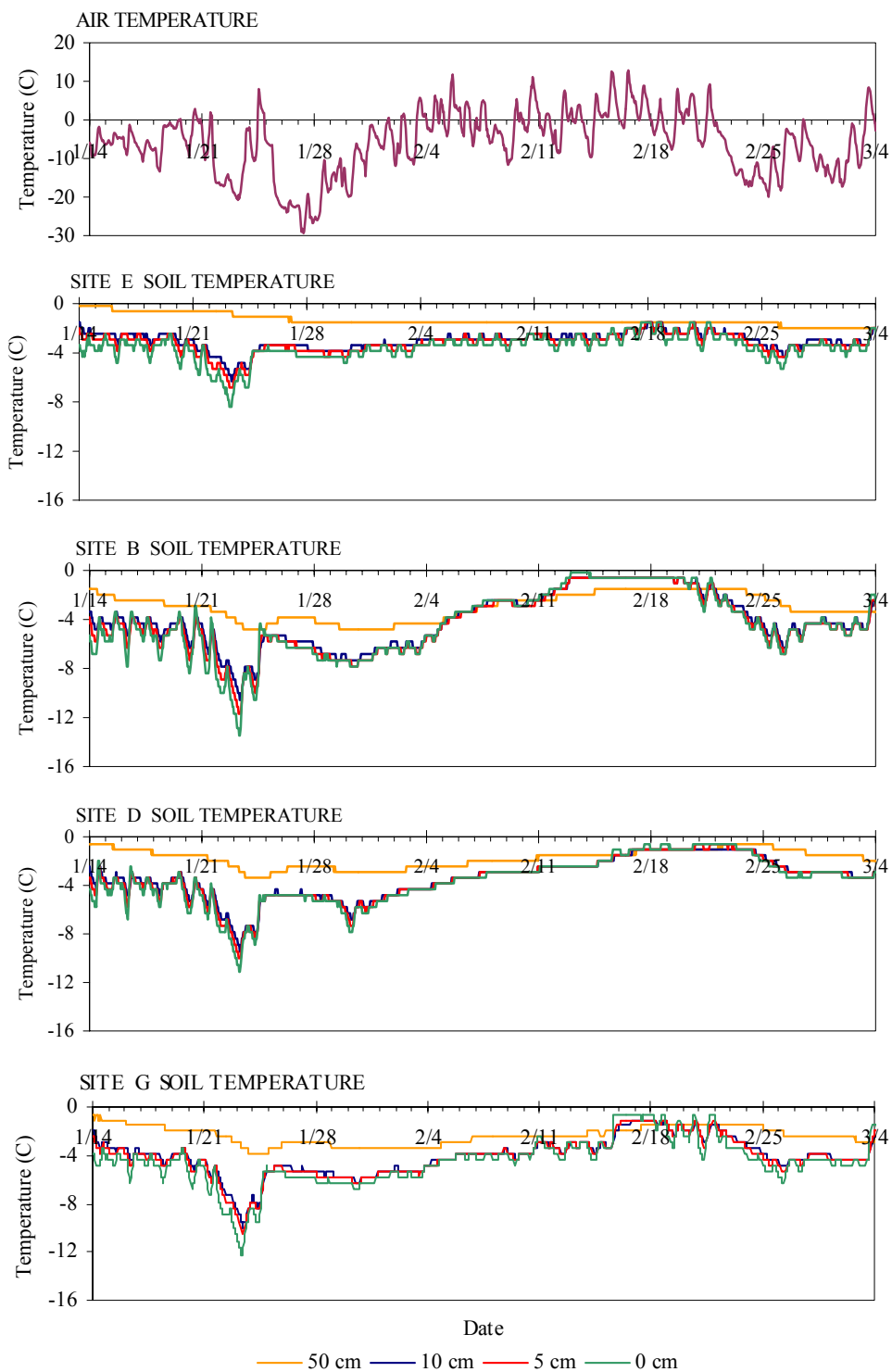


Figure 5.6: Hourly temperature fluxes from January 14, 2002 to March 4, 2002

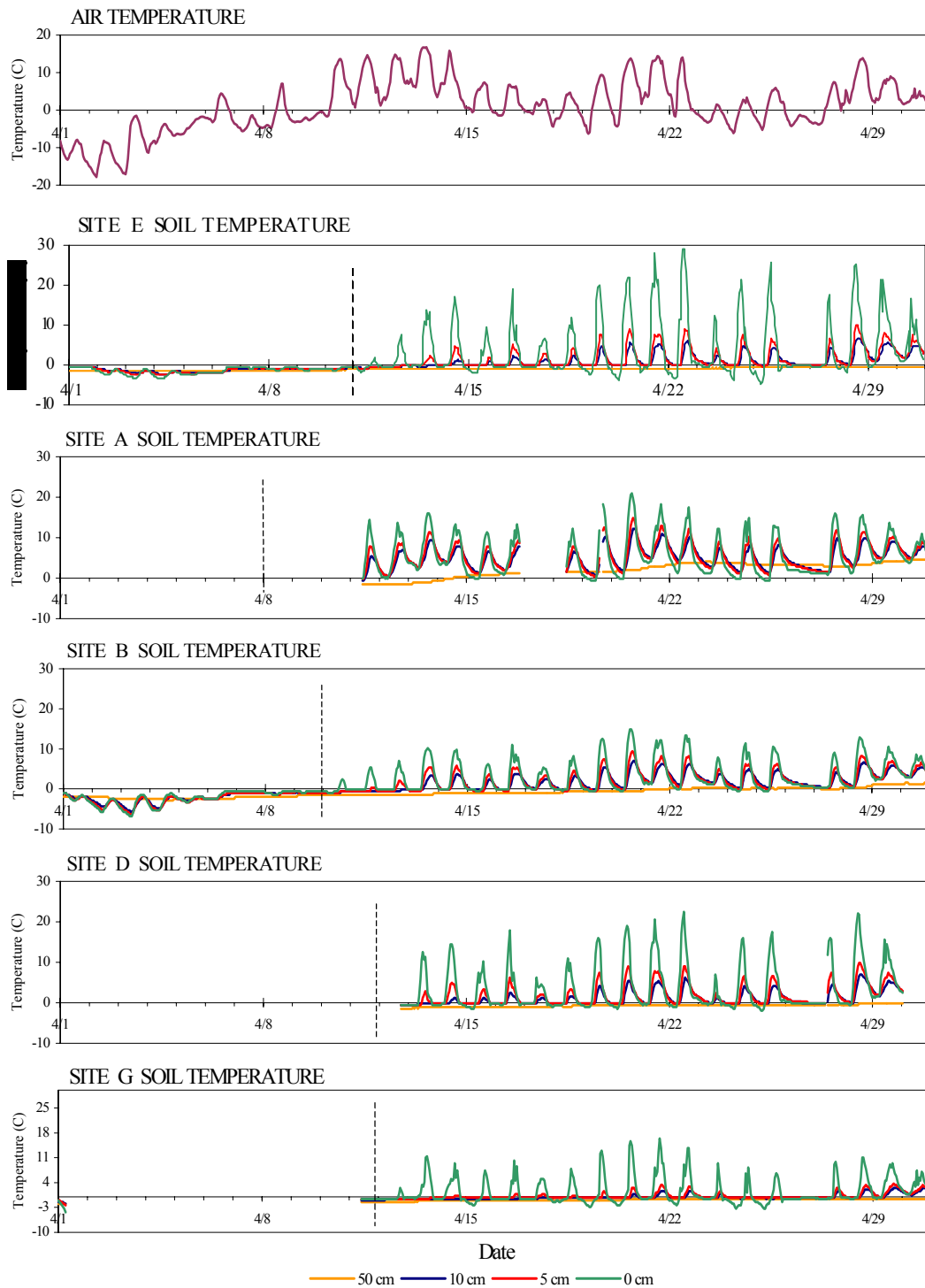


Figure 5.7: Hourly temperature fluxes for April, 2002 (Dashed line indicates date when complete ablation of snow cover is observed)

Figure 5.8 shows the vertical soil temperature profile measured at the University weather station on March 21<sup>st</sup>, 2002. Assuming a straight-line interpolation between measurement points, the depth of ground frost is estimated to be 160 cm.

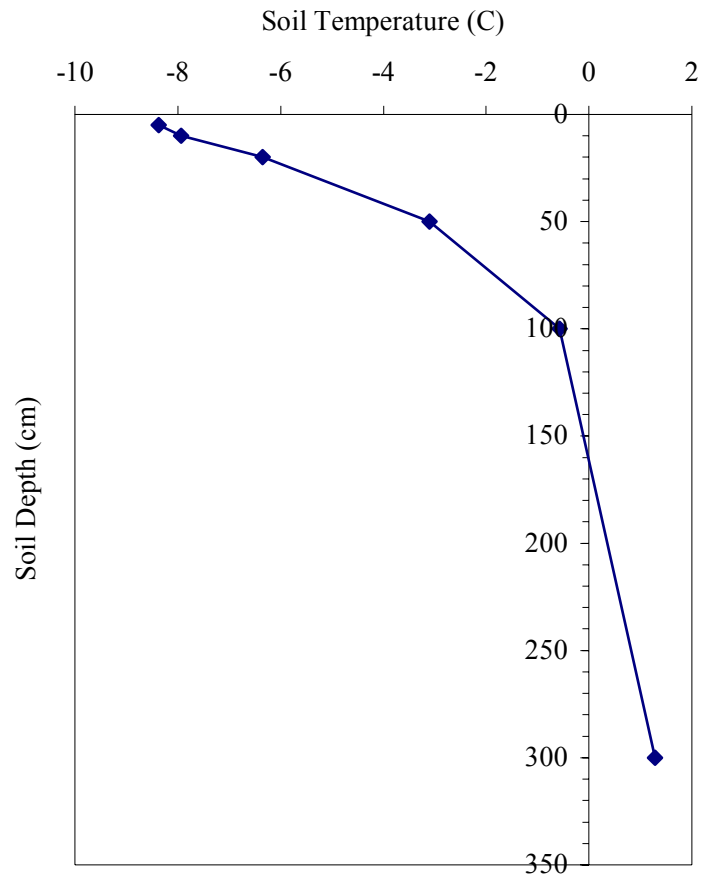


Figure 5.8: Soil temperature variation with depth

### 5.2.4 Infiltration into Frozen Ground

Infiltration into frozen ground is a function of the soil moisture at the shallow depth of 0-30 cm, prior to ground freeze-up and also a function of the snow water equivalent of the snowpack overlying the ground (Granger et. al, 1984). The amount of infiltration is inversely related to the soil moisture prior to ground freeze-up and directly related to the snow water equivalent of the snowpack (Granger et. al, 1984). Averaged soil moisture content measured at the study area revealed a dry condition, which indicates that substantial amount of infiltration should occur over the winter. Figure 5.9 shows the relationship between the total infiltration recorded over the winter and the SWE of the snowpack. In general, the infiltration amount increases as the SWE value increases. However, with the exception of one measurement site, the infiltration amount recorded was 5 mm or less. This shows that even with dry initial soil condition, the infiltration amount was relatively low compared to the available SWE. This suggests that the frozen ground acts as a near impervious area regardless of whether the initial soil moisture condition was dry or near saturation.

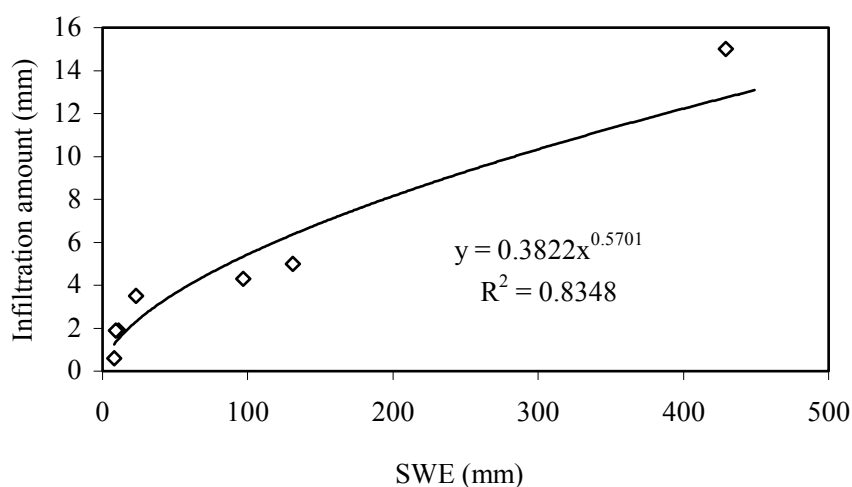


Figure 5.9: Infiltration amount vs. SWE

The soil temperature data showed that the ground remained frozen as long as the overlying snowpack had not completely ablated. This carries implications in the modelling of urban snowmelt runoff. Since infiltration is found to be minimal, runoff from snowpack on pervious areas essentially will flow to the nearest impervious areas, or to any nearby catchbasins.

### **5.2.5 Albedo of Snow**

Snow albedo measures the reflectance of the incident solar radiation by the snowpack. The albedo of snow is taken directly as the inverse ratio between observed incoming and outgoing solar radiation. Snow albedo measurements are used in the energy budget calculations of snowmelt, and the rate of change of snow albedo values is important in the continuous modelling of runoff from snowmelt. In this study, the shortwave radiation measurements commenced after a snowfall event that occurred from the 25<sup>th</sup> to the 27<sup>th</sup> of February. Snow albedo was measured for the four different types of snow cover classified earlier, and measurements were only taken on days with no significant cloud cover.

Figure 5.10 shows the snow albedo values measured over time for snowpacks in four different open areas. The albedo of snowpacks in open areas ranges between 0.9 – 1.0 for new snow and as ablation takes place, albedo of the snow decreases linearly to between 0.6 – 0.7, before the snow ablates completely. The final snow albedo value before complete ablation of the snowpack is relatively high because snowpacks in open areas are relatively undisturbed. Thus, the decrease of the snow albedo value is largely due to the melting of the snowpack.

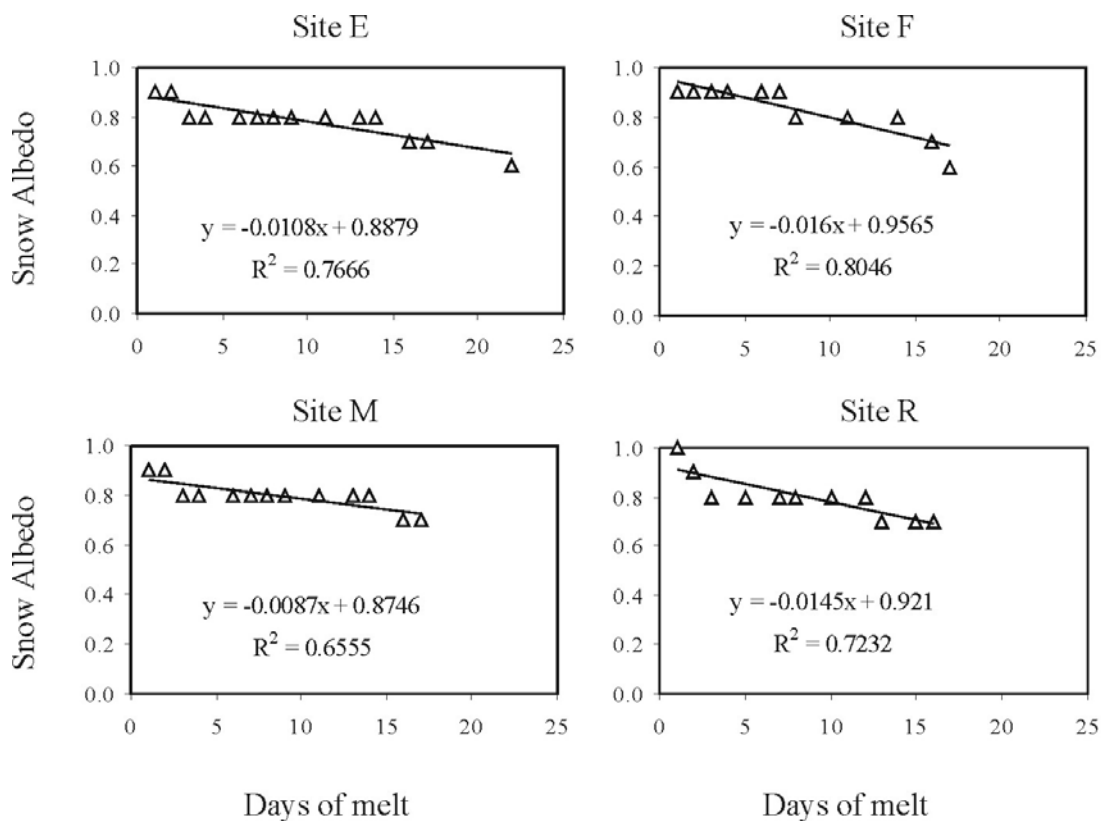


Figure 5.10: Snow albedo measurements at four open area sites

Albedo values measured for snow piles around the perimeter of parking Lot 10 are shown in Figure 5.11. Initial albedo values of snow piles are dependent on the snow/gravel content of the snow. Some snow piles are built from snow that has a much higher content of sand and gravel compared to other snow piles. These piles then will have a much lower snow albedo, due to its high dirt content. The albedo values for snow piles shown in Figure 5.11 decreases exponentially to 0.1 – 0.2. The low albedo values at the end of the melt period is due to both sand and gravel content of the snowpack as well as melting of the snowpack.

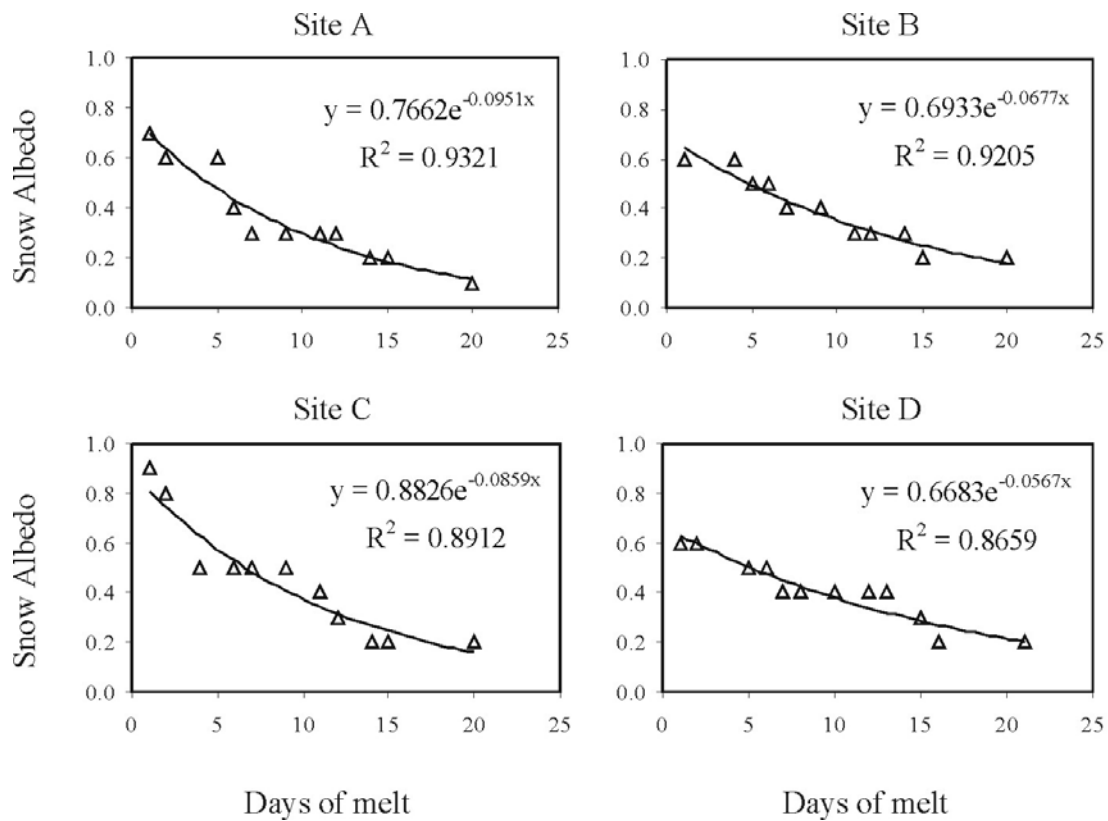


Figure 5.11: Snow albedo measurements for four sites with snow piles

Figure 5.12 shows the albedo of snowpacks on road shoulders. Newly plowed snow have albedo values of 0.7 – 0.8. Albedo of the snow decreases exponentially to 0.3 – 0.4 for sites I and L. Sites I and L are South facing sites, thus they receive maximum sun exposure. Snow albedo at site N decreases exponentially at a slower rate, but also reaches a very low value of 0.2. Site N is east facing and is shadowed by trees in the morning and in the late afternoon. Thus, snowpack at site N ablates at a slower rate compared to sites I and L.

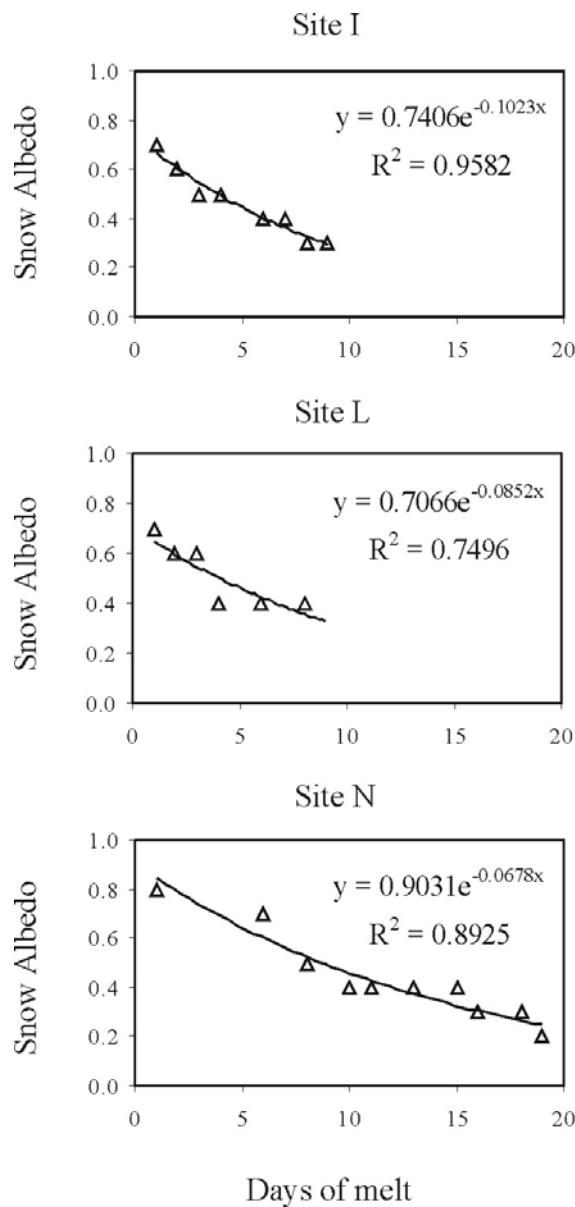


Figure 5.12: Albedo measurements for snow on road shoulders

Snow on sidewalk edges are accumulated from snow brushed off from the sidewalk. Snow brushed off the sidewalk usually has a very low content of sand because sidewalks are usually only slightly sanded. Figure 5.13 shows the albedo values for snow on

sidewalk edges. The snow albedo values decrease linearly to 0.5 - 0.6 at the end of the melt period. Snow at site K ablates faster than site H because site K is south facing while site H is north facing. Thus, site H is shaded in the morning and late afternoon, prolonging the ablation process. Similar to snow in open areas, the linear decrease of the albedo values for snow on road shoulders is largely due to melting of the snowpack.

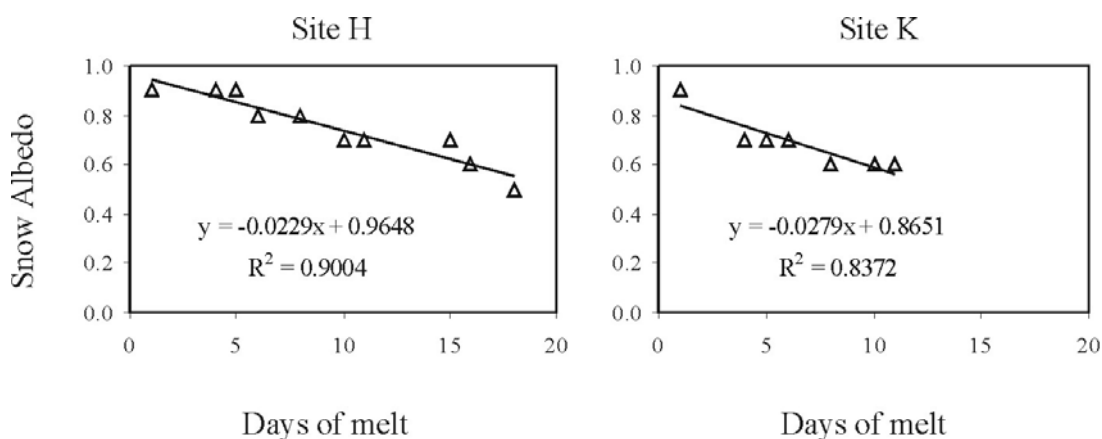


Figure 5.13: Albedo of snow on sidewalk edges

Comparison of the albedo values for the snow cover at different location shows that snow albedo varies for the different snow covers. Rate of the albedo changes also differs for the different sites. Snow in open areas and snow on sidewalk edges decreases linearly, whereas snow piles and snow on road shoulders decreases at an exponential rate. This demonstrates the spatial heterogeneity of the snow cover characteristics in urban areas in terms of its albedo values. Generally, snow albedo at various open areas remains quite high, up until complete ablation or melt takes place. On the other hand, snow on road shoulders and snow piles have a much lower albedo values. The albedo of snow on road shoulders can start out quite high, but quickly progresses to dirty, low albedo snow. Snow on sidewalk edges has similar albedo values as snow in open areas, but decreases to a

slightly lower albedo at the end of the melt period. Table 5.4 shows the summary of the initial and final snow albedo values for the four snow cover types classified.

Table 5.4: Snow albedo summary

<b>Types of snow cover</b>	<b>Initial snow albedo</b>	<b>Final snow albedo</b>
Piles	0.6 – 0.9	0.1 – 0.2
Road Shoulders	0.7 – 0.8	0.2 – 0.4
Sidewalk Edges	0.9	0.5 – 0.6
Open Areas	0.9	0.6 – 0.7

Measurements of the snow albedo on a cloudless, warm day revealed that higher albedos are recorded in the morning and in the evening compared to the albedo during the noon hour. This variation is due to the angle of the incident solar beam and the change in the structure of the snow. A higher angle of incidence results in higher albedos. In addition, a crust occurs on the snow surface in the morning and in the evening. However, during midday, the angle of the incident solar beam is smaller and as active melt is occurring, there is a higher concentration of liquid water in the top layers of the snowpack, which decreases the albedo. Table 5.5 shows albedo measurements taken at sites A, C, and D. Albedo values for sites A in the morning are not available because the aspect of its slope is west facing, and thus the snow cover is shaded in the morning. Similarly, site D is shaded in the late afternoon. The snow albedo values measured for the snow cover at sites A, C, and D reveals that the higher snow albedos are recorded in the morning and in the late afternoon compared to the noon hour. This shows that snow albedo values not only changes with time, it also exhibits a daily diurnal pattern on sunny, cloudless days.

Table 5.5: Albedo values for snow cover at sites A, C, and D

<b>Date</b>	<b>Time</b>	<b>Albedo values for snow cover at Site A</b>	<b>Albedo values for snow cover at Site C</b>	<b>Albedo values for snow cover at Site D</b>
07-Feb-02	9:30		0.74	0.51
	12:30	0.31	0.48	0.40
	15:30	0.44	0.61	
11-Feb-02	9:30		0.70	0.53
	12:30	0.30	0.43	0.41
	15:30	0.48	0.46	
14-Feb-02	9:30		0.49	0.43
	12:30	0.23	0.23	0.29
	15:30	0.33	0.29	

### 5.2.6 Net Longwave Radiation

In urban areas, the radiation exchanges of a snowpack is further complicated by the presence of building walls, which emits longwave radiation. The net longwave radiation of snowpacks near a North-facing wall and a South-facing wall as well as an open area is presented in Table 5.6. The net longwave radiation is calculated using radiation measurements taken on sunny and cloudless days. Table 5.6 shows that net longwave radiation of snowpacks near building walls can be significantly higher than net longwave radiation of snowpacks in an open area. The measurements of net longwave radiation on snowpacks at site P (near North-facing wall) and site E (open area) differs by as much as  $91 \text{ W/m}^2$ . This shows that the influence of building walls on the snowpacks' net radiation is significant.

Comparison of site P (near North-facing wall) and Q (near South-facing wall) reveals that a sun-facing building wall can increase the net longwave radiation into the snowpacks between 68-84  $W/m^2$ . Solar radiation is adsorbed by the building wall, which increases the longwave radiation emitted. The net longwave measurements showed that building walls have a significant effect on the radiation balance of a snowpack. This factor is important in the modelling of snowmelt runoff in a high-density urban area.

Table 5.6: Net longwave radiation measurements at sites E, P, and Q on cloudless days

<b>Date</b>	<b>Site E (Open area),  <math>W/m^2</math></b>	<b>Site P (North-facing building wall),  <math>W/m^2</math></b>	<b>Site Q (South-facing building wall),  <math>W/m^2</math></b>
31-Jan-02	-38	12	83
01-Feb-02	-84	7	91
02-Feb-02	-43	15	83
04-Feb-02	-68	8	83

### 5.2.7 Net Radiation Fluxes

Radiation heat flux drives melt in many environments. It usually dominates the snowpack's energy balance. Therefore, the net all-wave radiation of the snowpack is a strong indicator of snowmelt. Heat fluxes incident on the snowpack are considered positive values, and those away from the pack, negative values. Hence, positive values of net shortwave radiation would be the total adsorbed solar radiation by the snowpack. This applies to net longwave radiation and net all-wave radiation as well. The radiation measurements commenced after a snowfall event that occurred from the 25<sup>th</sup> to 27<sup>th</sup>

February. Measurements continued until the next significant snowfall event or when the snowpack has completely ablated.

The net radiation fluxes measured for snow piles are shown in Figure 5.14 and a progressively increasing trend for the net radiation fluxes can be observed over time. The net all-wave radiation values range between  $-50\text{W/m}^2$  to  $500\text{W/m}^2$ . Shortwave radiation dominates the all-wave radiation exchanges and measurements indicate that adsorbed shortwave radiation was high, which can be attributed to the low albedo for snow piles.

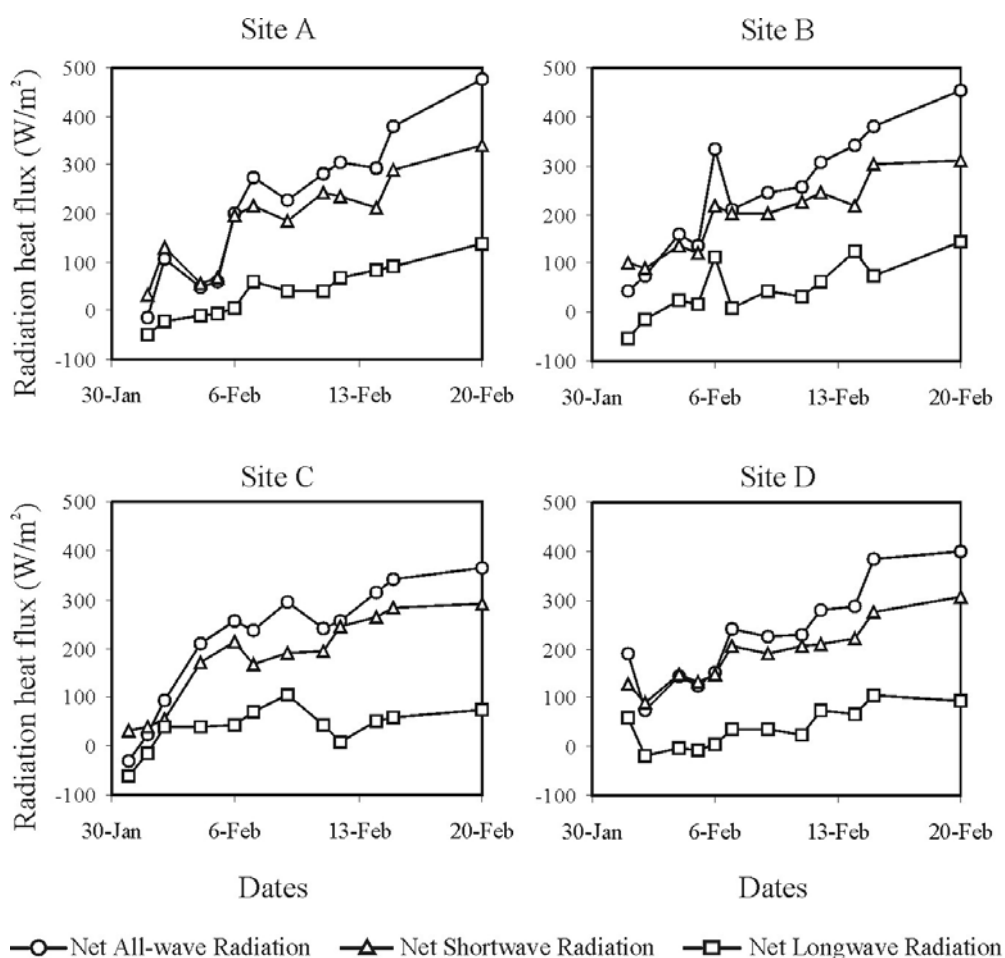


Figure 5.14: Net radiation fluxes measured for snow piles

Figure 5.15 shows the net radiation fluxes for snow in open areas, measured at four different sites. Net all-wave radiation values for snow in open areas ranges between  $-100 \text{ W/m}^2$  to  $150 \text{ W/m}^2$ , which is considerably lower than values measured for snow piles. Shortwave radiation also dominates the all-wave radiation exchanges, but had lower values compared to the shortwave radiation measured for snow piles. Snow in open areas has albedo values that remain above 0.5 during spring, resulting in higher shortwave radiation reflectance compared to snow piles.

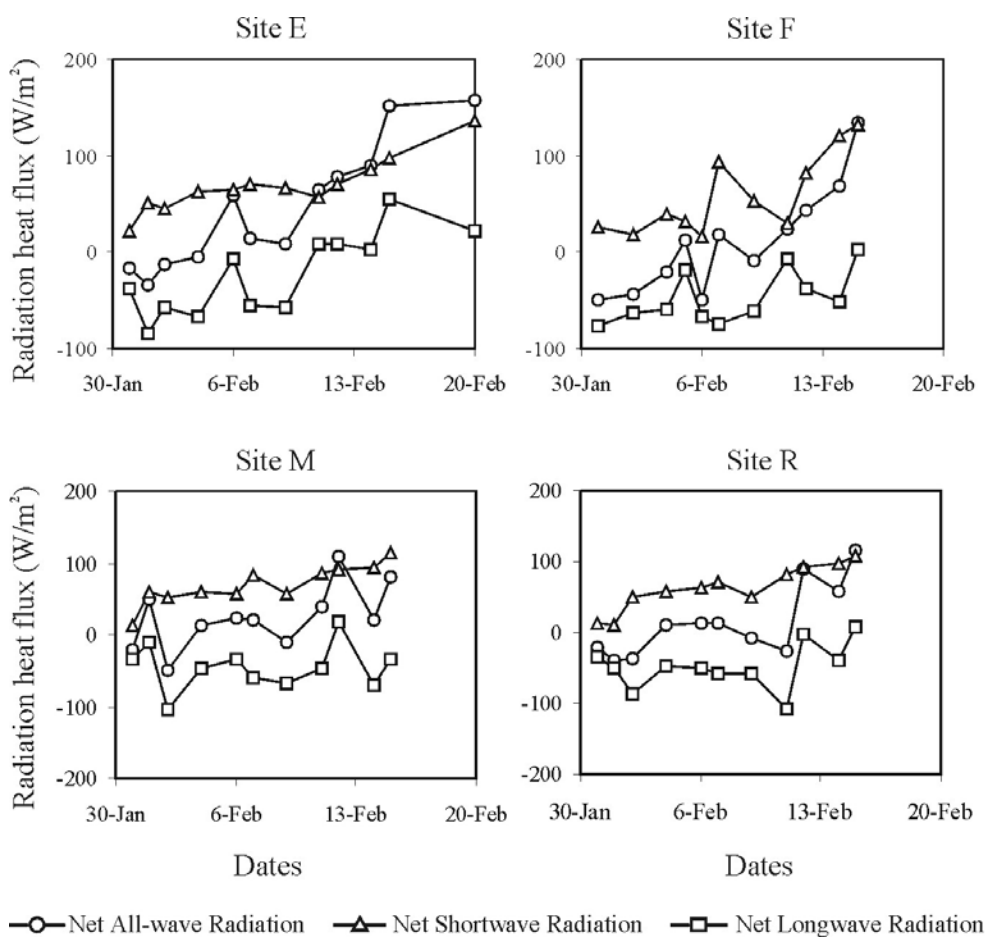


Figure 5.15: Net radiation fluxes measured for snow in open areas

The net radiation fluxes for snow on road shoulders are shown in Figure 5.16. The net all-wave radiation fluxes range between  $50 \text{ W/m}^2$  –  $250 \text{ W/m}^2$ . Initial albedo values for snow on road shoulders are typically 0.7 – 0.8, which results in higher adsorption of shortwave radiation. This leads to positive net all-wave radiation flux, and indicates active melt of the snowpack. Thus, even though the snow water equivalent of snow on road shoulders is higher than the snow water equivalent of snow in an open area, the snow on road shoulder experiences accelerated melt and a shorter melt period. Site N has a longer melt period compared to sites I and L, due to shadings in the morning and late afternoon.

Net radiation fluxes of snow near building walls are shown in Figure 5.17 and reveal the influence of building walls on the radiation exchanges of the snowpack. Site P shows radiation fluxes measured for snow near a North facing building wall (shaded), and site Q shows radiation fluxes measured for snow near a South (sun) facing building wall. In both cases, it can be observed that the net longwave radiation flux was positive throughout the measurement period. This is due to longwave radiation emitted by building walls. Site Q has a higher net longwave radiation compared to site P as it also emits adsorbed shortwave radiation as longwave radiation.

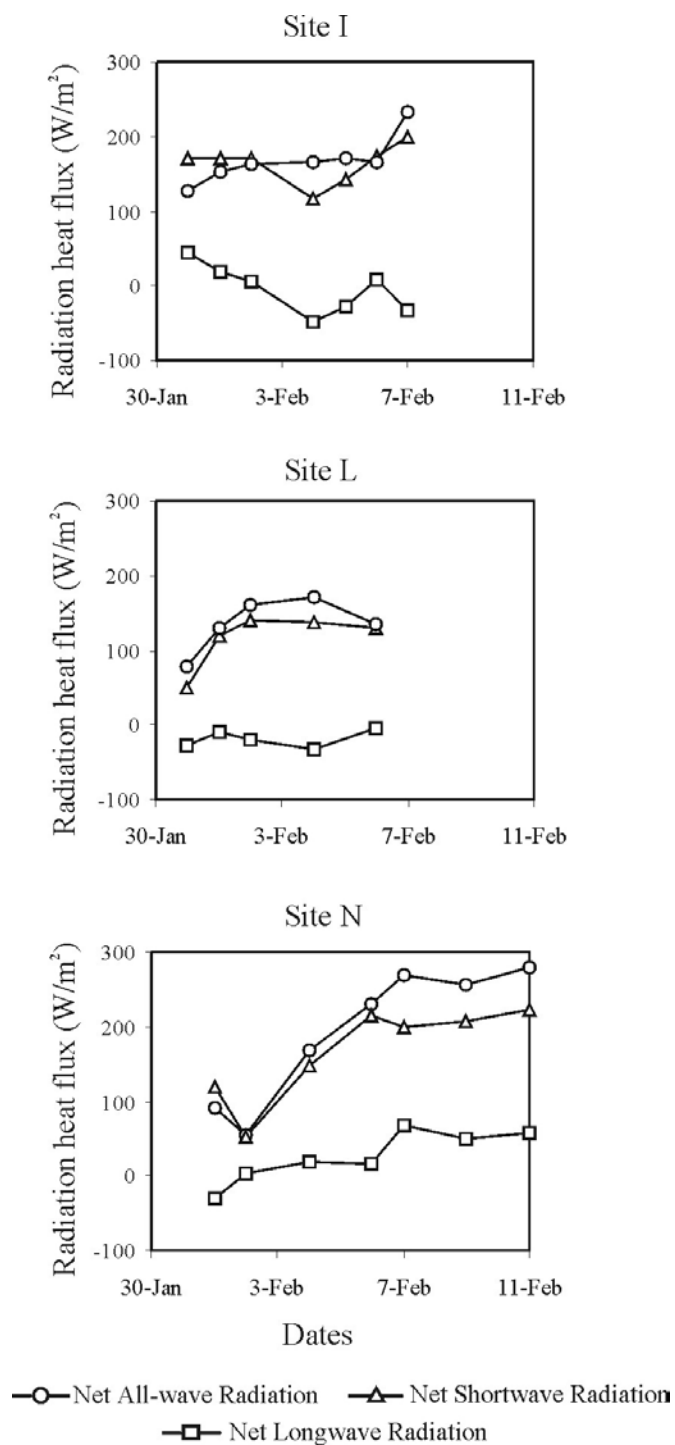


Figure 5.16: Net radiation fluxes measured for snow on road shoulders

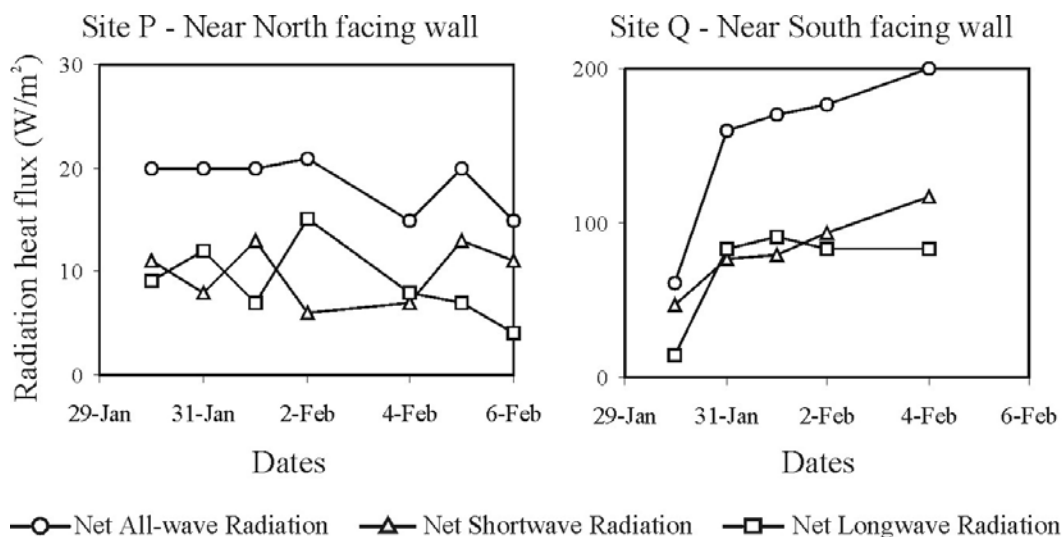


Figure 5.17: Net radiation fluxes measured for snow near building walls

### 5.2.8 Evaporation from the Snowpack

Evaporation from the snowpack is represented by latent energy lost from the snowpack in the energy budget for snowmelt. Evaporation was measured simultaneously for three different snow texture types: dry, fine-grained snow; crusty, larger-grained snow, and disturbed, piled snow. Table 5.7 shows the total evaporation measured in grams, and also in depths of mm for a dry, fine-grained snow. Similarly, Table 5.8 shows the total evaporation measured for a crusty, larger-grained snow. Table 5.9 shows evaporation measured for a disturbed, piled snow.

For the same-day measurements, comparison of the three tables revealed that the depths of evaporation loss in mm is consistently highest for fresh, dry, snow compared to the other snow texture types, and evaporation depth is consistently lowest for disturbed, piled snow. This is probably attributed to the texture of the snow. Disturbed, piled snow is

usually very icy and large-grained. Thus, it requires higher energy to evaporate than fresh, dry snow.

Table 5.7: Evaporation loss measurements for dry, fine-grained snow

<b>Date</b>	<b>Evaporation loss for dry, fine-grained snow (gram)</b>	<b>Evaporation loss for dry, fine-grained snow (mm)</b>
09-Feb-02	5.18	1.9
11-Feb-02	17.21	6.3
12-Feb-02	10.48	3.8
13-Feb-02	11.17	4.1
25-Feb-02	7.30	2.7
12-Mar-02	6.78	2.5
21-Mar-02	9.63	3.5

Table 5.8: Evaporation loss measurements for crusty, larger-grained snow

<b>Date</b>	<b>Evaporation loss for crusty, larger-grained snow (gram)</b>	<b>Evaporation loss for crusty, larger-grained snow (mm)</b>
9-Feb-02	4.82	1.4
11-Feb-02	17.88	5.1
13-Feb-02	12.44	3.6
14-Feb-02	7.31	2.1
15-Feb-02	7.85	2.2

Table 5.8: Evaporation loss measurements for crusty, larger-grained snow (continued)

<b>Date</b>	<b>Evaporation loss for crusty, larger-grained snow (gram)</b>	<b>Evaporation loss for crusty, larger-grained snow (mm)</b>
16-Feb-02	6.57	1.9
14-Mar-02	7.48	2.1
23-Mar-02	22.41	6.4

Table 5.9: Evaporation loss measurements for disturbed, piled snow

<b>Date</b>	<b>Evaporation loss for disturbed, piled snow (gram)</b>	<b>Evaporation loss for disturbed, piled snow (mm)</b>
9-Feb-02	7.52	0.6
11-Feb-02	23.14	1.9
13-Feb-02	17.58	1.3
14-Feb-02	10.08	0.7
16-Feb-02	7.91	0.6
20-Feb-02	14.21	1.1
21-Feb-02	9.39	0.7
25-Feb-02	7.58	1.6
11-Mar-02	10.45	1.2
12-Mar-02	14.96	1.2
14-Mar-02	11.36	0.9
21-Mar-02	20.49	1.6

Table 5.9: Evaporation loss measurements for disturbed, piled snow (continued)

<b>Date</b>	<b>Evaporation loss for disturbed, piled snow (gram)</b>	<b>Evaporation loss for disturbed, piled snow (mm)</b>
23-Mar-02	23.05	1.7
25-Mar-02	10.72	0.8
26-Mar-02	21.05	1.4
2-Apr-02	17.77	1.2
3-Apr-02	21.60	1.4
11-Apr-02	42.96	2.9

### 5.2.9 Net Energy Flux

Snowmelt rate is determined by the net energy flux to the snowpack. In this study, rain induced melt did not occur over the study period. Thus, the components of the energy budget that contribute to snowmelt are the net radiation, sensible heat transfer, and latent heat transfer. Figure 5.18 shows values of the respective fluxes for a melting snowpack in the study area over a 24-hour period on April 11<sup>th</sup>, 2002. Active melt was taking place, and Figure 5.18 shows that the energy balance is dominated by net radiation. The contribution of the turbulent exchanges to the total amount of energy available for melt is low compared to the net radiation. Net energy is negative at night, thus refreezing the liquid water held in the snowpack.

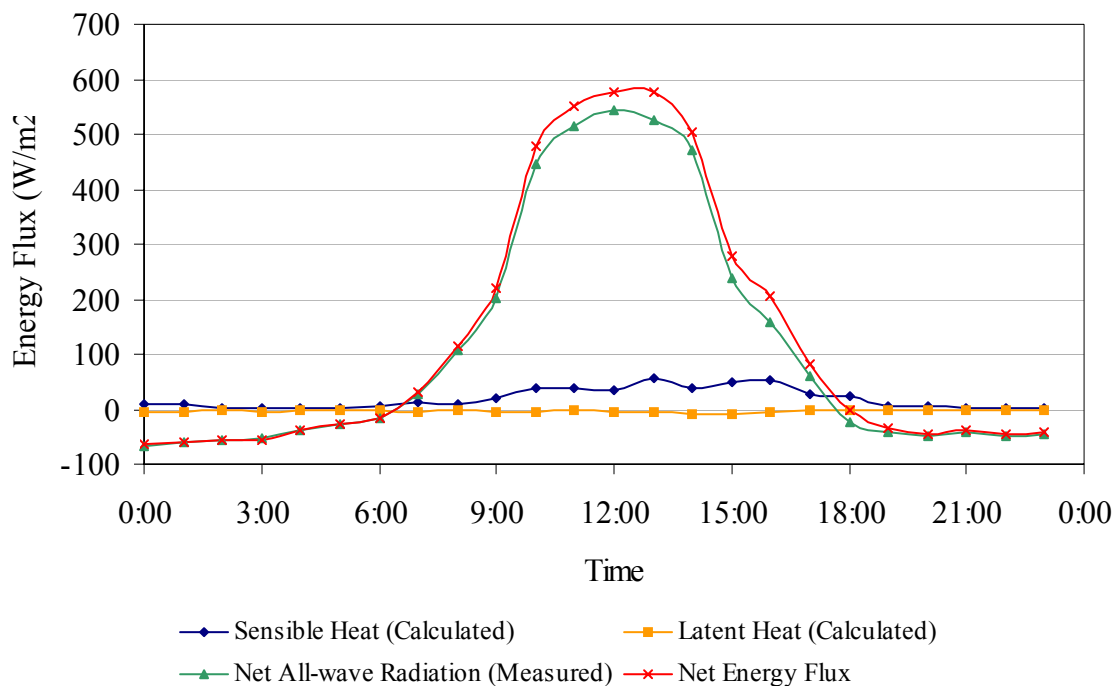


Figure 5.18: Energy fluxes for a melting snowpack

### 5.2.10 Surface Temperature

Temperatures of different surfaces were measured in the spring to monitor how different surfaces in the urban areas can contribute to snowmelt. Temperatures of the road surface were taken near a stationary car and bus, but with the engine running. Surface temperature measurements revealed that the temperature of the road pavement at the vicinity of a car exhaust can increase by  $1\text{ }^{\circ}\text{C}$ , and the temperature of the road pavement at the vicinity of a bus exhaust can increase by  $4\text{ }^{\circ}\text{C}$ . For a parked car, radiation from the body of the car also increases the pavement temperature substantially.

Vehicle traffic is a common element of an urban area. Vehicle traffic can increase the temperature of the road surface, and even parked vehicles can substantially increase the surface temperature of a parking lot. In a densely urbanized area, with heavy traffic flow, this can result in melting of snow on road surfaces in winter.

Temperatures of road pavements, sidewalk pavements, parking lot pavements and grassed area surfaces were measured randomly on April 10<sup>th</sup> and April 11<sup>th</sup>, 2002. Table 5.10 shows the averaged temperature measured for each surface type. The average temperature over the measurement period is 13 °C and 14 °C respectively for April 10<sup>th</sup> and April 11<sup>th</sup>. Even though average air temperature only differs by 1 °C for the two days, average surface temperatures for April 11<sup>th</sup> is higher than the average surface temperatures for April 10<sup>th</sup> by 3 – 5 °C. This difference can be accounted for by weather conditions prior to April 10<sup>th</sup>. Snowfall activities occurred on April 9<sup>th</sup> with an overcast sky. The weather condition on April 10<sup>th</sup> was mainly cloudy with intense melt of the snowcover occurring. Weather condition on April 11<sup>th</sup> was mainly sunny and this increases the exposure of the surfaces to solar radiation, which results in an increase of the surface temperature.

Comparison of the different surface types showed that grassed areas had the highest average temperature followed by the sidewalk pavements, with the road and parking lot pavements having the lowest temperatures. This could be the result of the different specific heat capacity for the different surface types. Table 5.11 shows the specific heat values for the different surface materials. Dry mineral soil has a very low heat capacity. The concrete sidewalk pavement has a slightly higher specific heat compared to the grassed surface and asphalt surfaces such as the road and the parking lot pavements have the highest specific heat capacities. This means that with the same energy input, soil temperature will increase more compared to concrete or asphalt surfaces. Similarly, temperature of concrete surfaces will increase more compared to asphalt surfaces.

The reason air measured above asphalt or concrete will have higher temperature than air measured above grassed area is because of the thermal conductivity properties of the material. Soil has a very low thermal conductivity value compared to concrete and asphalt. Thus, the transfer of heat from soil to air is much less compared to transfer of heat from asphalt or concrete to air. This also explains why concrete or asphalt is hotter when touched compared to grassed areas.

Table 5.10: Average surface temperature measurements

Surface type	Average temperature (°C)	
	Dry Surface	Wet or Water-ponded Surface
<u>10-Apr-02</u>		
Parking lot pavement	15	12
Sidewalk pavement	17	11
Road	15	12
Grassed area	18	11
<u>11-Apr-02</u>		
Parking lot pavement	20	15
Sidewalk pavement	21	16
Road	20	-
Grassed area	23	15

Table 5.11 Specific heat values

<b>Substance</b>	<b>Specific Heat (kJ/kg K)</b>
Asphalt	1.67
Concrete	0.962
Dry mineral soil	0.84

Source: Bolz and Tuve (eds.), 1973; Hanks and Ashcroft, 1980

## CHAPTER SIX

### URBAN SNOW MODELLING

#### 6.1 Introduction

An urban snowmelt model, named Urban Snow Model (USM), is created and programmed in Matlab to simulate generation of snowmelt runoff from an urban catchment. Although flow rates for urban winter runoff is typically low, it can be sustained over several days. In addition, a significant fraction of winter pollutants may be removed by snowmelt. Thus, snowmelt routines are important in simulation of winter water and pollutant storage for cold climate regions. The basic melt computations in this urban snow model are based on routines developed by the U.S. National Weather Service (Anderson, 1973). Therefore, some of the equations will be repeated here from chapter two for clarity. The program uses hourly times steps, allows redistribution of snow from impervious areas to pervious areas, and applies different snow albedo values for the different snow cover types found in urban areas. The following sections describe the methodology programmed in the urban snow model. It explains the various input parameters required, computations performed and output produced. All snow depths throughout the model are treated as depths of water equivalent.

The purpose of this model is to carry out a sensitivity analysis to show the impact of simulation with and without snow redistribution, and to determine the effect of rain-on-snow events on snowmelt runoff. Therefore, the catchment, and the precipitation events simulated are only hypothetical. Even though the study area in this research has a fairly low snowfall amount, cities such as Quebec and Winnipeg in Canada have high annual

winter precipitation. Thus, the model serves to demonstrate the impact of incorporating snow redistribution and urban snow characteristics on snowmelt generation, which is important for urban areas that receive high snowfall amount.

## **6.2 USM Time Steps**

The program uses hourly time steps for calculations of snowmelt and runoff.

## **6.3 Subcatchment Schematization**

### ***Land Surface – Snow Cover Combination***

Due to the snow removal activities that occur in urban areas, different combinations of snow cover and ground surface types can result after redistribution occurs. Seven such combinations are provided in USM, as described in Table 6.1. The combinations allow flexibility in the simulation of snowmelt from the different snow covered subcatchment types that can be found in an urban area. Snow cover on type 1 impervious subcatchment is usually plowed into big piles onto adjacent pervious area. Snow cover on type 2 and type 3 impervious subcatchments are treated identically; they are rolled or shoveled into small piles onto adjacent pervious areas. Type 4 impervious subcatchment and type 7 pervious subcatchment have natural snow covers that are not subject to redistribution. Types 1, 2, and 3 subcatchments are considered ‘normally bare’ due to probable snow removal, but are subject to snow cover as well.

Table 6.1: Subcatchment surface classification

Subcatchment Type	Perviousness	Snow cover and Extent	Examples of Land Surface	Simulation Treatment
1	Impervious	Normally bare	Parking lots	Snow cover redistributed
2	Impervious	Normally bare	All level roads	Snow cover redistributed
3	Impervious	Normally bare	Driveways and sidewalks	Snow cover redistributed
4	Impervious	Uniform snow cover	Miscellaneous unplowed impervious areas	Snow cover subject to areal depletion curve
5	Pervious	Covered with large snow piles	Perimeter area of parking lots	Snow cover subject to areal depletion curve
6	Pervious	Covered with small snow piles	Road shoulders, driveways/ sidewalk edges	Snow cover subject to areal depletion curve
7	Pervious	Uniform snow cover	Rooftops, parks, lawns, open areas	Snow cover subject to areal depletion curve

### ***Redistribution and Simulation of Snow Removal***

Snow removal practices in urban areas result in snow cover characteristics that are different from snow in rural areas. Much of the snow cover on impervious surfaces in urban areas is plowed into piles on adjacent pervious areas. This results in melt

characteristics that are significantly different from a uniform snow cover. In USM, it is assumed that all snow subject to redistribution resides on types 1, 2 and 3 subcatchments. For each of the subcatchment, a depth of snow, BaseDepth is an input for the subcatchment. All snow in excess of this depth is redistributed according to three options:

- (a) Plowed onto adjacent pervious area (into large piles)
- (b) Plowed onto adjacent pervious area (into small piles)
- (c) Removed altogether from simulated catchment

The fraction of the excess snow redistributed according to each option is an input parameter. The sum of the fractions for each subcatchment where redistribution occurs should equal to 1.0, and the transfers of snow from the impervious areas to pervious areas are area-weighted. The depth of snow, BaseDepth, remaining on the normally bare area is subject to a melting identical to a uniform snow cover. Default values for BaseDepth are provided in the model.

#### **6.4 Calculating Snow Melt Using the Energy Balance Method**

The energy balance equation for a snowpack is expressed as follows:

$$\Delta Q = Q_{sw} + Q_{lw} + Q_e + Q_h + Q_g + Q_m \quad (31)$$

where  $\Delta Q$  is the change in heat storage in the snowpack;  $Q_{sw}$  is the net shortwave radiation entering the snowpack;  $Q_{lw}$  is the net longwave radiation entering the snowpack;  $Q_e$  is the latent heat transfer;  $Q_h$  is the sensible heat transfer;  $Q_m$  is the advection of heat into the snowpack by rain; and  $Q_g$  is the conduction of heat into the snowpack from the underlying ground. Units for each energy balance term are  $W/m^2$ -hr.

It will be assumed that condition is for melt, and all heat added into the snowpack will produce liquid melt. For a melting snowpack, heat conduction from ground,  $Q_g$  is negligible compared to energy exchange at the snow surface. Thus, the term is neglected here.

It requires about 80 cal to melt one gram of water (the latent heat of fusion) or 93 W/m<sup>2</sup>-hr per 1 mm of melt. The melt rate is thus calculated as follows:

$$M_{sr} = \frac{\Delta Q}{93} \quad (32)$$

where  $M_{sr}$  is the melt rate (mm/hr); and  $\Delta Q$  is the change in heat storage of the snowpack (W/m<sup>2</sup>-hr).

### ***Net Shortwave Radiation***

The net shortwave radiation is calculated as follows:

$$Q_{sw} = Q_i * (1 - A) \quad (33)$$

where  $Q_{sw}$  is the net shortwave radiation (W/m<sup>2</sup>-hr);  $Q_i$  is the incoming shortwave radiation (W/m<sup>2</sup>-hr); and A is the snow albedo.

Measured hourly values of incoming shortwave radiation are obtained from meteorological stations. Snow albedo values are available for three different urban snow cover types; large snow piles, small snow piles, and a uniform snow cover. Large snow piles are the result of plowing from large impervious surfaces such as commercial

parking lots, and small snow piles are the results of shoveling from driveways, sidewalks, and snow rolled from sanding trucks on roads. Uniform snow covers are fairly undisturbed natural snow cover from unused parks, and open areas.

Figure 6.1 shows the snow albedo data documented for all large snow piles from the field study and the exponential relation between the snow albedo values and the days of melt. The exponential relationship is used to determine snow albedo values for large snow piles in USM.

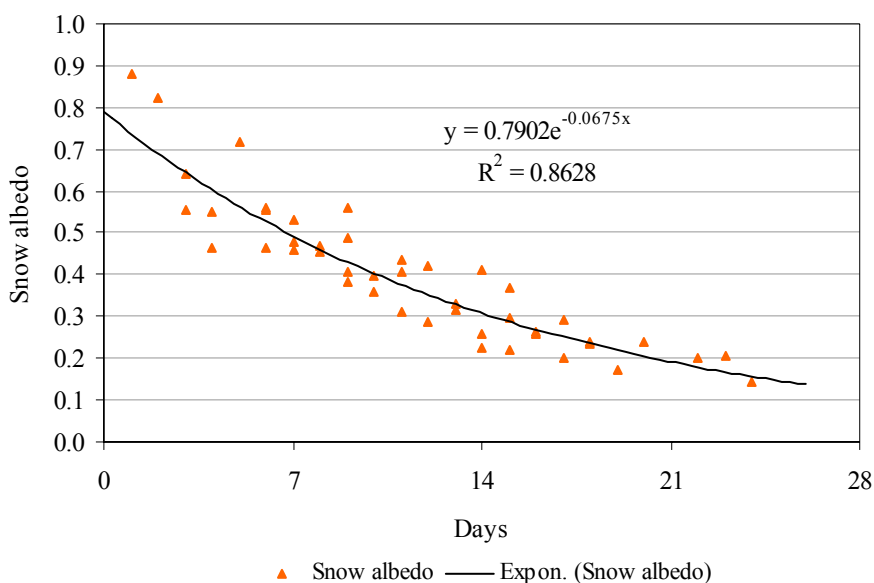


Figure 6.1: Snow albedo values for large snow piles

Figure 6.2 shows the snow albedo data documented for small snow piles from the field study and the exponential relation between snow albedo values and the days of melt. The data are compiled from both snow on sidewalk edges and snow on road shoulders. The exponential relationship is used to determine snow albedo values for small snow piles in USM.

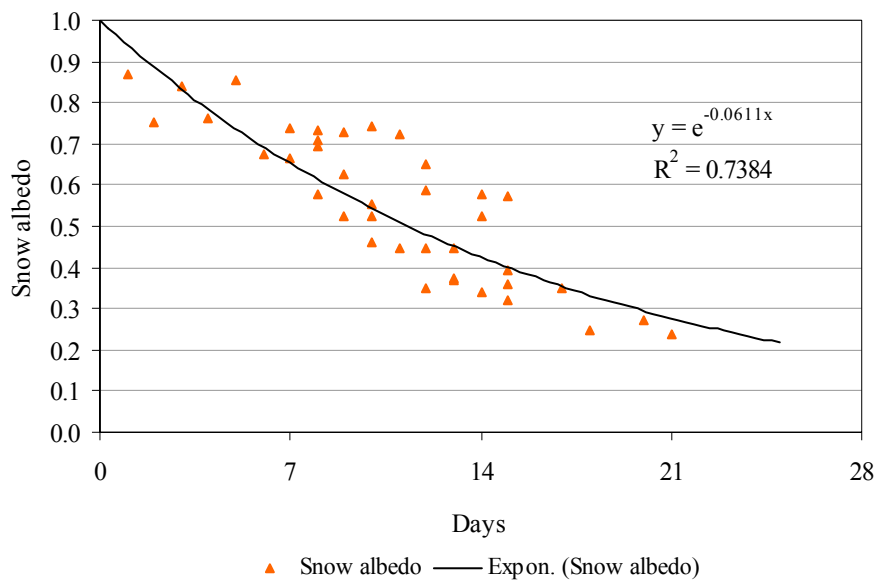


Figure 6.2: Snow albedo values for small snow piles

Figure 6.3 shows the snow albedo data documented for a natural snow cover from the field study and the linear relation between snow albedo values and the days of melt. The linear relation is used to determine snow albedo values for uniform snow covers in USM.

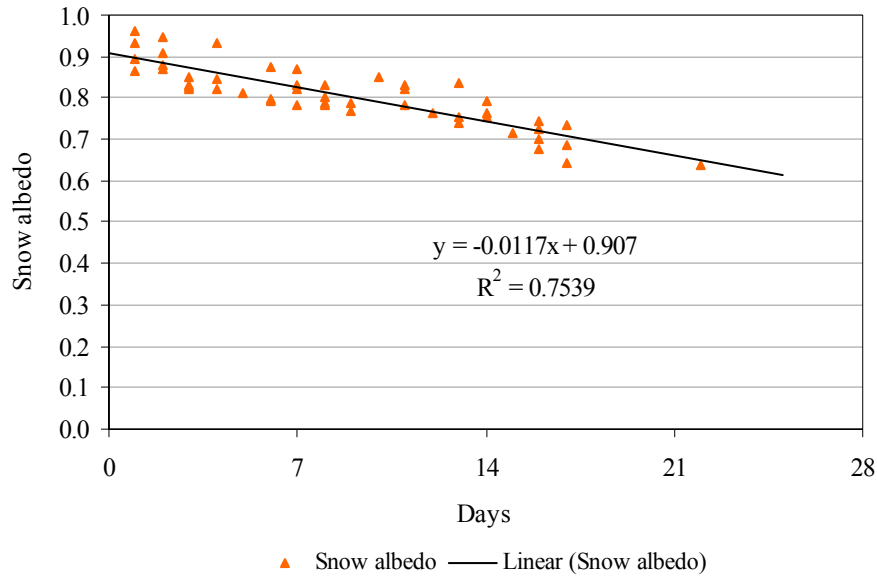


Figure 6.3: Snow albedo values for natural snow cover

### ***Net Longwave Radiation***

The net longwave radiation is calculated as follows:

$$Q_{lw} = Q_a - E_t \quad (34)$$

where  $Q_{lw}$  is the net longwave radiation ( $W/m^2$ -hr);  $Q_a$  is the incoming longwave radiation ( $W/m^2$ -hr); and  $E_t$  is the total emitted longwave radiation ( $W/m^2$ -hr). Measured hourly values of longwave radiation are obtained from meteorological stations.

The total emitted longwave radiation is given by Stefan-Boltzman law:

$$E_t = \varepsilon * \sigma * T^4 \quad (35)$$

where  $E_t$  is the total emitted longwave radiation ( $\text{W}/\text{m}^2$ );  $\epsilon$  is the emissivity in the longwave portion of the energy spectrum;  $\sigma$  is the Stefan-Boltzman constant ( $5.67 \times 10^{-13} \text{ W m}^{-2} \text{ }^\circ\text{K}^{-4}$ ); and  $T$  is the snow surface temperature ( $^\circ\text{K}$ ).

Assuming that the emissivity,  $\epsilon$  is 0.97; and the snow surface temperature is  $0^\circ\text{C}$ , so  $T = 273^\circ\text{K}$ . Substituting into equation 34, it is thus assumed that melting snow constantly emits longwave radiation at  $E_t = 305 \text{ W}/\text{m}^2$ .

### ***Latent and Sensible Heat Transfer***

Latent and sensible heat transfers are turbulent transfer processes. Latent heat is either energy lost from the snowpack due to evaporation and sublimation or energy gained from condensation. Sensible heat is attributed to the heat content of the air. A common equation for the latent heat transfer is (Eagleson, 1970):

$$Q_e = 2359.9 * 8.5 * k_e * (z_t * z_b)^{-\frac{1}{6}} * U_b * (e_a - e_s) \quad (36)$$

where  $z_t$  is the height above surface of air temperature measurements (ft);  $z_b$  is the height above surface of wind speed measurements (ft);  $U_b$  is the wind speed (mi/hr);  $e_a$  is the vapor pressure of atmosphere at temperature and relative humidity at height  $z_t$  (mb);  $e_s$  is the saturation vapor pressure at snow surface temperature (mb)

The factor 2359.9 converts inches to  $\text{W}/\text{m}^2\text{-hr}$ , and the factor 8.5 accounts for the fact that when the snowpack is ripe, the latent heat of condensation will supply latent heat of fusion to melt the snow. Due to the ratio of these latent heats ( $600/80 = 7.5$ ), each inch of

condensate will result in 8.5 (that is, 7.5 + 1) inches of melt. This applies to the evaporation process as well. The coefficient  $k_e$  has been measured in the Sierra Nevada mountain as:

$$k_e = 0.000265 \text{ in/hr ft}^{1/3} \text{ mi/hr mb}^{-1} \quad (37)$$

In USM, the coefficient  $k_e$  is obtained through calibration. Values of  $z_a$ ,  $z_b$ ,  $U_b$ ,  $e_a$ , and  $e_s$  were obtained from the University weather station, and used in the calculation of the latent heat transfer. The resultant values were compared to snow evaporation loss measured in the field study. Hence, the resultant  $k_e$  coefficient is:

$$k_e = 0.000035 \text{ in/hr ft}^{1/3} \text{ mi/hr mb}^{-1} \quad (38)$$

During snowmelt periods, heat is usually transferred from the air to the snowpack, because of the snowpack's colder temperature compared to the air (sensible heat transfer term positive). Similar to latent heat transfer, sensible heat transfer depends on the turbulence of the air. Assuming turbulent transfer coefficients for heat and vapor are equal, sensible heat transfer can be obtained using the Bowen's ratio (Anderson, 1973), expressed as:

$$\frac{Q_h}{Q_e} = \gamma * \frac{T_a - T_o}{e_a - e_o} \quad (39)$$

where  $Q_h$  is the sensible heat transfer ( $\text{W/m}^2\text{-hr}$ );  $Q_e$  is the latent heat transfer ( $\text{W/m}^2\text{-hr}$ );  $\gamma$  is the psychrometric constant ( $\text{mb } ^\circ\text{C}^{-1}$ ) ( $\gamma = 0.00057 P_a$ , where  $P_a$  (mb) is the atmospheric pressure);  $T_o$  is the snow surface temperature ( $^\circ\text{C}$ );  $T_a$  is the temperature of the air at  $z_a$  ( $^\circ\text{C}$ );  $e_a$  is the vapor pressure of the air at  $z_t$  (mb); and  $e_o$  is the vapor pressure

at the snow surface (mb) (assumed equal to the saturation vapor pressure at the snow surface temperature).

Thus, resulting expression for sensible heat transfer is:

$$Q_h = Q_e * \gamma * \frac{T_a - T_o}{e_a - e_o} \quad (40)$$

### ***Heat advection by Rain***

The temperature of rain falling upon the snowpack is usually higher than the temperature of the snowpack. Thus, heat transfer occurs from the raindrops into the snowpack. The quantity of heat transferred to the snowpack is dependent on the amount and temperature of the rain.

$$Q_m = \frac{2359.9}{144} * P_r * (T_r - T_s) \quad (41)$$

where  $Q_m$  is the heat advected by rain ( $W/m^2$ -hr);  $P_r$  is the rainfall intensity (in/hr);  $T_r$  is the air temperature ( $^{\circ}F$ ); and  $T_s$  is the snow surface temperature ( $^{\circ}F$ ).

Equation 40 is based on the relationship between heat required to melt ice (144 Btu/lb of ice) and the amount of heat released by a pound of water when its temperature is decreased by one degree.

## 6.5 Areal Depletion Curve

Areal depletion curve is used to determine the areal extent of the snow cover at any given time. The areal extent of snow cover on a catchment is determined by the fraction of area covered by snow, ASC, on the areal depletion curve. It is assumed that for all the subcatchments, there is a depth, SnowD, above which there is always 100% cover. In USM, the value of SnowD is fixed at 10 mm. The snow water equivalent depth present on the subcatchments at any time is indicated by the parameter Swe. This depth is nondimensionalized by SnowD to calculate ASC. Thus patches of bare ground will only appear after snowmelt reduces Swe to less than 10 mm. The fraction ASC is used to adjust the volume of melt that occurs, since heat transfer occurs only over the snow covered areas. Snow depth at time step 2 is then reduced from time step1 according to:

$$\text{Swe}_2 = \text{Swe}_1 - (\text{M}_{\text{sr}} * \text{ASC}) \quad (42)$$

Figure 6.4 shows the areal depletion curve used in this urban snow model to determine ASC. This curve is developed using data obtained from the University weather station. The University weather station carries out manual observations of depths of snow and the approximate percentages of snow covered area at the observation compound. There is insufficient documentation from the field study to develop different areal depletion curves for different snow cover types.

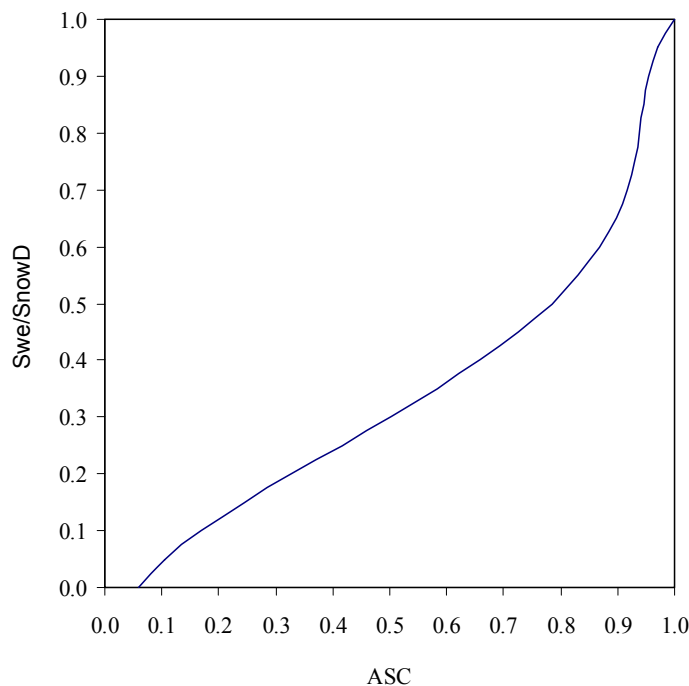


Figure 6.4: Areal Depletion Curve

## 6.6 Liquid Water Routing in Snowpack

Snowpack is a porous medium that has a certain “free water holding capacity” at any given time. Thus, not all melt immediately results in runoff. Following the computer model SWMM (Huber, 1988), the free water holding capacity is assumed to be a constant fraction,  $F_r$ , of the variable snow depth,  $Swe$  at each time step. The value of  $F_r$  is normally less than 0.10 and usually between 0.02-0.05 for deep snow packs (Huber, 1988). The free water holding capacity for each subcatchment is computed as follows (Huber, 1988):

$$FWC = F_r * Swe \quad (43)$$

where FWC is the free water holding capacity (mm);  $F_r$  is a fraction of snow depth; and Swe is the snow depth at any time step in water equivalent (mm). In USM,  $F_r$  is assumed to be 0.08 for natural snow cover, and 0.03 for snow piles.

The volume of the snowpack's free water holding capacity must be satisfied before runoff can be produced. By including the free water holding capacity of the snowpack in the simulation, runoff can be delayed and attenuated.

### **6.7 Infiltration into Frozen Ground**

Analysis from the field study revealed that frozen ground acts as a near impervious surface regardless of the condition of the initial soil moisture content. Thus, infiltration of snowmelt into frozen ground is minimal and assumed negligible in USM.

### **6.8 Net Runoff**

Runoff from snowmelt is produced after the free water holding capacity from snowpack is fulfilled. Net runoff is a combination of areal weighted snowmelt runoff from snow covered areas, and rainfall falling on bare grounds.

$$N \text{ Runoff} = ASC * M_{sr} + (1.0 - ASC) * P_{xmm} \quad (44)$$

where NRunoff is the net runoff (mm/hr); and  $P_{xmm}$  is the rainfall intensity (mm/hr).

## 6.9 Input Variables

Input variables in this program are divided into user-defined values and recorded values from a weather station. Table 6.2 shows the input variables that need user-defined values to simulate catchment schematization. All the values are hypothetical.

Table 6.2: User-defined input variables used to simulate catchment schematization

<b>Input Variables</b>	<b>Description</b>
$T_c$	Total catchment area (m <sup>2</sup> )
Perv	Total pervious area (m <sup>2</sup> )
Imperv	Total impervious area (m <sup>2</sup> )
$t_1$	Total Type 1 subcatchment area (m <sup>2</sup> )
$t_2$	Total Type 2 subcatchment area (m <sup>2</sup> )
$t_3$	Total Type 3 subcatchment area (m <sup>2</sup> )
$t_5$	Estimated Type 5 subcatchment area (m <sup>2</sup> )
$t_6$	Estimated Type 6 subcatchment area (m <sup>2</sup> )

Table 6.3 shows the user-defined input variables needed to simulate snow redistribution, and Table 6.4 shows the meteorological data needed by the program to calculate snow melt rate.

Table 6.3: User-defined input variables used to simulate snow redistribution

<b>Input Variables</b>	<b>Description</b>
$I_{swe}$	Initial SWE depth over the catchment area (mm)
BaseDeptht1	SWE depth for Type 1 subcatchment, above which redistribution occurs (mm)
BaseDeptht2	SWE depth for Type 2 subcatchment, above which redistribution occurs (mm)
BaseDeptht3	SWE depth for Type 3 subcatchment, above which redistribution occurs (mm)
$F_{t1a}$	Fraction of excess SWE in Type 1 subcatchment redistributed by plowing into big snow piles onto adjacent pervious area
$F_{t1b}$	Fraction of excess SWE in Type 1 subcatchment redistributed by plowing into small snow piles onto adjacent pervious area
$F_{t1c}$	Fraction of excess SWE in Type 1 subcatchment redistributed by trucking onto pervious area of another catchment
$F_{t2a}$	Fraction of excess SWE in Type 2 subcatchment redistributed by plowing into big snow piles onto adjacent pervious area
$F_{t2b}$	Fraction of excess SWE in Type 2 subcatchment redistributed by plowing into small snow piles onto adjacent pervious area
$F_{t2c}$	Fraction of excess SWE in Type 2 subcatchment redistributed by trucking onto pervious area of another catchment
$F_{t3a}$	Fraction of excess SWE in Type 3 subcatchment redistributed by plowing into big snow piles onto adjacent pervious area
$F_{t3b}$	Fraction of excess SWE in Type 3 subcatchment redistributed by plowing into small snow piles onto adjacent pervious area
$F_{t3c}$	Fraction of excess SWE in Type 3 subcatchment redistributed by trucking onto pervious area of another catchment

Table 6.3: User-defined input variables used to simulate snow redistribution (continued)

<b>Input Variables</b>	<b>Description</b>
$t_8$	Total area of pervious area of another catchment where redistributed snow is destined ( $m^2$ ) (only when option (c) is selected)

Table 6.4: Input variables needed to calculate snow melt rate

<b>Input Variables</b>	<b>Description</b>
$Q_i$	Incoming shortwave radiation ( $W/m^2$ -hr)
$Q_a$	Incoming longwave radiation ( $W/m^2$ -hr)
$U_b$	Wind speed (mi/hr)
$e_a$	Atmospheric vapor pressure (mb)
$P_a$	Surface atmospheric pressure (mb)
$T_a$	Air temperature ( $^{\circ}C$ )
$T_r$	Air temperature ( $^{\circ}F$ )
$P_r$	Rainfall intensity (in/hr)
$P_{xmm}$	Rainfall intensity (mm/hr)

## 6.10 Output Files

The program produces an output file that summarizes the simulation of the subcatchment schematization and also snow removal and redistribution. The simulation also produces 22 figures as listed in Table 6.5:

Table 6.5: Resultant graphs from simulation

<b>Figures</b>	<b>Titles</b>
1	(a) Hourly Incoming Shortwave Radiation (b) Hourly Net Shortwave Radiation for Large Snow Piles
2	(a) Hourly Net Shortwave Radiation for Small Snow Piles (b) Hourly Net Shortwave Radiation for Uniform Snow Cover
3	(a) Hourly Incoming Longwave Radiation (b) Hourly Net Longwave Radiation
4	(a) Hourly Latent Heat Transfer (b) Hourly Sensible Heat Transfer
5	Hourly Advected Heat Transfer from Rain
6	(a) Melt Rate for Large Snow Piles (b) Melt Rate for Small Snow Piles (c) Melt Rate for Uniform Snow Cover
7	Net Runoff Rate for Type 1 subcatchment
8	Net Runoff Rate for Type 2 subcatchment
9	Net Runoff Rate for Type 3 subcatchment
10	Net Runoff Rate for Type 4 subcatchment
11	Net Runoff Rate for Type 5 subcatchment
12	Net Runoff Rate for Type 6 subcatchment
13	Net Runoff Rate for Type 7 subcatchment
14	Net Runoff Volume for Type 1 subcatchment
15	Net Runoff Volume for Type 2 subcatchment
16	Net Runoff Volume for Type 3 subcatchment
17	Net Runoff Volume for Type 4 subcatchment

Table 6.5: Resultant graphs from simulation (continued)

<b>Figures</b>	<b>Titles</b>
18	Net Runoff Volume for Type 5 subcatchment
19	Net Runoff Volume for Type 6 subcatchment
20	Net Runoff Volume for Type 7 subcatchment
21	Total Net Runoff Volume for the Whole Catchment

### 6.11 Simulations of Urban Snowmelt

Urban snowmelt is simulated for three different scenarios. The three different scenarios determine the effects of simulation of snow redistribution on runoff, and the effects of rain-on-snow event on the runoff. Table 6.6 describes the three simulation scenarios.

Table 6.6: Simulation scenarios description

<b>Simulation</b>	<b>Description</b>
A	Single event snowfall with no rain-on-snow event, and snow is redistributed
B	Single event snowfall with rain-on-snow event, and snow is redistributed
C	Single event snowfall with no rain-on-snow event, and snow is not redistributed. Snow on impervious area uses snow albedo values for small piles

### ***Objectives of Simulation A***

Simulation A is carried out to discern any similarities or differences between different urban snow cover types. It also determines the contribution of each snow cover types to the total runoff volume. Results from simulation A will also be used as a basis of comparison for results from simulation B and simulation C.

### ***Objectives of Simulation B***

Simulation B is carried out to determine the effects of rain during snowmelt period on the runoff.

### ***Objectives of Simulation C***

Simulation C is carried out to determine the effects of simulation of a snow cover without redistribution on the runoff.

## **6.12 Results and Analysis of Simulations**

This section describes the results and analysis of each simulation. Only pertinent resultant graphs will be presented here.

### 6.12.1 Results and Analysis of Simulation A

#### *User-defined input values*

Simulation A is a single event simulation with no rain-on-snow event. The input values for the user-defined variables for simulation A are shown in Table 6.7.

Table 6.7: Values for the user-defined input variables for simulation A

<b>Input Variables</b>	<b>Values</b>
$T_c$	2,000,000 m <sup>2</sup>
Perv	700,000 m <sup>2</sup>
Imperv	1,300,000 m <sup>2</sup>
$t_1$	500,000 m <sup>2</sup>
$t_2$	645,000 m <sup>2</sup>
$t_3$	150,000 m <sup>2</sup>
$t_5$	15,000 m <sup>2</sup>
$t_6$	100,000 m <sup>2</sup>
$I_{swe}$	15 mm
BaseDeptht1	5 mm
BaseDeptht2	8 mm
BaseDeptht3	2 mm
$F_{t1a}$	1.0
$F_{t1b}$	0
$F_{t1c}$	0

Table 6.7: Values for the user-defined input variables for simulation A (continued)

<b>Input Variables</b>	<b>Values</b>
$F_{t2a}$	0.3
$F_{t2b}$	0.7
$F_{t2c}$	0
$F_{t3a}$	0
$F_{t3b}$	1.0
$F_{t3c}$	0
$t_8$	0

### ***Meteorological data***

Recorded hourly meteorological data used in this simulation was obtained from the University weather station. Wind speed and air temperature are measured at heights of 2 meters. The atmospheric vapor pressure is calculated using air temperature and relative humidity.

### ***Snow redistribution***

Snow is redistributed from the impervious areas onto adjacent pervious areas. This result in three different snow cover types: large snow piles, small snow piles and a uniform snow cover. The redistribution also results in the seven snow cover-land surface combinations discussed earlier in Section 6.2. Large snow piles results from snow plowed

from parking lots and roadways. Small snow piles comprised of snow on road shoulders, snow on sidewalk edges, and snow shoveled from driveways. Uniform snow cover is natural snow cover on unused parks, undisturbed lawns and snow on rooftops. The snow on impervious areas that is not redistributed, BaseDepth, is melted the same way as a uniform snow cover.

***Snow water equivalent available after redistribution***

After redistribution, the available snow depth for melt for each snow cover-land surface subcatchment combination will be different. The snow water equivalent available for each subcatchment type for simulation1 is shown in Table 6.8.

Table 6.8: Snow depth available for melt for each subcatchment type

<b>Subcatchment type</b>	<b>Snow Depth (mm)</b>
1	5.00
2	8.00
3	2.00
4	15.00
5	438.63
6	66.10
7	15.00

### *Change in heat storage of the snowpack*

The change in heat storage of the snowpack is the sum of all the energy transfer to or from the snowpack. Figure 6.5 shows the energy flux for large snow piles. The energy balance is dominated by radiation, and the main source of energy to melt the snowpack comes from the shortwave radiation. Thus, snow albedo is an important factor as it influences the amount of shortwave radiation adsorbed by the snowpack.

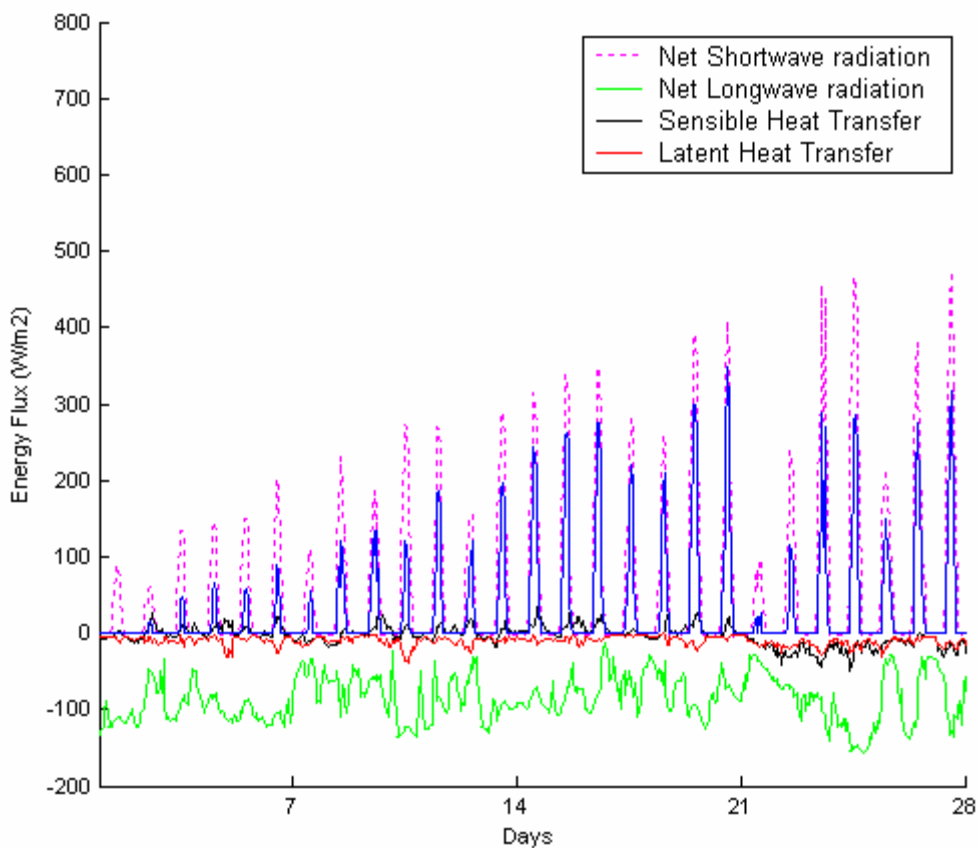


Figure 6.5: Energy flux for large snow piles

### ***Melt rates***

Three different melt rates are produced for the three different snow cover types due to the influence of the different snow albedo values and the rates of decrease of the snow albedo. Figure 6.6 shows the resultant melt rates for simulation A. Large snow piles produces the highest melt rate, and melt also starts several days earlier than a uniform snow cover. Melt rates for small snow piles are similar to the large snow piles, only the intensity of melt is lower. The uniform snow cover has the lowest melt rate due to its high snow albedo values and slow rate of decrease for snow albedo compared to the other two snow cover types. For all three snow cover types, melt rates increases with time largely due to the decreasing snow albedo values.

### ***Runoff rates and runoff period***

Runoff rates for each of the subcatchment type is influenced by their available snow depth (in water equivalent), and melt rates. Figure 6.7 shows the runoff rates for type 5 subcatchment, Figure 6.8 shows the runoff rates for type 6 subcatchment, and Figure 6.9 shows the runoff rates for type 7 subcatchment. Runoff rates for subcatchment types 1, 2, 3, and 4 are not of real interest as they have low snow depths and the snow are melted the same way as a uniform snow cover.

A comparison of the runoff rates for subcatchment types 5, 6, and 7 revealed significant differences. For subcatchment type 5, which is covered with snow piles, the runoff rates are significantly higher than subcatchment type 6 (covered with small snow piles), and subcatchment type 7 (uniformly snow covered). This is the result of the high melt rates for large snow piles. A distinct difference between runoffs for the three subcatchment types is the runoff period. Uniform snow cover has the shortest runoff period followed by

small snow piles. Runoff for large snow piles can be extended for several weeks compared to the uniform snow cover. However, regardless of the intensity of the runoff, all types of snow cover produces runoff that is sustained over a period of days to weeks.

Runoff rates for uniformly snow covered subcatchments shows a sharp increase, which is then sustained over several days. This is attributed to the low snow depth over the subcatchment. As free water holding capacity of the snowpack is filled, liquid melt is released from the snowpack, causing a sudden peak in runoff rates. The runoff rate is sustained at similar intensity probably due to the slow decrease in snow albedo values that prevents higher adsorption of shortwave radiation, and thus higher melt release.

Runoff rates for small snow piles show a general trend of increase at a high rate. It is due to the exponential decrease in snow albedo, thus resulting in higher adsorption of shortwave radiation. Similarly, runoff rates for large snow piles also show a high rate of increase in runoff intensity over time.

### ***Runoff volume***

To investigate the effects of the characteristics of each of the snow cover types on runoff, it is important to compare their runoff volumes. The runoff volume for subcatchment types 5, 6, and 7 is shown in Figure 6.10, 6.11, and 6.12 respectively. A comparison of these three figures show that uniformly snow covered subcatchments produces the highest runoff volume, followed by subcatchments covered by small snow piles, and subcatchments covered by large snow piles produces the lowest runoff volume. This is due to the fact that total subcatchment area covered by a uniform snow cover is much larger than total subcatchment area covered by large snow piles.

The three figures also show significant difference in the flow of the runoff. For uniformly snow covered subcatchments, flow peaks sharply for several days and then drops quite sharply too. For subcatchments covered with small snow piles, runoff flow increases gradually but then drops sharply. For subcatchments covered with large snow piles, runoff flow remains quite low but increases in volume with time, and runoff is sustained over a long period. The distinct flow pattern for each subcatchment type is the result of the combination of its available snow depth, runoff rates, and area size.

### ***Total runoff over the whole catchment***

Figure 6.13 shows the total runoff volume for the whole catchment simulated. Runoff at the onset of the melt period consists mainly of melt from small snow piles. The peak runoff volume is contributed mainly by both small snow piles and uniform snow cover. Runoff at the end of the melt period is contributed mainly by large snow piles. This simulation demonstrates that the various urban snow cover each contributes significantly to the net runoff volume.

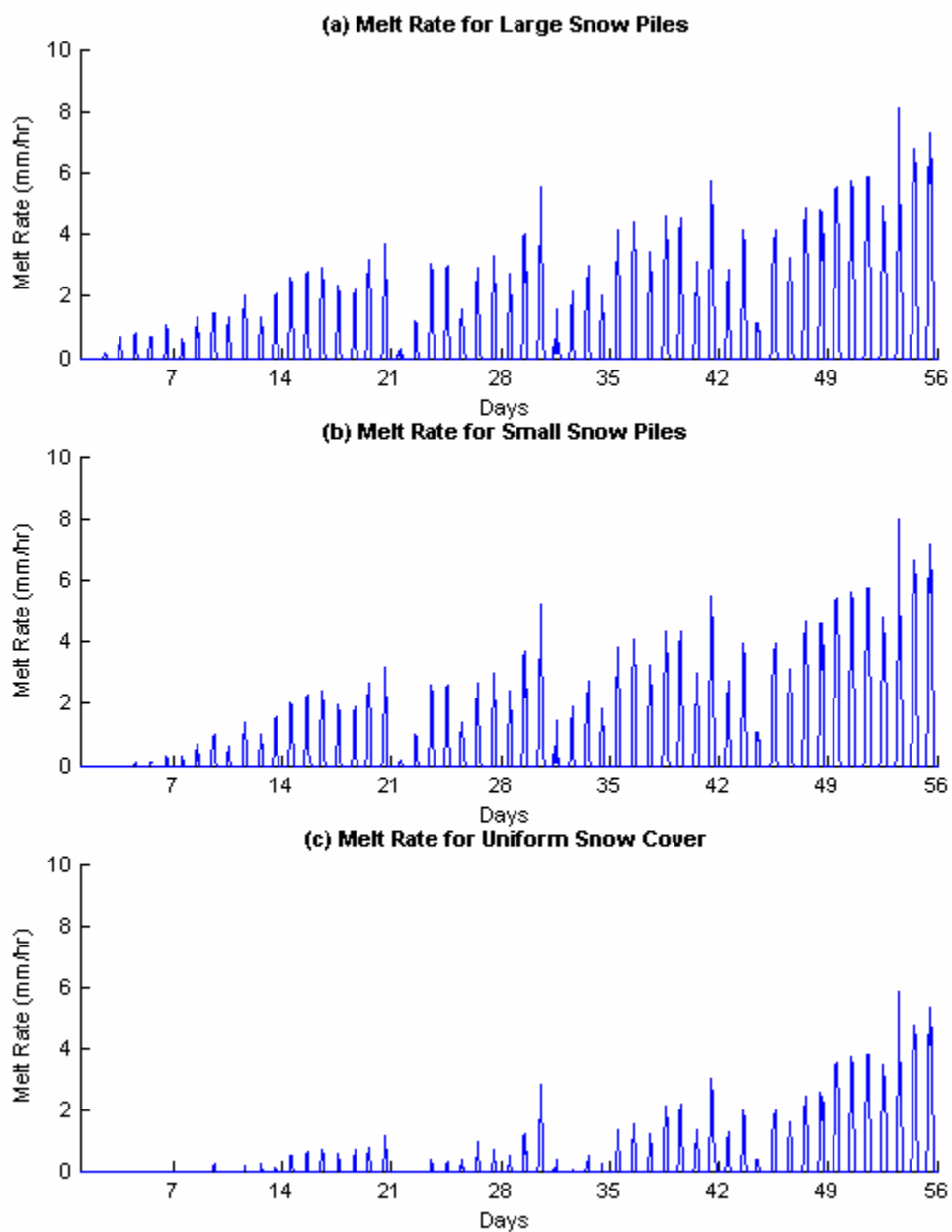


Figure 6.6: (a) Melt rate for large snow piles; (b) Melt rate for small snow piles; and (c) Melt rate for uniform snow cover

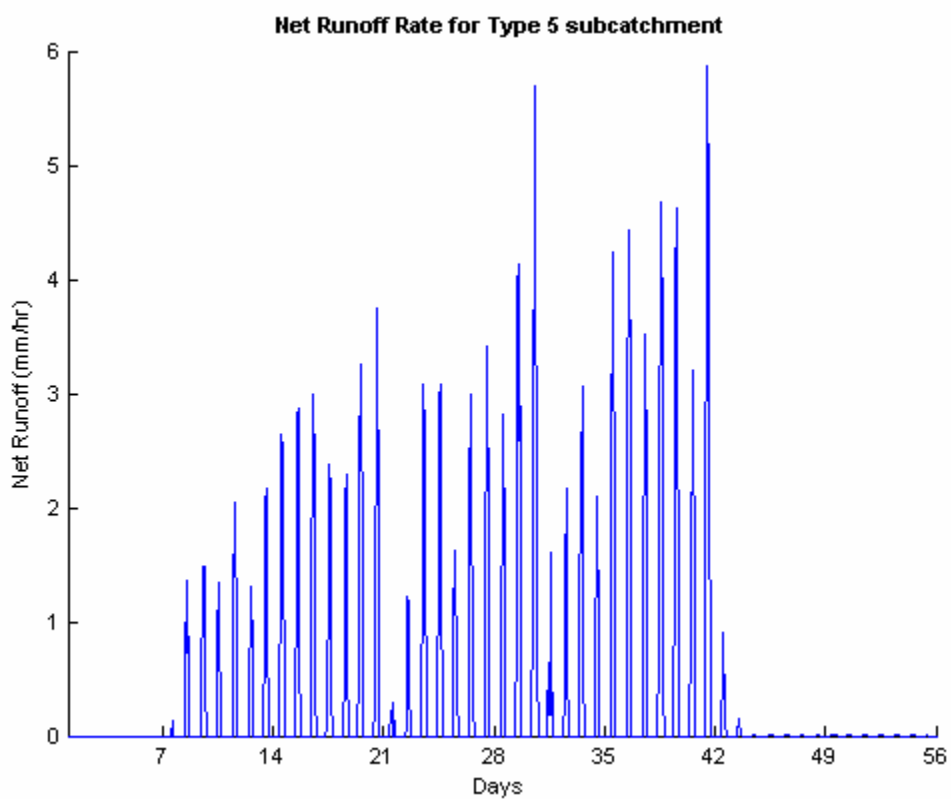


Figure 6.7: Runoff rates for subcatchment type 5 (large snow piles)

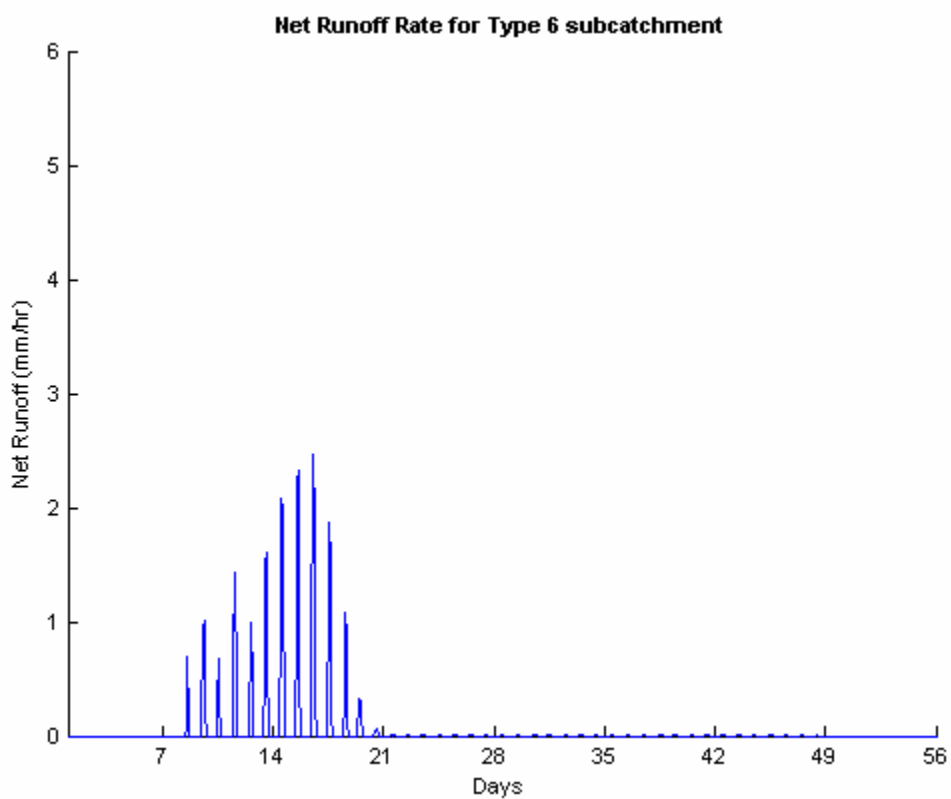


Figure 6.8: Runoff rates for subcatchment type 6 (small snow piles)

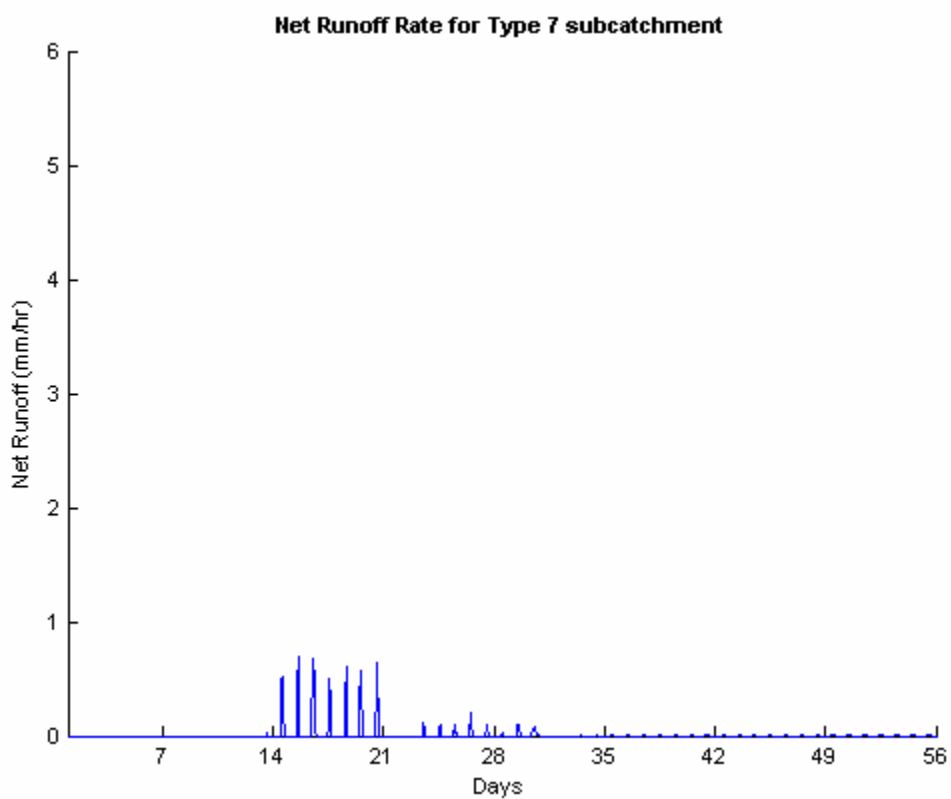


Figure 6.9: Runoff rates for subcatchment type 7 (uniform snow cover)

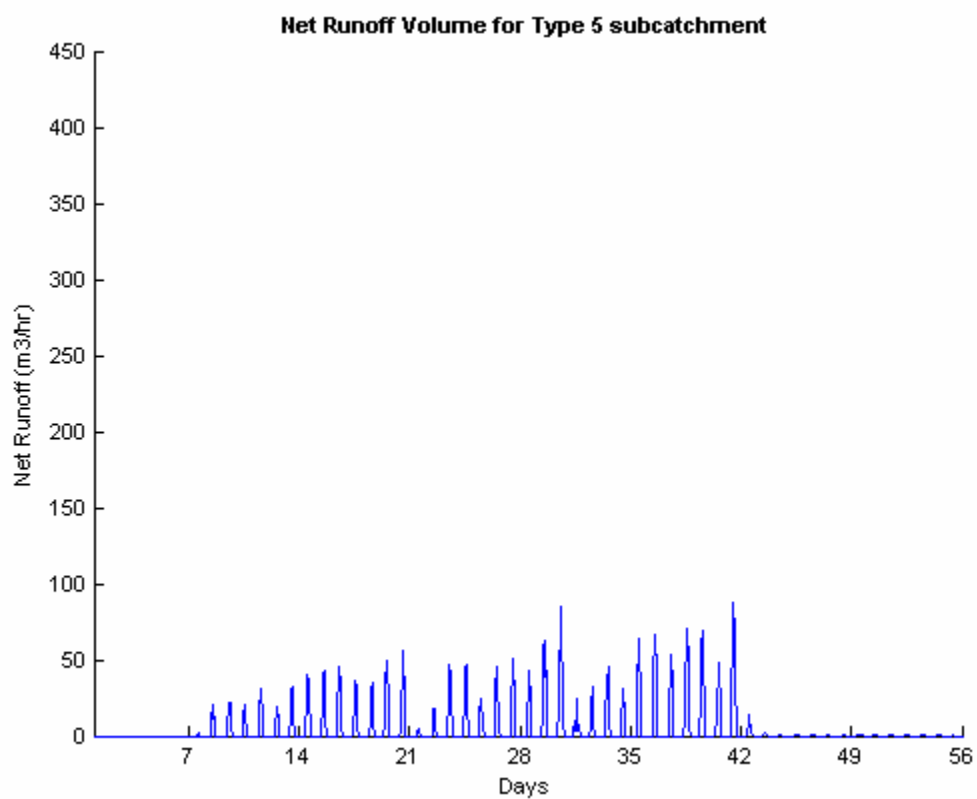


Figure 6.10: Runoff volume for subcatchment type 5 (large snow piles)

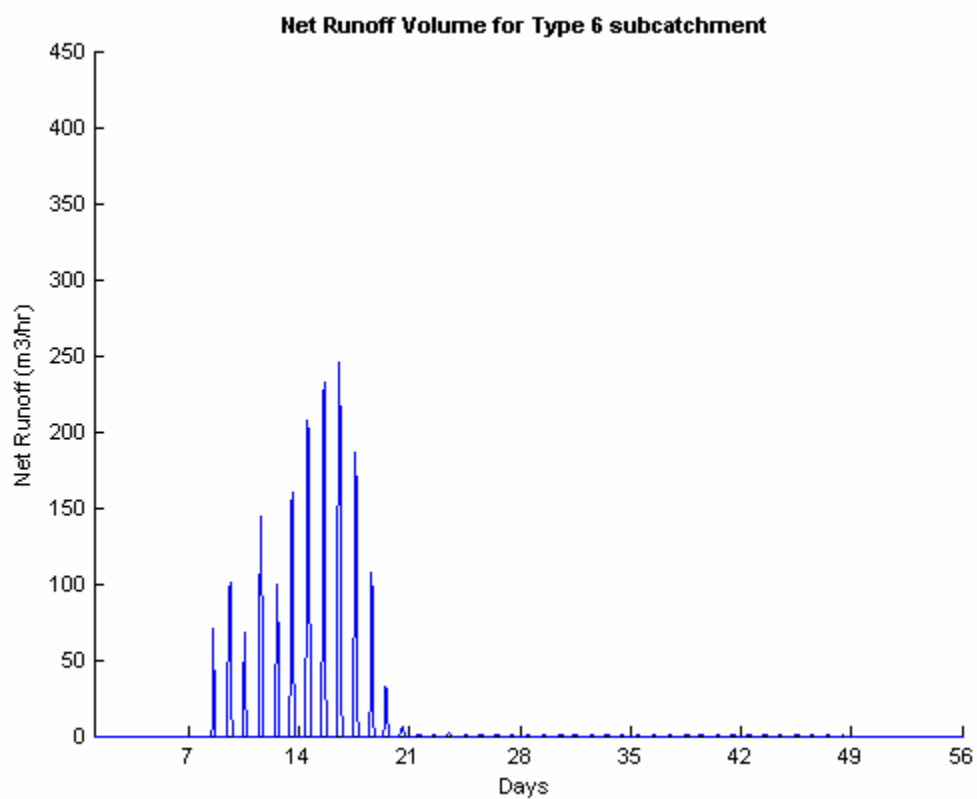


Figure 6.11: Runoff volume for subcatchment type 6 (small snow piles)

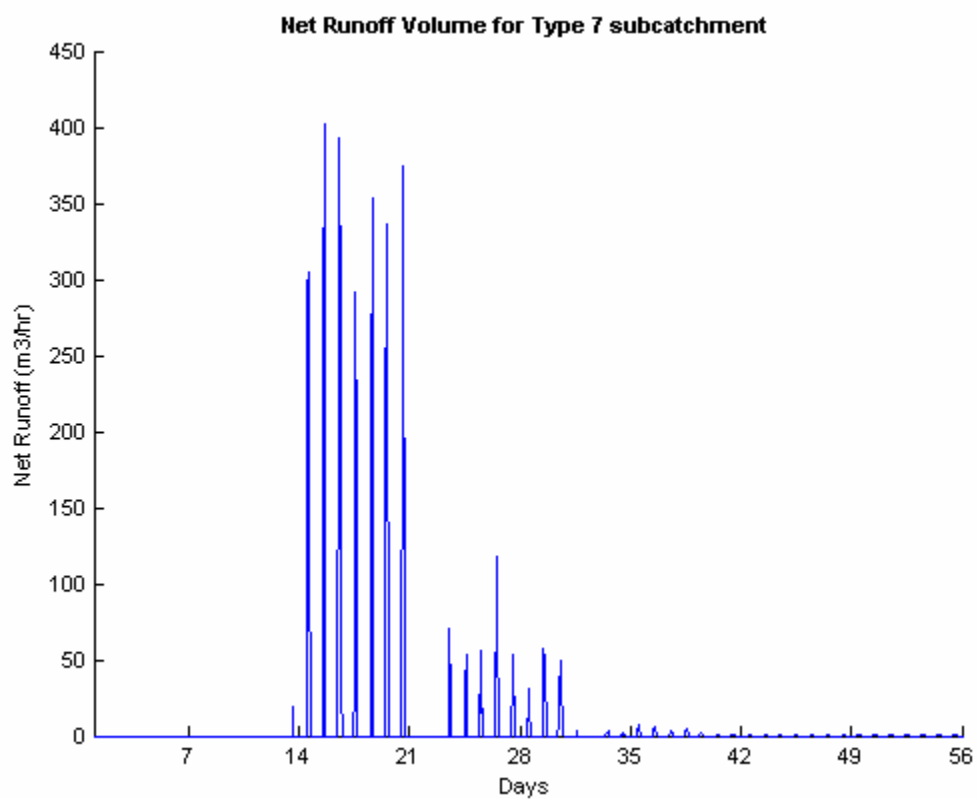


Figure 6.12: Runoff volume for subcatchment type 7 (uniform snow cover)

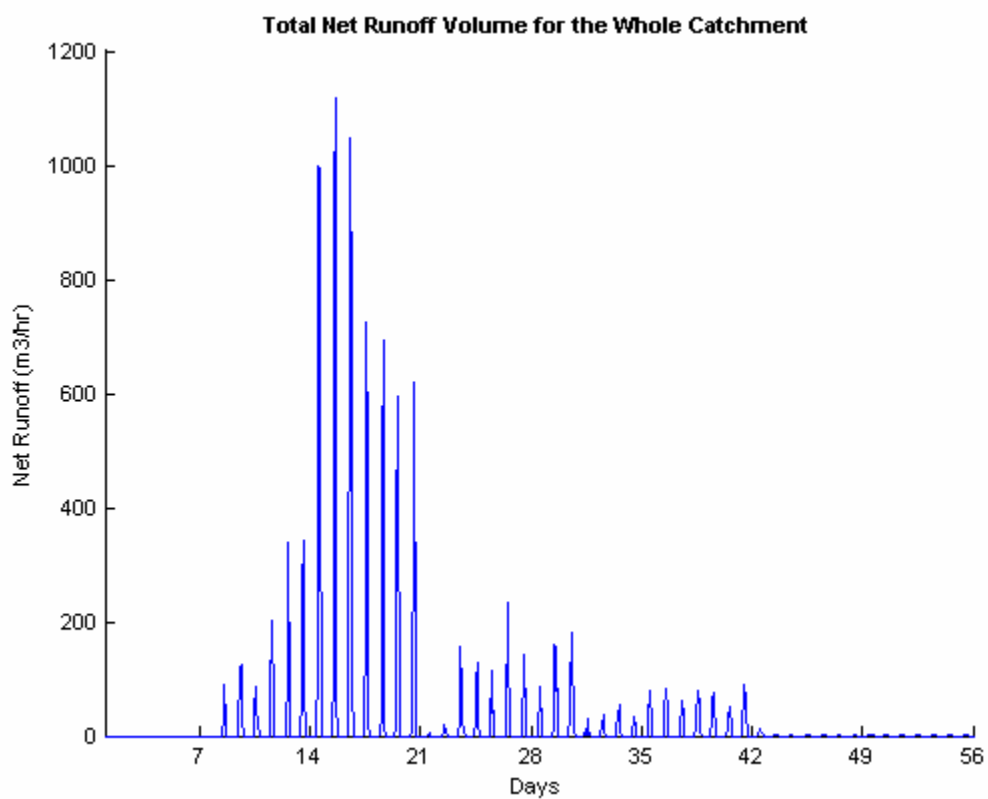


Figure 6.13: Total runoff volume for the whole catchment

### 6.12.2 Results and Analysis of Simulation B

Simulation B is a repetition of simulation A, but with an added component to the heat transfer of the snowpack. Rainfall of 2 – 2.5 mm per hour is simulated over a nine hour period on day 14 into the snowmelt period.

#### *Change in heat storage of the snowpack and melt rates*

Change in heat storage of the snowpack for this simulation only differs from simulation A on day 14 where there is an added heat into the snowpack from the rain. Figure 6.14 shows the advected heat from rain into the snowpack. For the rain intensity simulated, the contribution of advected heat from rain is still small compared to energy adsorbed from shortwave radiation. Therefore, there is only a slight increase in the melt rate of the snowpack.

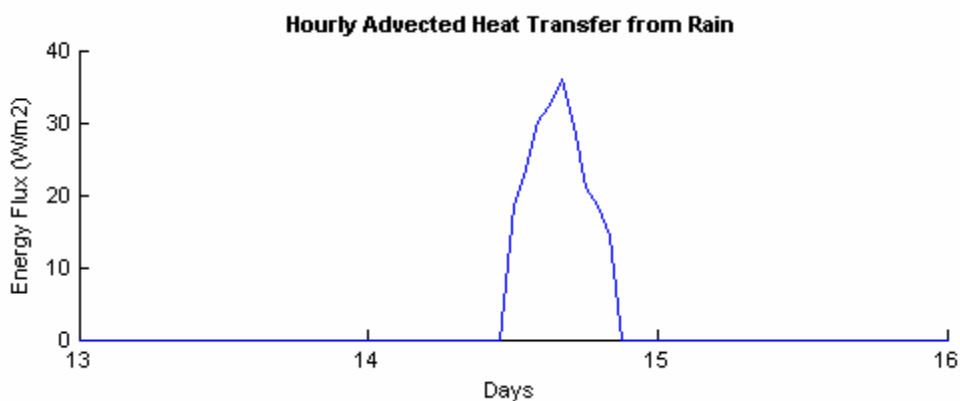


Figure 6.14: Advected heat rain from rain into the snowpack

### *Runoff rates*

Runoff rates for large impervious areas with very thin snow cover such as parking lots experience an instantaneous spike due to the fact that by day 14 of the melt period, a large portion of the subcatchment is bare, thus facilitating immediate runoff. Figure 6.15 shows the runoff rates for subcatchment type 1 (parking lots). Similarly, impervious subcatchment types 2 and 3 experience similar spikes in their runoff rates.

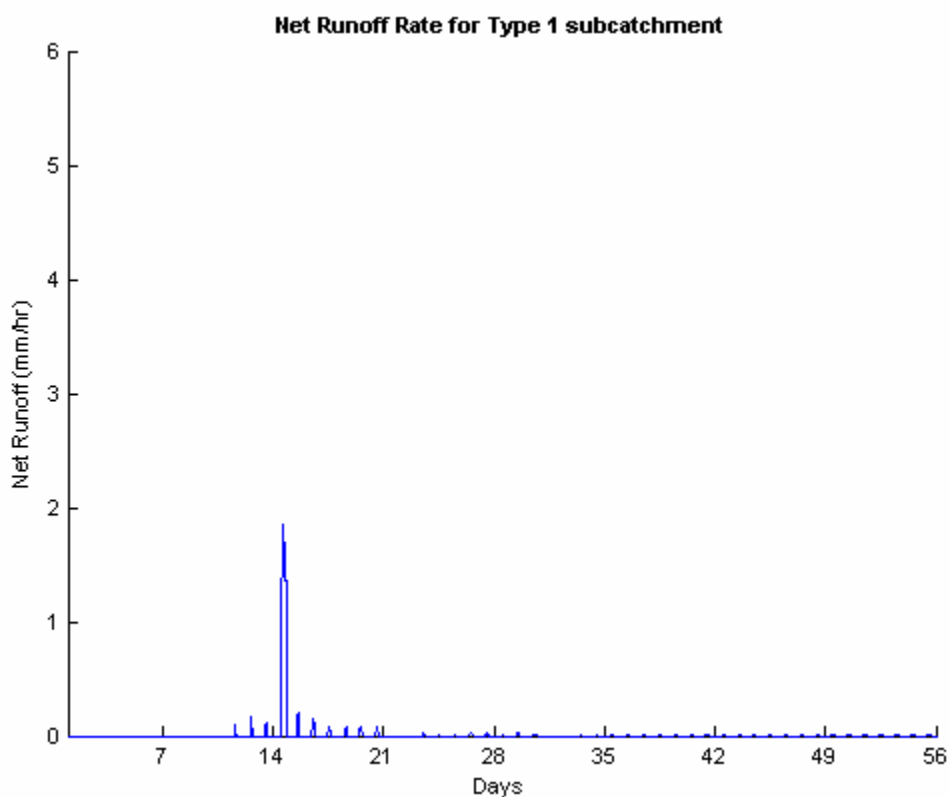


Figure 6.15: Runoff rates for impervious subcatchment type 1 (parking lots)

Runoff rates for subcatchments covered with snow piles, large or small shows a very slight increase in the runoff rates on the day when the rain was simulated. Since snow depth for these two subcatchments are very high, the whole area is still 100% snow covered when the rain was simulated. Thus, any increase in runoff rate is due to increase in snowmelt from additional heat advected from rain. For uniform snow cover in pervious areas, at the time of the simulation of the rainfall, the subcatchment is also 100% snow covered. Thus, the increase in runoff rates for subcatchment type 7 is also small.

### ***Runoff volume***

Runoff volume for subcatchment types 1, 5 and 7 is shown in Figure 6.16, Figure 6.17, and Figure 6.18 respectively. Runoff volume for impervious areas shows a dramatic increase in runoff volume on the day the rain was simulated due to the high runoff rate and the large area size that is no longer snow covered. Runoff volume for areas covered with large snow piles shows no discernible change in the runoff volume, while runoff volume for pervious areas with uniform snow cover experiences an increase of about 200 m<sup>3</sup>/hr. Area size for snow piles is very small compared to the uniform snow cover, so this is reflected in the runoff volume difference between the two cover types, although both have similar increase in runoff rates.

### ***Total runoff over the whole catchment***

Total runoff over the whole catchment for simulation B is shown in Figure 6.19. The total runoff demonstrates the effects of rain-on-snow. Runoff volume peak increases about 1600 m<sup>3</sup>/hr and the time to peak changed from day 15 of the melt period to day 14, when the rainfall was simulated. This simulation shows that rain-on-snow can easily increase

the volume of winter runoff and causes flood conditions. In addition, frozen ground results in minimal infiltration, and thus flood can easily occur during spring melt when pervious areas are also largely bare.

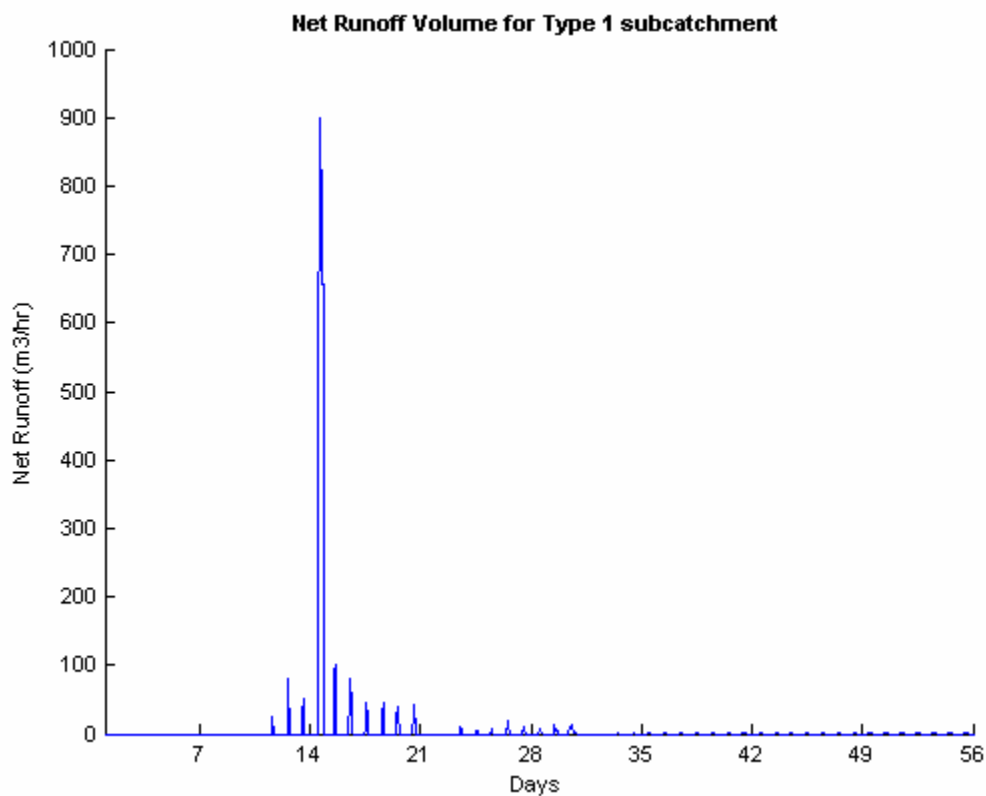


Figure 6.16: Runoff volume for subcatchment type 1 (parking lots)

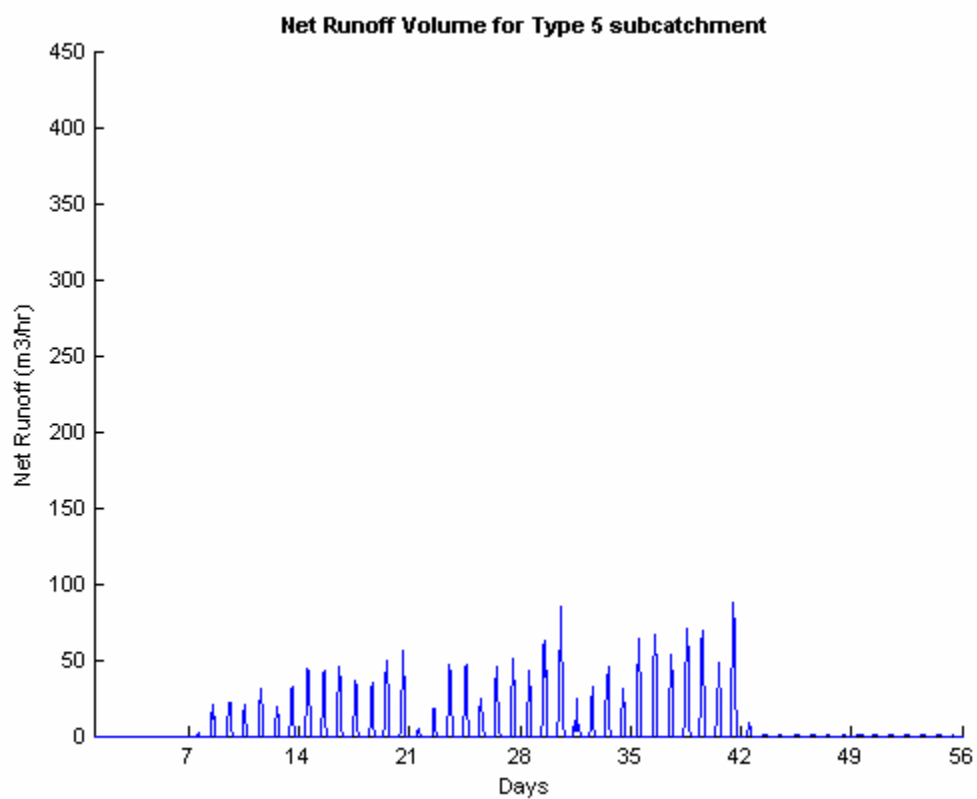


Figure 6.17: Runoff volume for subcatchment type 5 (large snow piles)

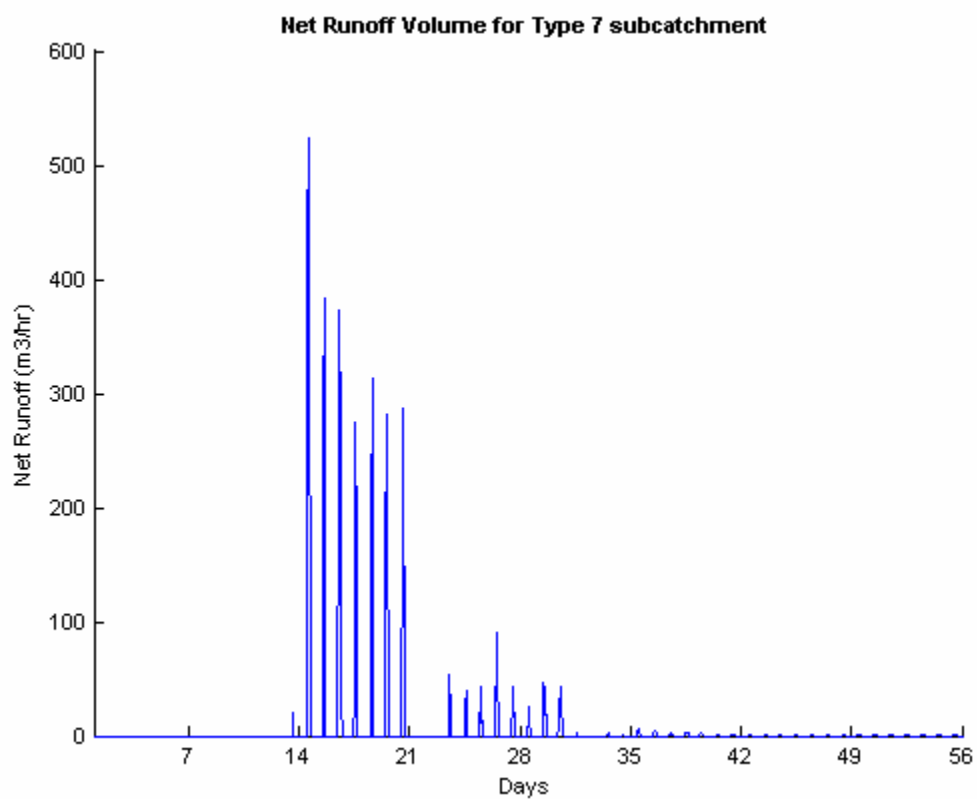


Figure 6.18: Runoff volume for subcatchment type 7 (uniform snow cover)

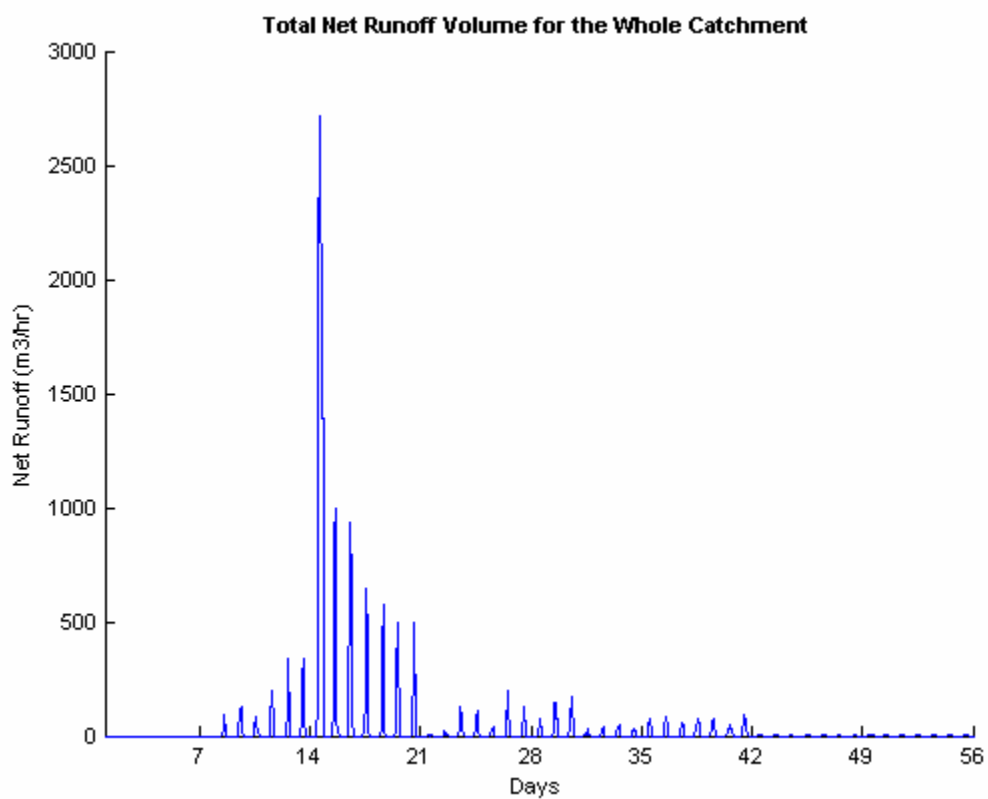


Figure 6.19: Total runoff volume for the whole catchment

### 6.12.3 Results and Analysis of Simulation C

Simulation C is also a repetition of simulation A, but without simulating snow redistribution. Therefore, all snow cover in simulation C is uniform, and subcatchment types 5 and 6 are not simulated. All the snow on impervious areas adopts snow albedo values from small snow piles. This is done to reflect the typically low albedo values of snow on impervious surfaces in urban areas.

#### *Change in heat storage of the snowpack and melt rates*

Since albedo of snow on impervious areas are simulated following small snow piles, melt rate of snow on impervious areas then mirrors melt rates for small snow piles in simulation A. Melt rates for snow on pervious areas remains the same as that of a uniform snow cover.

#### *Runoff rates*

Runoff rates for snow on all impervious areas increases at a high rate and peaks within a few days after free water holding capacity of the snowpack is filled. This is due to the exponential decrease of snow albedo, which allows higher adsorption of shortwave radiation, the main source of melt energy. Runoff is sustained for a period of ten days. Figure 6.20 shows the runoff rates for snow on impervious subcatchment type 1. As for snow on pervious areas, runoff rates remains unchanged from those observed on simulation A.

### ***Runoff volume***

Runoff volumes for impervious areas are much higher in this simulation compared to simulation A. As expected, runoff volume pattern is the same for all impervious area types. Figure 6.21 shows the runoff volume for subcatchment type 1. Compared to runoff from simulation A, intense runoff from impervious areas in this simulation begins on day 7, whereas in simulation A, it only begins on day 11.

### ***Total runoff over the whole catchment***

Total runoff for the whole catchment for simulation C is shown in Figure 6.22. The total runoff for this simulation shows a marked difference from total runoff for simulation A. Peak runoff for this simulation increases about 200 m<sup>3</sup>/hr compared to peak runoff from simulation A. Time to peak also changed from day 15 on simulation A to day 11 in this simulation. The earlier onset of peak is probably a combination of thin snow depth throughout the whole catchment and the high rate of melt increase for the impervious areas. Runoff period is also shortened by 12 days in this simulation. Runoff for this simulation demonstrates that assuming a uniform cover for snow in urban areas can be very misleading. Simulation of the redistribution of snow changes runoff flow, runoff period, and the time to peak.

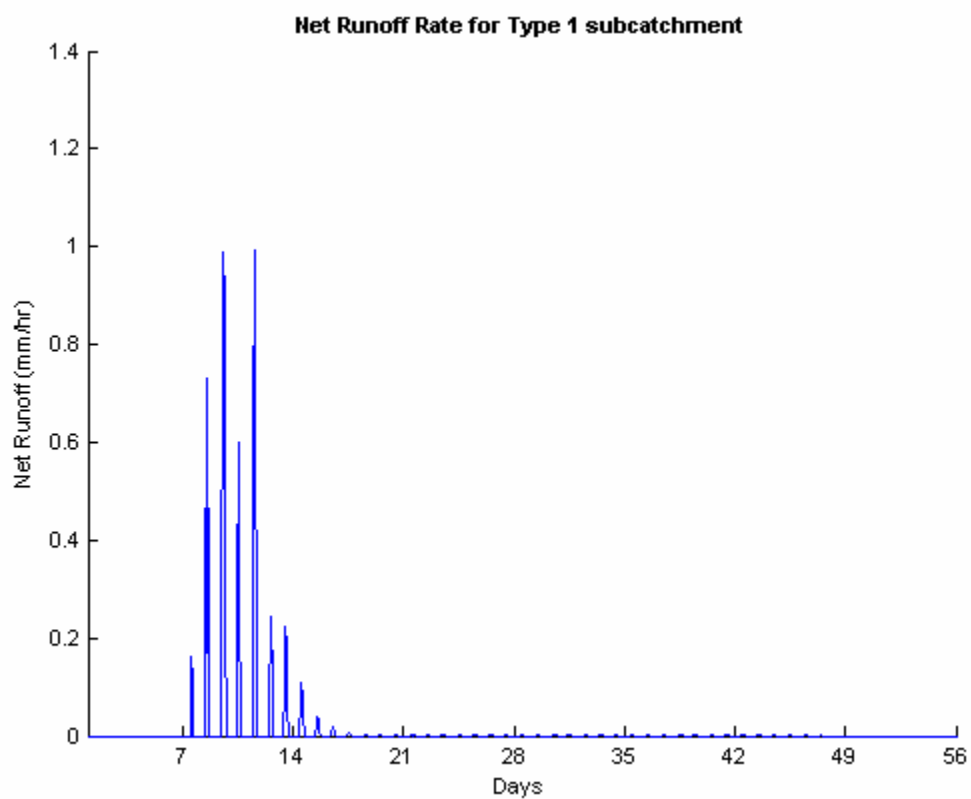


Figure 6.20: Runoff rates for impervious subcatchment type 1 (parking lots)

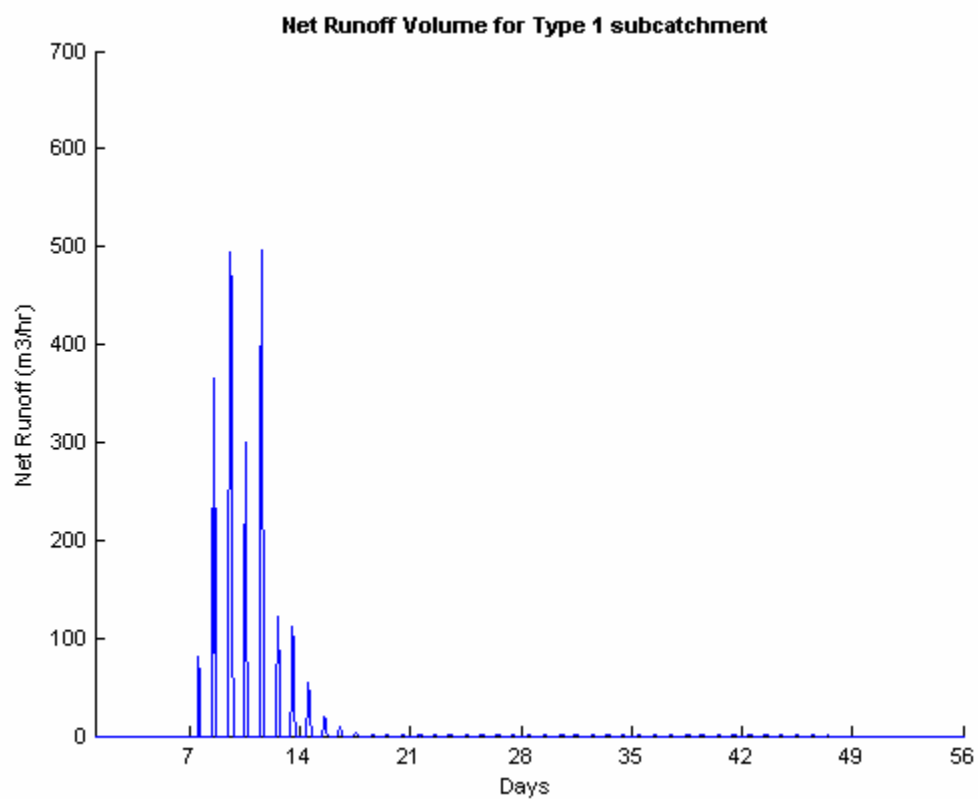


Figure 6.21: Runoff volume for subcatchment type 1 (parking lots)

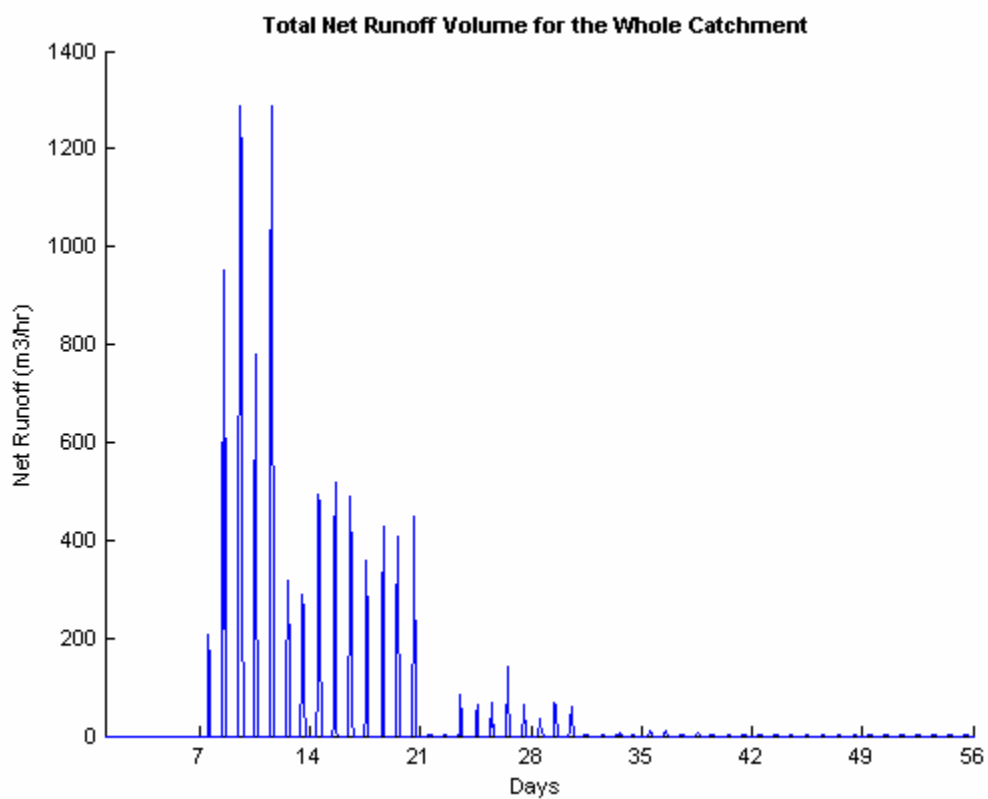


Figure 6.22: Total runoff volume for the whole catchment

## CHAPTER SEVEN

### CONCLUSION AND RECOMMENDATIONS

This research investigated the different aspects of urban snow hydrology. Focus was placed on the study of the spatial and temporal distribution of the characteristics of urban snow, and the impact of incorporating the different characteristics of urban snow in a snowmelt model.

#### 7.1 Major Results of Field Study

In the field study conducted over the winter of 2002, the urban snow cover was classified into four types; snow piles, snow on road shoulders, snow on sidewalk edges, and snow in open areas. The field study revealed that urban snow is highly heterogeneous in terms of the spatial distribution of snow water equivalent, and the temporal distribution of snow albedo. Four separate functions for the snow albedo change over time were developed. Albedo for snow piles decreased exponentially to 0.1-0.2. For snow on road shoulders, albedo also decreased exponentially to 0.2-0.4. Snow on sidewalk edges had albedo values that decreased linearly to 0.5-0.6, and for snow in open areas, albedo values decreased linearly to 0.6-0.7. Average snow density was found to be 490 kg/m<sup>3</sup> for snow piles, 220 kg/m<sup>3</sup> for snow on road shoulders, 240 kg/m<sup>3</sup> for snow on sidewalk edges, and 210 kg/m<sup>3</sup> for snow in open areas. Energy balance of the urban snowpack was dominated by net radiation, and the main source of energy for melt was the shortwave radiation. Therefore, the albedo rate of change for urban snow cover is a very important factor in urban snowmelt generation. Snow cover has also been found to act as an insulating layer for the ground to a certain degree with the result of dampening the fluctuations in the soil

temperature in reaction to the changes in air temperature. However, this effect is more pronounced when the snow cover is uniformly covering a larger extent of area. The characteristics of the urban cover coupled with the factors dominating melt for urban snow cover makes the suitability of applying the temperature index method in calculating urban snowmelt highly questionable.

The field study conducted also revealed that frozen ground acts as a near impervious area regardless of whether the initial soil moisture condition was dry or near saturation. The start of ground thaw in spring coincides with the end of the snow cover depletion. This carries a large impact for the modelling of rain-on-snow events in the spring during periods when snow cover is largely depleted but ground thaw has not progressed sufficiently. The adverse combination of frozen ground, spring melt and rainfall can easily cause spring flooding.

## **7.2 Major Results of Modelling**

The urban snowmelt model simulated in this study demonstrates that simulation of snow redistribution and the incorporation of urban snow characteristics can significantly impact urban runoff. Three simulations were tested to demonstrate the differences in simulations with and without snow piles, and to demonstrate the impact of rain-on-snow events on runoff. The simulation of snow piles resulted in extended period of melt, and decreased peak volume as less areas of thin snow cover with shorter periods of intense melt rate were simulated. The simulation of rain-on-snow increased the peak runoff volume and changed the time to peak. All three simulations were carried out using hourly time steps. If the meteorological data was averaged over a day, the resultant runoff would have a decreased peak volume, since the main source of melt energy is shortwave radiation. In urban areas, snow piles, large or small is a common occurrence. Neglecting this aspect of

the urban snow cover in urban snowmelt models or applying rural snowmelt computations in simulations of urban winter runoff can easily render the simulation results inaccurate.

### **7.3 Recommendation for Future Field Study**

In the urban snowmelt model developed in this study, the areal depletion curve for a uniform snow cover is applied to all snow cover types. For a more accurate result, it is recommended that an areal depletion curve for snow piles should be developed. Snow piles have higher densities that can change or influence the areal depletion curve.

**REFERENCES**

Anderson, E.A. 1968. "Development and testing of snowpack energy balance equations," *Water Resources Research*, 4(1): 19-37.

Anderson, E.A. 1973. "National Weather Service river forecast system – Snow accumulation and ablation model," *NOAA Tech. Memo. NWS HYDRO-17*, U.S. Department of Commerce, Washington, D.C.

Anderson, E.A. 1996. "SNOW-17: SNOW-17 Snow Model," *NWSRFS User's Manual II.2*, <[http://hydrology.nws.noaa.gov/oh/hrl/nwsrfs/users\\_manual/htm/xrfsdocwpd.htm](http://hydrology.nws.noaa.gov/oh/hrl/nwsrfs/users_manual/htm/xrfsdocwpd.htm)>, 2001.

Anderson, E.A. and N.H. Crawford. 1964. "The Synthesis of Continuous Snowmelt Runoff Hydrographs on a Digital Computer," *Technical Report No. 36*, Department of Civil Engineering, Stanford University, California.

Bengtsson, L. 1976. "Snowmelt estimated from energy budget studies," *Nordic Hydrology*, 7: 3-18.

Bengtsson, L. 1984. "Modelling snowmelt induced runoff with short time resolution," *Proc. 3<sup>rd</sup> Int. Conf. Urban Storm Drainage*, Chalmers University of Technology, Gothenburg, pp. 305-314.

Bengtsson, L. 1986. "Snowmelt simulation models in relation to space and time," *Proc. Budapest Symp. 1986, Modelling Snowmelt-Induced Processes*, International Association of Hydrological Sciences, Wallingford, U.K., pp. 115-123.

Bengtsson, L. and Westerström, G. 1992. "Urban snowmelt and runoff in northern Sweden," *Hydrological Sciences Journal*, 37: 263-275.

Bicknell B.R., Imhoff, J.C., Kittle, Jr. J.L., Donigian Jr. A.S., and Johanson, R.C. 1997. "Hydrological simulation program- FORTRAN: User's Manual for Version 11," EPA/600/R-97/080, U.S. Environmental Protection Agency (EPA).

Bolz, R.E. and Tuve, G.L. (Ed.) 1973. "CRC Handbook of Tables for Applied Engineering Science," CRC Press, Ohio, U.S.A., pp. 177

Buttle, J.M. 1989. "Soil moisture and groundwater responses to snowmelt on a drumlin sideslope," *Journal of Hydrology*, 105: 335-355.

Buttle, J.M. and Xu, F. 1988. "Snowmelt runoff in suburban environments," *Nordic Hydrology*, 19:19-40.

Conway, H., Gades, A. and Raymond, C.F. 1996. "Albedo of dirty snow during conditions of melt," *Water Resources Research*, 32(6): 1713-1718.

Danish Hydraulic Institute (DHI). 2000. "MOUSE RDII user guide," Danish Hydraulic Institute, Hørsholm, Denmark.

Dickinson, W.T. and Whitley, H.R. 1972. "A sampling scheme for shallow snowpacks," *Bull. Int. Assoc. Hydrol. Sci.*, 17:247-258.

Dingman, S.L. 1975. "Hydrologic effects of frozen ground: Literature review and synthesis," *CRREL Special report 218, U.S. Army Corps of Engineers, Cold Regions Research and Engineering Laboratory, Hanover, NH.*

Donigian, Jr. A.S., Bicknell, B.R., Imhoff, J.C. 1995. "Hydrological Simulation Program – Fortran (HSPF)," *Computer Models of Watershed Hydrology*, Vijay P. Singh, Ed., Water Resources Publication, Colorado USA., pp. 395-442.

Eagleson, P.S. 1970. "Dynamic Hydrology," McGraw-Hill, U.S.A., pp. 254-257.

Farrell, A. C., Scheckenberger, R. B., Guther, R. T. 2001. "A Case In Support Of Continuous Modelling For Stormwater Management System Design," *Models and Applications to Urban Water Systems, Monograph 9*, William James, Ed., CHI, pp. 113-130.

Granger, R.J., Gray, D.M. and Dyck, G.E. 1984. "Snowmelt infiltration to frozen prairie soils," *Canadian Journal of Earth Sciences*, 21: 669-677.

Gray, D.M. and Male, D.H. (Ed.) 1981. "Handbook of snow: principles, processes, management & use," Pergamon Press, Toronto.

Hanks, R.J. and Ashcroft, G.L. 1980. "Applied Soil Physics: Soil Water and Temperature Application," Springer-Verlag, Berlin, Hiedelberg, 1980

Huber, W.C. and Dickinson, R.E. 1988. "Storm water management model, version 4: User's manual," EPA/600/3-88/001a. (NTIS PB88-236641/AS), U.S. Environmental Protection Agency (EPA), Athens, Georgia., pp. 350-379.

Huber, W.C. 1995. "EPA storm water management model -- SWMM," *Computer Models of Watershed Hydrology*, Vijay P. Singh, Ed., Water Resources Publication, Colorado USA., pp. 783-808.

Ishikawa, N., Narita, H., and Kajiya, Y. 1999. "Contributions of heat from traffic vehicles to snow melting on roads," *Transportation Research Record No.1672*, National Academy Press, Washington D.C., pp. 28-33.

Marks, D., and Dozier, J. 1992. "Climate and energy exchange at the snow surface in the alpine region of the Sierra Nevada 2. Snow cover energy balance," *Water Resources Research*, 28(11): 3043-3054.

Marks, D., Winstral, A., Van Vactor, S.S., Robertson, D., and Davis, R.E. 2000. "Topographic and canopy controls on snow deposition, snow-cover energy balance and snowmelt," *Proc. Symp. Remote Sensing and Hydrology*, Santa Fe, New Mexico, U.S.A., IAHS Publication No. 267, pp. 129-135.

Matheussen, B.V., and Thorolfsson, S.T. 1999. "Simulation errors due to insufficient temporal resolution in urban snowmelt models," *Proc. 8<sup>th</sup> Int. Conf. Urban Storm Drainage*, Sydney, Australia, pp. 1-8.

Moran, S.R. 1986. "Surficial geology of the Calgary urban area," Alberta Research Council, Bulletin 53.

National Weather Service Hydrology Laboratory (NWSHL). 1996. "Overview of NWSRFS," *NWSRFS User's Manual I.1.1*, <[http://hydrology.nws.noaa.gov/oh/hrl/nwsrfs/users\\_manual/part1/html/overview.htm](http://hydrology.nws.noaa.gov/oh/hrl/nwsrfs/users_manual/part1/html/overview.htm)>, 2001.

Osborn, G., and Rajewicz, R. 1998. "Urban geology of Calgary," *Urban geology of Canadian Cities*, Karrow, P.F and White, O.L., Ed., Geological Association of Canada Special Paper 42, pp. 93-115.

Semádeni-Davies, A.F., and Bengtsson, L. 1998. "Snowmelt sensitivity to radiation in the urban environment," *Hydrological Sciences Journal*, 43(1): 67-89.

Semádeni-Davies, A.F. 1999. "Urban snowmelt processes: Modelling and observation," Report No. 1026, Department of Water Resources Engineering, Lund Institute of Technology, Lund University, Sweden.

Semádeni-Davies, A.F. 2000. "Representation of snow in urban drainage models," *Journal of Hydrologic Engineering*, 5(4): 363-370.

Speers, D.D. 1995. "SSARR model," *Computer Models of Watershed Hydrology*, Vijay P. Singh, Ed., Water Resources Publication, Colorado USA., pp. 367-394.

Sundin, E., Andreasson, P., and Viklander, M. 1999. "An energy budget approach to urban snow deposit melt," *Nordic Hydrology*, 30: 39-56.

Thorolfsson, S.T., and Brandt, J. 1996. "The influence of snowmelt on urban runoff in Norway," *Proc. 7<sup>th</sup> Int. Conf. Urban Storm Drainage*, Hanover, Germany, pp. 133-138.

Thorolfsson, S.T., and Sand, K. 1991. "Urban snowmelt research in Norway: Measurements and modelling approach," *Proc. Int. Conf. Urban Drainage and New Technol.*, Č. Maksimović, Ed., Elsevier Science, New York, pp. 309-316.

U.S. Army Corps of Engineers (USACE). 1991. "User Manual, SSARR model, streamflow synthesis and reservoir regulation," USACE North Pacific Division, pp. 35-40.

U.S. Army Corps of Engineers (USACE). 1998. "Runoff from snowmelt," *Engineering Manual 1110-2-1406*, USACE Washington, D.C., pp. 2-6 – 2-7.

Watt, W.E. et. al. (ed.) 1989. "Hydrology of Floods in Canada: A Guide to Planning and Design," National Research Council Canada, Ottawa, pp. 95-168.

Westerström, G. 1981. "Snowmelt runoff from urban plot," *Proc. 2<sup>nd</sup> Int. Conf. Urban Storm Drainage*, Urbana, Illinois USA, pp. 452-459.

Westerström, G. 1984. "Snowmelt runoff from Porsön residential area, Luleå, Sweden," *Proc. 3<sup>rd</sup> Int. Conf. Urban Storm Drainage*, Chalmers University of Technology, Gothenburg, pp. 315-323.

Westerström, G. 1990. "Snowmelt - Runoff from small urban catchments," *Proc. Int. Conf. of Urban Hydrology Under Wintry Conditions*, Narvik, Norway.

Woo, Ming-ko. 1997. "A guide for ground-based measurement of the arctic snow cover," <<http://www.crysys.uwaterloo.ca/science/documents/Woo.pdf>>

World Meteorological Organization (WMO). 1986. "Intercomparisons of models of snowmelt runoff operational hydrology," *Rep. No. 23 (WMO No. 646)*, Geneva.

Yackel, J.J. 1995. "An Analysis of the spatial and temporal character of the chinook in southern Alberta," *Thesis (M.Sc.)*, National Library of Canada, Ottawa.